Scientific
Research
Publishing

International Journal of Modern Nonlinear Theory and Application

Scientific
Research
Publishing

Table of Contents

Volume 4   Number 2   **June 2015**

The figure on the front cover is from the article published in International Journal of Modern Nonlinear Theory and Application, 2015, Vol. 4, No. 2, pp. 127-141 by Jiangyong Hou, Wenjing Yan and Jie Chen.

International Journal of Modern Nonlinear Theory and Application (IJMNTA)

Journal Information

SUBSCRIPTIONS

The *International Journal of Modern Nonlinear Theory and Application* (Online at Scientific Research Publishing, www.SciRP.org) is published quarterly by Scientific Research Publishing, Inc., USA.

Subscription rates:
Print: $59 per issue.
To subscribe, please contact Journals Subscriptions Department, E-mail: sub@scirp.org

SERVICES

Advertisements
Advertisement Sales Department, E-mail: service@scirp.org

Reprints (minimum quantity 100 copies)
Reprints Co-ordinator, Scientific Research Publishing, Inc., USA.
E-mail: sub@scirp.org

COPYRIGHT

PRODUCTION INFORMATION

For manuscripts that have been accepted for publication, please contact:
E-mail: ijmnta@scirp.org

Output Feedback Nonlinear General Integral Control

Baishun Liu

Academy of Naval Submarine, Qingdao, China
Email: baishunliu@163.com

Abstract

This paper proposes an output feedback nonlinear general integral controller for a class of uncertain nonlinear system. By solving Lyapunov equation, we demonstrate a new proposition on Equal ratio gain technique. By using Equal ratio gain technique, Singular perturbation technique and Lyapunov method, theorem to ensure regionally as well as semi-globally exponential stability is established in terms of some bounded information. Moreover, a real time method to evaluate the ratio coefficients of controller and observer are proposed such that their values can be chosen moderately. Theoretical analysis and simulation results show that not only output feedback nonlinear general integral control has the striking robustness but also the organic combination of Equal ratio gain technique and Singular perturbation technique constitutes a powerful tool to solve the output feedback control design problem of dynamics with the nonlinear and uncertain actions.

Keywords

1. Introduction

Integral control [1] plays an important role in practice because it ensures asymptotic tracking and disturbance rejection when exogenous signals are constants or planting parametric uncertainties appear. However, output feedback nonlinear general integral control design is not a trivial matter because it depends on not only the uncertain nonlinear actions, disturbances and nonlinear control actions but also the uncertain estimation error dynamics. Therefore, it is of important significance to develop the design method for output feedback nonlinear general integral control since some states cannot be measured in practice.

For general integral control design, there were various design methods, such as general integral control design based on linear system theory, sliding mode technique, feedback linearization technique and singular perturbation technique and so on, which were presented by [2]-[5], respectively. In addition, general concave integral control [6], general convex integral control [7], constructive general bounded integral control [8] and the generalization of the integrator and integral control action [9] were all developed by using Lyapunov method and resorting to a known stable control law. Equal ratio gain technique firstly was proposed by [10] and was used to address the linear general integral control design. After that Equal ratio gain technique was extended to the canonical interval system matrix [11] and was used to deal with nonlinear general integral control design. All these design methods and general integral controls above are all based on the state feedback. Presently, output feedback general integral control along with its design method has not been developed.

Motivated by the cognition above, this paper proposes an output feedback nonlinear general integral controller for a class of uncertain nonlinear system. The main contributions are that: 1) as any row integrator and its controller gains of a canonical interval system matrix tend to infinity with the same ratio, if it is always Hurwitz, and then the same row solutions of Lyapunov equation all tend to zero; 2) theorem to ensure regionally as well as semi-globally exponential stability is established in terms of some bounded information; 3) a real time method to evaluate the ratio coefficients of controller and observer are proposed such that their values can be chosen moderately. Moreover, theoretical analysis and simulation results show that not only output feedback nonlinear general integral control has the striking robustness but also the organic combination of Equal ratio gain technique and Singular perturbation technique constitutes a powerful tool to solve the output feedback control design problem of dynamics with the nonlinear and uncertain actions.

Throughout this paper, we use the notation $\lambda_m(A)$ and $\lambda_M(A)$ to indicate the smallest and largest eigenvalues, respectively, of a symmetric positive define bounded matrix $A(x)$, for any $x \in R^n$. The norm of vector x is defined as $\|x\| = \sqrt{x^T x}$, and that of matrix A is defined as the corresponding induced norm $\|A\| = \sqrt{\lambda_M(A^T A)}$.

The remainder of the paper is organized as follows: Section 2 describes the system under consideration, assumption and output feedback nonlinear general integral control. Section 3 demonstrates a new proposition on Equal ratio gain technique. Section 4 addresses the design method. Examples and simulation are provided in Section 5. Conclusions are presented in Section 6.

2. Problem Formulation

Consider the following controllable nonlinear system,

$$\begin{cases} \dot{x}_1 = x_2 \\ \dot{x}_2 = x_3 \\ \vdots \\ \dot{x}_n = f(x,w) + g(x,w)u \end{cases} \tag{1}$$

where $x \in R^n$ is the state; $u \in R$ is the control input; $w \in R^l$ is a vector of unknown constant parameters and disturbances. The uncertain nonlinear functions $f(x,w)$ and $g(x,w)$ are all continuous in (x,w) on the control domain $D_x \times D_w \subset R^n \times R^l$. We want to design an output feedback control law u such that $x(t) \to 0$ as $t \to \infty$.

Assumption 1: There is a unique pair $(0, u_0)$ that satisfies the equation,

$$0 = f(0,w) + g(0,w)u_0 \tag{2}$$

so that $x = 0$ is the desired equilibrium point and u_0 is the steady-state control that is needed to maintain equilibrium at $x = 0$, irrespective of the value of w.

Assumption 2: Suppose that the functions $f(x,w)$ and $g(x,w)$ satisfy the following inequalities,

$$\|f(x,w) - f(0,w)\| \le l_f^x \|x\| \tag{3}$$

$$0 < g_m < g(x,w) < g_M \tag{4}$$

$$\left\| g(x,w) - g(0,w) \right\| \le l_g^x \left\| x \right\| \tag{5}$$

$$\left\| f(0,w) g^{-1}(0,w) \right\| \le \gamma_g^f \tag{6}$$

for all $x \in D_x$ and $w \in D_w$, where l_f^x, l_g^x, g_m, g_M and γ_g^f are all positive constants.

For the purpose of this paper, it is convenient to introduce the following definition.

Definition 1: $F_\Phi(a_\Phi, b_\Phi, x)$ with $a_\Phi > 0$, $b_\Phi > 0$, and $x \in R$ denotes the set of all continuous differential increasing function [12], $\Phi(x)$, such that

$$\Phi(0) = 0,$$

$$\left| \Phi(x) \right| \ge b_\Phi, \quad \forall x \in R : |x| > a_\Phi$$

$$d\Phi(x)/dx > 0, \quad \forall x \in R$$

where $|\cdot|$ stands for the absolute value.

Figure 1 depicts the example curves for the functions belonging to the function set F_Φ. For instance, for all $x \in R$, the functions, $\operatorname{arcsin}h(x)$, $\tanh(x)$, $ax + bx^3$ $(a > 0, b > 0)$, $\sinh(x)$, ax and so on, all belong to function set F_Φ.

The output feedback nonlinear general integral controller [11] and observer [12] are given as,

$$\begin{cases} u = -\mu^{-1}\left(u_1(\hat{x}_1) + u_2(\hat{x}_2) + \cdots + u_n(\hat{x}_n) + \alpha_\sigma \sigma \right) - \phi(\hat{x}) - \varphi(\sigma) \\ \dot{\sigma} = \mu^{-1}\theta(\sigma)\left(v_1(\hat{x}_1) + v_2(\hat{x}_2) + \cdots + v_n(\hat{x}_n) \right) \end{cases} \tag{7}$$

$$\begin{cases} \dot{\hat{\sigma}} = \left(d\Phi(\hat{\sigma})/d\hat{\sigma} \right)^{-1}(x_1 - \hat{x}_1) \\ \dot{\hat{x}}_1 = \hat{x}_2 + \varepsilon^{-1}h_1(x_1 - \hat{x}_1) \\ \dot{\hat{x}}_2 = \hat{x}_3 + \varepsilon^{-2}h_2(x_1 - \hat{x}_1) \\ \vdots \\ \dot{\hat{x}}_n = \hat{f}(\hat{x}, \hat{w}) + \varepsilon^{-n}h_n(x_1 - \hat{x}_1) + \varepsilon^{-n-1}h_{n+1}\Phi(\hat{\sigma}) - \hat{g}(\hat{x}, \hat{w})\mu^{-1}\left(u_1(\hat{x}_1) + u_2(\hat{x}_2) + \cdots + u_n(\hat{x}_n) + \alpha_\sigma \sigma \right) \\ \quad - \hat{g}(\hat{x}, \hat{w})\left(\phi(\hat{x}) + \varphi(\sigma) \right) \end{cases} \tag{8}$$

where $\hat{x} \in R^n$ is the estimated state; $\hat{w} \in R^l$ is the prescient constant parameters and disturbances; μ, ε, α_σ and h_j $(j = 1, 2, \cdots, n+1)$ are all positive constants;

$$u_i(\hat{x}_i) = \alpha_i(\hat{x}_i)\hat{x}_i \quad \left(0 < \alpha_i^m \le \alpha_i(\hat{x}_i) \le \alpha_i^M \right),$$
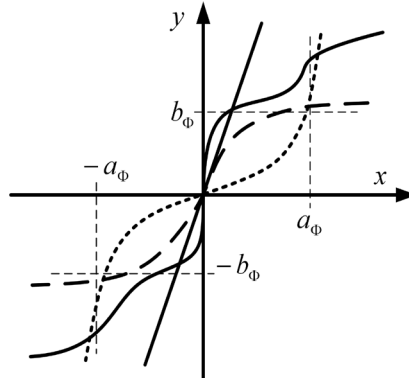
Figure 1. Example curves for the functions belonging to the function set F_Φ.

$$v_i(\hat{x}_i) = \beta_i(\hat{x}_i)\hat{x}_i \quad \left(0 < \beta_i^m \le \beta_i(\hat{x}_i) \le \beta_i^M\right),$$

$\alpha_i(\hat{x}_i)$ and $\beta_i(\hat{x}_i)$ are the slopes of the line segment connecting $\hat{x}_i$ to the origin $(i=1,2,\cdots,n)$; $\phi(\hat{x})$ $(\phi(0)=0)$ is used to attenuate the uncertain nonlinear action of $f(x,w)$; $\theta(\sigma)$ $(0<\theta_m<\theta(\sigma)<\theta_M)$ is applied to reorganize the integrator output; $\varphi(\sigma)$ $(\varphi(0)=0)$ is utilized to improve the integral control performance $(0<\alpha_\sigma^m<\alpha_\sigma+\mathrm{d}\varphi(\sigma)/\mathrm{d}\sigma\le\alpha_\sigma^M)$; $\hat{f}(\hat{x},\hat{w})$ and $\hat{g}(\hat{x},\hat{w})$ are the normal models of $f(x,w)$ and $g(x,w)$, respectively. $\Phi(\bullet)$ belongs to the function set F_Φ.

Assumptions 3: By the definition of controller (7), it is convenient to suppose that the following inequalities,

$$\|f(x,w)-f(0,w)-g(x,w)\phi(x)\|\le l_{f\phi}^x\|x\| \tag{9}$$

$$\|\varphi(\sigma)-\varphi(\sigma_0)\|\le l_\varphi^\sigma\|\sigma-\sigma_0\| \tag{10}$$

hold for all $x\in D_x$, $w\in D_w$ and σ, $\sigma_0\in R$, where $l_{f\phi}^x$ and l_φ^σ are all positive constants.

By the definitions of $u_i(\hat{x}_i)$, $v_i(\hat{x}_i)$ and $\theta(\sigma)$, and letting $e_i=x_i-\hat{x}_i$ $(i=1,2,\cdots,n)$, the controller (7) can be written as,

$$\begin{cases} u=-\mu^{-1}\left(\alpha_1\hat{x}_1+\alpha_2\hat{x}_2+\cdots+\alpha_n\hat{x}_n+\alpha_\sigma\sigma\right)-\phi(\hat{x})-\varphi(\sigma) \\ \dot{\sigma}=\mu^{-1}\left(\beta_1\hat{x}_1+\beta_2\hat{x}_2+\cdots+\beta_n\hat{x}_n\right) \end{cases} \tag{11}$$

and the whole closed-loop system can be written as,

$$\begin{cases} \dot{x}_1=x_2 \\ \dot{x}_2=x_3 \\ \vdots \\ \dot{x}_n=f(x,w)-g(x,w)\phi(\hat{x})-g(x,w)\varphi(\sigma)-\mu^{-1}g(x,w)\left(\alpha_1x_1+\alpha_2x_2+\cdots+\alpha_nx_n+\alpha_\sigma\sigma\right) \\ \qquad +\mu^{-1}g(x,w)\left(\alpha_1e_1+\alpha_2e_2+\cdots+\alpha_ne_n\right) \\ \dot{\sigma}=\mu^{-1}\left(\beta_1x_1+\beta_2x_2+\cdots+\beta_nx_n\right)-\mu^{-1}\left(\beta_1e_1+\beta_2e_2+\cdots+\beta_ne_n\right) \end{cases} \tag{12}$$

$$\begin{cases} \Phi(\hat{\sigma})=e_1 \\ \dot{e}_1=e_2-\varepsilon^{-1}h_1e_1 \\ \dot{e}_2=e_3-\varepsilon^{-2}h_2e_1 \\ \vdots \\ \dot{e}_n=\Delta_f-\varepsilon^{-n}h_ne_1-\varepsilon^{-n-1}h_{n+1}\Phi(\hat{\sigma})-\mu^{-1}\Delta_g\left(\alpha_1x_1+\alpha_2x_2+\cdots+\alpha_nx_n+\alpha_\sigma\sigma\right) \\ \qquad +\mu^{-1}\Delta_g\left(\alpha_1e_1+\alpha_2e_2+\cdots+\alpha_ne_n\right)-\Delta_g\left(\phi(\hat{x})+\varphi(\sigma)\right) \end{cases} \tag{13}$$

where

$$\Delta_f=f(x,w)-\hat{f}(\hat{x},\hat{w}), \quad \Delta_g=g(x,w)-\hat{g}(\hat{x},\hat{w}),$$

and $\theta(\sigma)$ is integrated into β_i $(i=1,2,\cdots,n)$.

By the equation (2) and inequality (4), and choosing μ^{-1} and $\varepsilon^{-n-1}h_{n+1}$ to be large enough, and then setting $\dot{x}=\dot{e}=0$ and $x=e=0$ of the systems (12) and (13), we obtain

$$f(0,w)g^{-1}(0,w)=\mu^{-1}\alpha_\sigma\sigma_0+\varphi(\sigma_0) \tag{14}$$

$$\Delta_{f0}-\Delta_{g0}\left(\mu^{-1}\alpha_\sigma\sigma_0+\varphi(\sigma_0)\right)=\varepsilon^{-n-1}h_{n+1}\Phi(\hat{\sigma}_0) \tag{15}$$

where

$$\Delta_{f0}=f(0,w)-\hat{f}(0,\hat{w}) \text{ and } \Delta_{g0}=g(0,w)-\hat{g}(0,\hat{w}).$$

Thus, we ensure that σ_0 and $\hat{\sigma}_0$ are the unique solutions of the systems (12) and (13), respectively.

Defining $z = \begin{bmatrix} x^T & \sigma - \sigma_0 \end{bmatrix}^T$, $e_0 = \Phi(\hat{\sigma}) - \Phi(\hat{\sigma}_0)$ and $\eta_i = \varepsilon^{-n+i} e_i$ $(i = 0,1,2,\cdots,n)$, and substituting (14) and (15) into (12) and (13), respectively, the whole closed-loop system can be rewritten as,

$$\begin{cases} \dot{z} = A_z z + F_z(z,e) \\ \varepsilon \dot{\eta} = A_\eta \eta + \varepsilon F_\eta(z,e) \end{cases} \tag{16}$$

where

$$A_z = \begin{bmatrix} 0 & 1 & \cdots & 0 & 0 \\ 0 & 0 & \ddots & 0 & 0 \\ 0 & 0 & \cdots & 1 & 0 \\ -\mu^{-1}\alpha_1 & -\mu^{-1}\alpha_2 & \cdots & -\mu^{-1}\alpha_n & -\mu^{-1}\alpha_\sigma \\ \mu^{-1}\beta_1 & \mu^{-1}\beta_2 & \cdots & \mu^{-1}\beta_n & 0 \end{bmatrix},$$

$$A_\eta = \begin{bmatrix} 0 & 1 & 0 & 0 & 0 & 0 \\ 0 & -h_1 & 1 & 0 & 0 & 0 \\ \vdots & -h_2 & 0 & \ddots & 0 & 0 \\ 0 & \vdots & 0 & 0 & 1 & 0 \\ 0 & -h_{n-1} & 0 & 0 & 0 & 1 \\ -h_{n+1} & -h_n & 0 & 0 & 0 & 0 \end{bmatrix},$$

$$F_z(z,e) = \begin{bmatrix} 0 & \cdots & 0 & \delta_1 + \mu^{-1}\delta_2 & -\mu^{-1}\delta_3 \end{bmatrix}^T,$$

$$F_\eta(z,e) = \begin{bmatrix} 0 & \cdots & 0 & 0 & \Delta_1 + \mu^{-1}\Delta_2 \end{bmatrix}^T,$$

$$\delta_1 = f(x,w) - g(x,w)\phi(\hat{x}) - f(0,w) - g(x,w)(\varphi(\sigma) - \varphi(\sigma_0)) - [g(x,w) - g(0,w)]f(0,w)g^{-1}(0,w),$$

$$\delta_2 = g(x,w)(\alpha_1 e_1 + \alpha_2 e_2 + \cdots + \alpha_n e_n),$$

$$\delta_3 = \beta_1 e_1 + \beta_2 e_2 + \cdots + \beta_n e_n,$$

$$\Delta_1 = \Delta_f - \Delta_{f0} - \Delta_g \phi(\hat{x}) - \Delta_g(\varphi(\sigma) - \varphi(\sigma_0)) - (\Delta_g - \Delta_{g0})f(0,w)g^{-1}(0,w),$$

$$\Delta_2 = \Delta_g(\alpha_1 e_1 + \alpha_2 e_2 + \cdots + \alpha_n e_n) - \Delta_g(\alpha_1 x_1 + \alpha_2 x_2 + \cdots + \alpha_n x_n + \alpha_\sigma(\sigma - \sigma_0)),$$

and $g(x,w)$ is integrated into α_i and α_σ.

By **Assumptions 2** and **3**, the uncertain terms δ_1, δ_2, δ_3, Δ_1 and Δ_2 satisfy the linear growth bound,

$$\|\delta_1\| \le \gamma_{\delta_1}^z \|z\| + \gamma_{\delta_1}^\eta(\varepsilon)\|\eta\| \tag{17}$$

$$\|\delta_2\| \le \gamma_{\delta_2}^\eta(\varepsilon)\|\eta\| \tag{18}$$

$$\|\delta_3\| \le \gamma_{\delta_3}^\eta(\varepsilon)\|\eta\| \tag{19}$$

$$\|\Delta_1\| \le \gamma_{\Delta_1}^z \|z\| + \gamma_{\Delta_1}^\eta(\varepsilon)\|\eta\| \tag{20}$$

$$\|\Delta_2\| \le \gamma_{\Delta_2}^z \|z\| + \gamma_{\Delta_2}^\eta(\varepsilon)\|\eta\| \tag{21}$$

where $\gamma_{\delta_1}^z$, $\gamma_{\delta_1}^\eta(\varepsilon)$, $\gamma_{\delta_2}^\eta(\varepsilon)$, $\gamma_{\delta_3}^\eta(\varepsilon)$, $\gamma_{\Delta_1}^z$, $\gamma_{\Delta_1}^\eta(\varepsilon)$, $\gamma_{\Delta_2}^z$ and $\gamma_{\Delta_2}^\eta(\varepsilon)$ are all positive constants.

3. Propositions on Equal Ratio Gain Technique

Equal ratio gain technique is firstly proposed by [10] and is extended to the canonical interval system matrix in [11]. For analyzing the stability of the closed-loop system (16), it is necessary to review two important propositions on Equal ratio gain technique as follows.

Proposition 1 [10]: as any row controller gains, or controller and its integrator gains of a canonical system matrix tend to infinity with the same ratio, if it is always Hurwitz, and then the same row solutions of Lyapunov equation all tend to zero.

Proposition 2 [11]: a canonical interval system matrix can be designed to be Hurwitz as any row controller gains, or controller and its integrator gains increase with the same ratio.

Based on two **Propositions** above, it is not enough to analyze the stability of the closed-loop system (16). So, a new proposition on Equal ratio gain technique is demonstrated in the next two subsections.

3.1. New Proposition

Consider the following controllable canonical interval system matrix A,

$$A = \begin{bmatrix} 0 & 1 & \cdots & 0 & 0 \\ 0 & 0 & \ddots & 0 & 0 \\ 0 & 0 & \cdots & 1 & 0 \\ -\mu^{-1}\alpha_1 & -\mu^{-1}\alpha_2 & \cdots & -\mu^{-1}\alpha_n & -\mu^{-1}\alpha_{n+1} \\ \mu^{-1}\beta_1 & \mu^{-1}\beta_2 & \cdots & \mu^{-1}\beta_n & 0 \end{bmatrix}$$

where

$$0 < \alpha_i^m \leq \alpha_i \leq \alpha_i^M \quad (i = 1, 2, \cdots, n+1),$$

$$0 < \beta_j^m \leq \beta_j \leq \beta_j^M \quad (j = 1, 2, \cdots, n),$$

and μ is a positive constant.

By **Proposition 2**, the interval system matrix A can be designed to be Hurwitz for all $0 < \alpha_i^m \leq \alpha_i \leq \alpha_i^M$, $0 < \beta_j^m \leq \beta_j \leq \beta_j^M$ and $0 < \mu < \mu^*$. Thus, for any given positive define symmetric matrix Q there exists a unique positive define symmetric matrix P that satisfies Lyapunov equation $PA + A^{\mathrm{T}}P = -Q$, and the solution of Lyapunov equation can be obtained by skew symmetric matrix approach [13], that is,

$$P = 0.5(S - Q)A^{-1}$$

where

$$S = PA - A^{\mathrm{T}}P \quad \text{and} \quad A^{\mathrm{T}}S + SA = A^{\mathrm{T}}Q - QA.$$

The inversion of the matrix A with $\mu = 1$ is,

$$A^{-1} = \begin{bmatrix} * & * & \cdots & * & 0 & (\beta_1)^{-1} \\ 1 & 0 & \cdots & 0 & 0 & 0 \\ 0 & 1 & \cdots & 0 & 0 & 0 \\ 0 & 0 & \ddots & 0 & \vdots & \vdots \\ 0 & 0 & \cdots & 1 & 0 & 0 \\ * & * & \cdots & * & -\alpha_{n+1}^{-1} & -\alpha_1(\alpha_{n+1}\beta_1)^{-1} \end{bmatrix} \tag{22}$$

where the elements $*$ are omitted since it is useless to achieve our object. The interesting reader can evaluate them by $AA^{-1} = I$.

It is well known that the solution P of Lyapunov equation is more and more complex as the order of the system matrix A increases. Therefore, for clearly showing the results, we consider a simple case, that is, taking

$Q = I$ and $n = 2$ of the system matrix A. Thus, taking $\mu = 1$, obtain,

$$S - Q = \begin{bmatrix} -1 & s_{12} & s_{13} \\ -s_{12} & -1 & s_{23} \\ -s_{13} & -s_{23} & -1 \end{bmatrix}$$

$$A^{-1} = \begin{bmatrix} * & 0 & (\beta_1)^{-1} \\ 1 & 0 & 0 \\ * & -(\alpha_3)^{-1} & -\alpha_1(\alpha_3\beta_1)^{-1} \end{bmatrix}$$

where

$$s_{12} = \frac{\alpha_1 + (\alpha_1 + \alpha_3\beta_2)\alpha_1 + \beta_1\beta_1 + \alpha_1\beta_2\beta_2 - \alpha_2\beta_1\beta_2}{\alpha_2(\alpha_3\beta_2 + \alpha_1) - \alpha_3\beta_1}$$

$$s_{13} = \frac{\alpha_1\alpha_2\beta_2 - \alpha_3\beta_2\beta_1 - \alpha_2\alpha_2\beta_1 - \alpha_2\alpha_3 - \alpha_3\alpha_3\beta_1}{\alpha_2(\alpha_3\beta_2 + \alpha_1) - \alpha_3\beta_1}$$

$$s_{23} = -\frac{\alpha_3 + \alpha_3(\alpha_3\beta_2 + \alpha_1) + \alpha_3\beta_2\beta_2 + \alpha_2\beta_1}{\alpha_2(\alpha_3\beta_2 + \alpha_1) - \alpha_3\beta_1}$$

and then we have,

$$p_{13} = -\frac{1}{2\beta_1} - s_{13}\frac{\alpha_1}{2\alpha_3\beta_1}$$

$$p_{23} = \frac{1}{2\alpha_3}$$

$$p_{33} = -\frac{s_{13}}{2\beta_1} + \frac{\alpha_1}{2\alpha_3\beta_1}$$

Now, α_3, α_2, α_1, β_2 and β_1 are multiplied by μ^{-1}, then we obtain,

$$s_{12}^{\mu} = \frac{\alpha_1\mu^2 + (\alpha_1\mu + \alpha_3\beta_2)\alpha_1 + \beta_1\beta_1\mu + \alpha_1\beta_2\beta_2 - \alpha_2\beta_1\beta_2}{\alpha_2(\alpha_3\beta_2 + \mu\alpha_1) - \mu\alpha_3\beta_1}$$

$$s_{13}^{\mu} = \frac{\alpha_1\alpha_2\beta_2 - \alpha_3\beta_2\beta_1 - \alpha_2\alpha_2\beta_1 - \mu\alpha_2\alpha_3 - \alpha_3\alpha_3\beta_1}{\alpha_2(\alpha_3\beta_2 + \mu\alpha_1) - \mu\alpha_3\beta_1}$$

$$s_{23}^{\mu} = -\frac{\mu^2\alpha_3 + \alpha_3\alpha_3\beta_2 + \mu\alpha_1\alpha_3 + \alpha_3\beta_2\beta_2 + \mu\alpha_2\beta_1}{\alpha_2(\alpha_3\beta_2 + \mu\alpha_1) - \mu\alpha_3\beta_1}$$

$$p_{13} = -\frac{1}{2\beta_1}\mu - s_{13}^{\mu}\frac{\alpha_1}{2\alpha_3\beta_1}\mu$$

$$p_{23} = \frac{1}{2\alpha_3}\mu$$

$$p_{33} = -\frac{s_{13}^{\mu}}{2\beta_1}\mu + \frac{\alpha_1}{2\alpha_3\beta_1}\mu$$

It is obvious that s_{12}^{μ}, s_{23}^{μ} and s_{13}^{μ} all tend to the constants as $\mu \to 0$, and then we have,

$$\left\| P_3 \right\| = \left\| P_3^\mu \right\| \mu \to 0 \quad \text{as} \quad \mu \to 0$$

where $P_3 = P_3^\mu \mu = \begin{bmatrix} p_{31} & p_{32} & p_{33} \end{bmatrix}$.

From the statements above, it is easy to see that for $n = 2$ of the system matrix A, $\left\| P_3 \right\|$ can be formulated as the linear form on μ and tends to zero as $\mu \to 0$. Moreover, the solution of the matrix S is more and more complex as the order of the system matrix A increases. Thus, by the inversion of system matrix A^{-1} (22), $\left\| P_{n+1} \right\|$ can be formulated as the linear form on μ for the $n+1$-order system matrix A, and with the help of computer, it can be verified that the solution of P_{n+1}^μ still tends to the constant as $\mu \to 0$. Therefore, for the $n+1$-order system matrix A, we can conclude that $\left\| P_{n+1} \right\| \to 0$ as $\mu \to 0$. As a result, the following theorem can be established.

Theorem 1: If the interval system matrix A is Hurwitz for all $0 < \alpha_i^m \le \alpha_i \le \alpha_i^M$, $0 < \beta_j^m \le \beta_j \le \beta_j^M$ and $0 < \mu < \mu^*$, and then we have,

$$\left\| P_{n+1} \right\| = \left\| P_{n+1}^\mu \right\| \mu \to 0 \quad \text{as} \quad \mu \to 0.$$

where

$$P_{n+1} = P_{n+1}^\mu \mu = \begin{bmatrix} p_{n+1,1} & p_{n+1,2} & \cdots & p_{n+1,n+1} \end{bmatrix},$$

$$P_{n+1}^\mu = -0.5 \beta_1^{-1} \begin{bmatrix} 1 + s_{1,n+1}^\mu \alpha_1 \alpha_{n+1}^{-1} & s_{12}^\mu + s_{2,n+1}^\mu \alpha_1 \alpha_{n+1}^{-1} & \cdots & s_{1,n-1}^\mu + s_{n-1,n+1}^\mu \alpha_1 \alpha_{n+1}^{-1} & \beta_1 \alpha_{n+1}^{-1} & s_{1,n+1}^\mu + \alpha_1 \alpha_{n+1}^{-1} \end{bmatrix}.$$

Discussion 1: From the statements above, the solution of the matrix S is more and more complex as the order of the system matrix A increases. So, although **Theorem 1** is demonstrated by taking $Q = I$ and the single variable system matrix A, it is very easy to extend **Theorem 1** to any given positive define symmetric matrix Q and the multiple variable system matrix A with the help of computer since there is not any difficulty to obtain the solution of the matrix S in theory, that is, Lyapunov equation applies to not only the single system matrix but also the multiple system matrix. Thus, there is the following proposition.

Proposition 3: as any row integrator and its controller gains of a canonical interval system matrix tend to infinity with the same ratio, if it is always Hurwitz, and then the same row solutions of Lyapunov equation all tend to zero.

3.2. Example

For testifying the justification of **Theorem 1** and **Proposition 3**, we consider a 6-order two variable system matrix A as follows,

$$A = \begin{bmatrix} 0 & 0 & 0 & 0 & 1 & 0 \\ 0 & 0 & 0 & 0 & 0 & 1 \\ \beta_1^x & \beta_2^x & 0 & 0 & \beta_3^x & \beta_4^x \\ \beta_1^y & \beta_2^y & 0 & 0 & \beta_3^y & \beta_4^y \\ -\alpha_1^x & -\alpha_2^x & -\alpha_3^x & 0 & -\alpha_4^x & -\alpha_5^x \\ -\alpha_1^y & -\alpha_2^y & 0 & -\alpha_3^y & -\alpha_4^y & -\alpha_5^y \end{bmatrix}$$

The inversion of the system matrix A is,

$$A^{-1} = \begin{bmatrix} * & * & a_{13} & a_{14} & 0 & 0 \\ * & * & a_{23} & a_{24} & 0 & 0 \\ * & * & a_{33} & a_{34} & a_{35} & 0 \\ * & * & a_{43} & a_{44} & 0 & a_{46} \\ 1 & 0 & 0 & 0 & 0 & 0 \\ 0 & 1 & 0 & 0 & 0 & 0 \end{bmatrix}$$

where

$$a_{13} = -\frac{\beta_2^y}{\beta_2^x \beta_1^y - \beta_1^x \beta_2^y}, \quad a_{23} = \frac{\beta_1^y}{\beta_2^x \beta_1^y - \beta_1^x \beta_2^y}, \quad a_{33} = \frac{\alpha_1^x \beta_2^y - \alpha_2^x \beta_1^y}{\alpha_3^x \left(\beta_2^x \beta_1^y - \beta_1^x \beta_2^y \right)}$$

$$a_{43} = \frac{\alpha_1^y \beta_2^y - \alpha_2^y \beta_1^y}{\alpha_3^y \left(\beta_2^x \beta_1^y - \beta_1^x \beta_2^y \right)}, \quad a_{14} = -\frac{\beta_2^x}{\beta_2^y \beta_1^x - \beta_1^y \beta_2^x}, \quad a_{24} = \frac{\beta_1^x}{\beta_2^y \beta_1^x - \beta_1^y \beta_2^x}$$

$$a_{34} = \frac{\alpha_1^x \beta_2^x - \alpha_2^x \beta_1^x}{\alpha_3^x \left(\beta_2^y \beta_1^x - \beta_1^y \beta_2^x \right)}, \quad a_{44} = \frac{\alpha_1^y \beta_2^x - \alpha_2^y \beta_1^x}{\alpha_3^y \left(\beta_2^y \beta_1^x - \beta_1^y \beta_2^x \right)}, \quad a_{35} = -\frac{1}{\alpha_3^x}, \quad a_{46} = -\frac{1}{\alpha_3^y}.$$

By the equation $A^{\mathrm{T}}S + SA = A^{\mathrm{T}}Q - QA$, it is very easy to obtain the fifteen linear equations with fifteen elements of the matrix S. So, it is omitted.

Thus, taking

$$A = \begin{bmatrix} 0 & 0 & 0 & 0 & 1 & 0 \\ 0 & 0 & 0 & 0 & 0 & 1 \\ 8 & 2 & 0 & 0 & 3 & 1 \\ 2 & 7 & 0 & 0 & 1 & 5 \\ -8 & -2 & -8 & 0 & -3 & -1 \\ -2 & -8 & 0 & -8 & -1 & -3 \end{bmatrix}$$

$$Q = \begin{bmatrix} 3.0 & 1.0 & -0.8 & 0.6 & 0.5 & 0.3 \\ 1.0 & 5.0 & 1.3 & 1.0 & 0.8 & 0.2 \\ -0.8 & 1.3 & 6 & 0.8 & 0.4 & 1.0 \\ 0.6 & 1.0 & 0.8 & 2.0 & 1.3 & 0.5 \\ 0.5 & 0.8 & 0.4 & 1.3 & 3.0 & 0.8 \\ 0.3 & 0.2 & 1.0 & 0.5 & 0.8 & 6.0 \end{bmatrix}.$$

Now, by Routh's stability criterion and with the help of computer, we have: 1) if α_i^x $(i = 1,2,\cdots,5)$ and β_j^x $(j = 1,2,\cdots,4)$ of the system matrix A are multiplied by μ^{-1}, then it is still Hurwitz for all $0 < \mu \le \mu^* = 1.45$, and the numerical solutions of P_3 are shown in **Table 1**; 2) if α_i^y and β_j^y of the system matrix A are multiplied by μ^{-1}, then it is still Hurwitz for all $0 < \mu \le \mu^* = 2.90$, and the numerical solutions of P_4 are shown in **Table 2**.

From the example above, it is obvious that: 1) as shown in **Table 1, Table 2**, the absolute values of p_{3i} and p_{4i} $(i = 1,2,\cdots,6)$ are all decrease as μ reduces; 2) although the result above is obtained by a constant system matrix, it is easy to be extended to the interval system matrix. This not only verifies the justification of **Theorem 1** and **Proposition 3** but also shows that for the high order and multiple variable system matrix, it is convenient and practical with the help of computer.

Table 1. Numerical Solutions of P_3 for all α_i^x and β_j^x multiplied by μ^{-1}.

	$\mu = 1.0$	$\mu = 0.1$	$\mu = 0.01$
p_{31}	21.38	4.54e-1	4.27e-2
p_{32}	−5.90	1.66e-1	1.81e-2
p_{33}	25.78	5.65e-1	5.32e-2
p_{34}	−10.86	−2.32e-1	−2.24e-2
p_{35}	0.75	7.50e-2	7.5e-3
p_{36}	−0.84	2.36e-1	2.46e-2

Table 2. Numerical Solutions of P_4 for all α_i^y and β_j^y multiplied by μ^{-1}.

	$\mu = 1.0$	$\mu = 0.1$	$\mu = 0.01$
p_{41}	−6.73	6.23e-2	7.70e-3
p_{42}	6.27	3.09e-1	2.97e-2
p_{43}	−10.86	−3.13e-1	−3.10e-2
p_{44}	9.45	4.10e-1	3.93e-2
p_{45}	0.94	1.55e-1	1.60e-2
p_{46}	0.25	2.50e-2	2.50e-3

4. Stability Analysis

The asymptotic stability of the closed-loop system (16) can be achieved by Equal ratio gain technique and Singular perturbation technique as follows:

By **Proposition 2** [11], the interval system matrix A_z can be designed to be Hurwitz for all

$$0 < \alpha_i^m \leq \alpha_i \leq \alpha_i^M, \quad 0 < \beta_j^m \leq \beta_j \leq \beta_j^M, \quad \alpha_\sigma \text{ and } 0 < \mu < \mu^*,$$

and by choosing h_j $(j = 1, 2, \cdots, n+1)$, the matrix A_η can be designed to be Hurwitz, too. Thus, by linear system theory, two quadratic Lyapunov functions,

$$V_z(z) = z^{\mathrm{T}} P_z z \tag{23}$$

$$V_\eta(\eta) = \eta^{\mathrm{T}} P_\eta \eta \tag{24}$$

can be obtained. Where P_z and P_η are the solutions of Lyapunov equations,

$$P_z A_z + A_z^{\mathrm{T}} P_z = -Q_z \text{ and } P_\eta A_\eta + A_\eta^{\mathrm{T}} P_\eta = -Q_\eta$$

with any given positive define symmetric matrices Q_z and Q_η, respectively.

Using $V(z, \eta) = (1-d) V_z(z) + d V_\eta(\eta)$ [1] as Lyapunov function candidate, and then its time derivative along the trajectories of the closed-loop system (16) is,

$$\dot{V}(z, \eta) = (1-d)\dot{V}_z(z) + d\dot{V}_\eta(\eta)$$
$$= (1-d) z^{\mathrm{T}} \left(A_z^{\mathrm{T}} P_z + P_z A_z \right) z + d\varepsilon^{-1} \eta^{\mathrm{T}} \left(A_\eta^{\mathrm{T}} P_\eta + P_\eta A_\eta \right) \eta + (1-d) \frac{\partial V_z(z)}{\partial z} F_z(z, e) + d \frac{\partial V_\eta(\eta)}{\partial \eta} F_\eta(z, e), \tag{25}$$

Substituting $F_z(z, e)$ and $F_\eta(z, e)$ into (25), obtain,

$$\dot{V}(z, \eta) = (1-d) z^{\mathrm{T}} \left(A_z^{\mathrm{T}} P_z + P_z A_z \right) z + d\varepsilon^{-1} \eta^{\mathrm{T}} \left(A_\eta^{\mathrm{T}} P_\eta + P_\eta A_\eta \right) \eta + (1-d) z^{\mathrm{T}} P_{zn} \left(\delta_1 + \mu^{-1} \delta_2 \right)$$
$$+ (1-d) \left(\delta_1 + \mu^{-1} \delta_2 \right)^{\mathrm{T}} P_{zn} z - (1-d) \mu^{-1} z^{\mathrm{T}} P_{zn+1} \delta_3 - (1-d) \mu^{-1} \delta_3^{\mathrm{T}} P_{zn+1} z \tag{26}$$
$$+ d\eta^{\mathrm{T}} P_{\eta n+1} \left(\Delta_1 + \mu^{-1} \Delta_2 \right) + d \left(\Delta_1 + \mu^{-1} \Delta_2 \right)^{\mathrm{T}} P_{\eta n+1} \eta,$$

where

$$P_{zn} = \begin{bmatrix} p_{n1} & p_{n2} & \cdots & p_{n,n+1} \end{bmatrix},$$

$$P_{zn+1} = \begin{bmatrix} p_{n+1,1} & p_{n+1,2} & \cdots & p_{n+1,n+1} \end{bmatrix},$$

$$P_{\eta n+1} = \begin{bmatrix} p_{n+1,1} & p_{n+1,2} & \cdots & p_{n+1,n+1} \end{bmatrix}.$$

Now, by **Propositions 1** and **3**, we have,

$$\|P_{zn}\| = \|P_{zn}^{\mu}\| \mu \to 0 \quad \text{as} \quad \mu \to 0,$$

$$\|P_{zn+1}\| = \|P_{zn+1}^{\mu}\| \mu \to 0 \quad \text{as} \quad \mu \to 0.$$

Substituting them and (17) - (21) into (26), obtain,

$$
\begin{aligned}
\dot{V}(z,\eta) \le & -(1-d)\left(\lambda_m(Q_z) - 2\mu\gamma_{\delta_1}^z \|P_{zn}^{\mu}\|\right)\|z\|^2 \\
& + 2\left((1-d)\left(\mu\gamma_{\delta_1}^\eta(\varepsilon) + \gamma_{\delta_2}^\eta(\varepsilon)\right)\|P_{zn}^{\mu}\| + (1-d)\gamma_{\delta_3}^\eta(\varepsilon)\|P_{zn+1}^{\mu}\| + d\left(\gamma_{\Delta_1}^z + \mu^{-1}\gamma_{\Delta_2}^z\right)\|P_{\eta n+1}\|\right)\|z\|\|\eta\| \\
& -\left(\frac{1}{\varepsilon}\lambda_m(Q_\eta) - 2d\left(\gamma_{\Delta_1}^\eta(\varepsilon) + \mu^{-1}\gamma_{\Delta_2}^\eta(\varepsilon)\right)\|P_{\eta n+1}\|\right)\|\eta\|^2 \\
= & -\zeta^{\mathrm{T}}\Lambda\zeta,
\end{aligned}
\tag{27}
$$

where

$$\zeta = \begin{bmatrix} \|z\| & \|\eta\| \end{bmatrix}^{\mathrm{T}},$$

$$\rho_z^z = \lambda_m(Q_z) - 2\mu\gamma_{\delta_1}^z \|P_{zn}^{\mu}\|,$$

$$\rho_z^\eta = \left(\mu\gamma_{\delta_1}^\eta(\varepsilon) + \gamma_{\delta_2}^\eta(\varepsilon)\right)\|P_{zn}^{\mu}\| + \gamma_{\delta_3}^\eta(\varepsilon)\|P_{zn+1}^{\mu}\|,$$

$$\rho_\eta^z = \left(\gamma_{\Delta_1}^z + \mu^{-1}\gamma_{\Delta_2}^z\right)\|P_{\eta n+1}\|,$$

$$\rho_\eta^\eta = \lambda_m(Q_\eta),$$

$$\gamma_\eta = 2\left(\gamma_{\Delta_1}^\eta(\varepsilon) + \mu^{-1}\gamma_{\Delta_2}^\eta(\varepsilon)\right)\|P_{\eta n+1}\|,$$

$$\Lambda = \begin{bmatrix} (1-d)\rho_z^z & -(1-d)\rho_z^\eta - d\rho_\eta^z \\ -(1-d)\rho_\eta^\eta - d\rho_z^z & d\left(\frac{1}{\varepsilon}\rho_\eta^\eta - \gamma_\eta\right) \end{bmatrix}.$$

The right-hand side of the inequality (27) is a quadratic form, which is negative define when,

$$(1-d)d\rho_z^z\left(\varepsilon^{-1}\rho_\eta^\eta - \gamma_\eta\right) > \left((1-d)\rho_z^\eta + d\rho_\eta^z\right)^2 \tag{28}$$

This is equivalent to,

$$\varepsilon < \varepsilon_d = \frac{(1-d)d\rho_z^z\rho_\eta^\eta}{(1-d)d\rho_z^z\gamma_\eta + \left((1-d)\rho_z^\eta + d\rho_\eta^z\right)^2} \tag{29}$$

By the dependence of ε_d on d, it is obvious that the maximum of ε_d occurs at $d^* = \rho_z^\eta / (\rho_z^\eta + \rho_\eta^z)$ [1] and is given by,

$$\varepsilon^* < \varepsilon_d = \frac{\rho_z^z\rho_\eta^\eta}{\rho_z^z\gamma_\eta + 4\rho_z^\eta\rho_\eta^z} \tag{30}$$

Although $\|P_{zn}^{\mu}\|$ and $\|P_{zn+1}^{\mu}\|$ are dependent on $\hat{x}$, they are fixed for any given moment t and all tend to the constants as $\mu \to 0$, and then there exists $\mu^{**}(t)$ such that $\rho_z^z > 0$ holds for all $0 < \mu(t) < \mu^{**}(t)$. Thus, by choosing a moderate $\mu(t)$ and solving the Equation (30), $\varepsilon^*(\mu(t))$ can be obtained, and then $\Lambda > 0$ holds for all $0 < \mu(t) < \mu^{**}(t)$ and $0 < \varepsilon(t) < \varepsilon^*(\mu(t))$. Consequently, if $\Lambda > 0$ holds for all

$t \in [0, \infty)$, then we conclude that $\dot{V}(z, \eta) \leq 0$ holds uniformly in t.

Using the fact that Lyapunov function $V(z, \eta)$ is a positive define function and its time derivative is a negative define function if $\Lambda > 0$ holds for all $t \in [0, \infty)$, we conclude that the closed-loop system (16) is stable. In fact, $\dot{V}(z, \eta) = 0$ means $x = 0$, $e = 0$, $\sigma = \sigma_0$ and $\hat{\sigma} = \hat{\sigma}_0$. By invoking LaSalle's invariance principle, it is easy to know that the closed-loop system (16) is uniformly exponentially stable. As a result, we have the following theorem.

Theorem 2: Under **Assumptions 1**, **2** and **3**, if the matrix A_η is Hurwitz and the interval system matrix A_z is Hurwitz for all $0 < \mu < \mu^*$, $0 < \alpha_i^m \leq \alpha_i \leq \alpha_i^M$, $0 < \beta_j^m \leq \beta_j \leq \beta_j^M$ and α_σ, and then the equilibrium point $x = 0$, $e = 0$, $\sigma = \sigma_0$ and $\hat{\sigma} = \hat{\sigma}_0$ of the closed-loop system (16) is uniformly exponentially stable for all $0 < \mu(t) < \mu^{**}(t)$ and $0 < \varepsilon(t) < \varepsilon^*(\mu(t))$. Moreover, if all assumptions hold globally, and then it is globally uniformly exponentially stable.

By the demonstration above, there exist $\mu^{**}(t)$ and $\varepsilon^*(\mu(t))$ such that $\rho_z^z > 0$ and $\Lambda > 0$ hold for all $t \in [0, \infty)$. So, it is practical and feasible to find a real method to evaluate the instantaneous values $\mu^{**}(t)$ and $\varepsilon^*(\mu(t))$, that is, as follows:

Step 1: by the inequality $\lambda_m(Q_z) > 2\mu\gamma_{\delta_1}^z \|P_{zn}^\mu(t)\|$, the impermissible minimum of $\|P_{zn}(t)\|_m$ is,

$$\|P_{zn}(t)\|_m = 0.5\lambda_m(Q_z)/\gamma_{\delta_1}^z$$

Step 2: by the definitions of $\alpha_i(\hat{x}_i)$ and $\beta_i(\hat{x}_i)$, the instantaneous values $\alpha_i(t)$ and $\beta_i(t)$ can be given as,

$$\begin{cases} \alpha_i(t) = \dfrac{u_i(\hat{x}_i(t))}{\hat{x}_i(t)}, & \text{if } \hat{x}_i(t) \neq 0; \\[2mm] \alpha_i(t) = \dfrac{du_i(\hat{x}_i(t))}{d\hat{x}_i(t)}\bigg|_{\hat{x}_i(t)=0} & \text{if } \hat{x}_i(t) = 0. \end{cases}$$

$$\begin{cases} \beta_i(t) = \dfrac{v_i(\hat{x}_i(t))}{\hat{x}_i(t)}, & \text{if } \hat{x}_i(t) \neq 0; \\[2mm] \beta_i(t) = \dfrac{dv_i(\hat{x}_i(t))}{d\hat{x}_i(t)}\bigg|_{\hat{x}_i(t)=0} & \text{if } \hat{x}_i(t) = 0. \end{cases}$$

Step 3: by the values $\|P_{zn}(t)\|_m$, $\alpha_i(t)$, $\beta_i(t)$ and the condition $0 < \mu < \mu^*$, and using the iterative method to solve Lyapunov equation,

$$P_z(t)A_z(t) + A_z^T(t)P_z(t) = -Q_z$$

$\mu^{**}(t)$ can be obtained. Thus, by choosing a moderate $\mu(t)$ and solving Lyapunov equation above again, $\|P_{zn}^\mu(t)\|$ and $\|P_{zn+1}^\mu(t)\|$ can be evaluated.

Step 4: by the values $\alpha_i(t)$, $\beta_i(t)$ and definitions of $\eta_i = \varepsilon^{-n+i}e_i$, δ_1 δ_2, δ_3, Δ_1 and Δ_2, $\gamma_{\delta_1}^z$, $\gamma_{\Delta_1}^z$, $\gamma_{\Delta_2}^z$, $\gamma_{\delta_1}^\eta(\varepsilon)$, $\gamma_{\delta_2}^\eta(\varepsilon)$, $\gamma_{\delta_3}^\eta(\varepsilon)$, $\gamma_{\Delta_1}^\eta(\varepsilon)$ and $\gamma_{\Delta_2}^\eta(\varepsilon)$ can be obtained for given ε. $\|P_{\eta n+1}\|$ can be evaluated by solving Lyapunov equation $P_\eta A_\eta + A_\eta^T P_\eta = -Q_\eta$.

Step 5: by the values $\|P_{zn}^\mu(t)\|$, $\|P_{zn+1}^\mu(t)\|$, $\|P_{\eta n+1}\|$, $\gamma_{\delta_1}^z$, $\gamma_{\Delta_1}^z$, $\gamma_{\Delta_2}^z$, $\gamma_{\delta_1}^\eta(\varepsilon)$, $\gamma_{\delta_2}^\eta(\varepsilon)$, $\gamma_{\delta_3}^\eta(\varepsilon)$, $\gamma_{\Delta_1}^\eta(\varepsilon)$ and $\gamma_{\Delta_2}^\eta(\varepsilon)$, and using the iterative method to solve the inequality (30), $\varepsilon^*(\mu(t))$ can be obtained.

Discussion 2: From the procedure of stability analysis above, it is obvious that: although $\varepsilon(t)$ is dependent on $\mu(t)$, $\varepsilon(t)$ can be chosen arbitrarily small. Thus, so long as the bounded conditions (17) - (21) are satisfied, the asymptotically stable control can be achieved. This shows that the striking feature of output feedback nonlinear general integral control, that is, its robustness with respect to the nonlinearities, uncertainties and disturbances from the real system, control input and estimated error dynamics, is clearly demonstrated by Equal ratio gain technique and Singular perturbation technique. This means that the organic combination of Equal ratio gain technique and Singular perturbation technique constitutes a powerful tool to solve the output feedback control design problem of dynamics with the nonlinear and uncertain actions.

5. Example and Simulation

Consider the pendulum system [1] described by,

$$\ddot{\theta} = -a\sin(\theta) - b\dot{\theta} + cT$$

where $a, b, c > 0$, θ is the angle subtended by the rod and the vertical axis, and T is the torque applied to the pendulum. View T as the control input and suppose we want to regulate θ to r. Now, taking $x_1 = \theta - r$, $\dot{x}_2 = \dot{\theta}$, the pendulum system can be written as,

$$\begin{cases} \dot{x}_1 = x_2 \\ \dot{x}_2 = -a\sin(x_1 + r) - bx_2 + cu \end{cases}$$

and then it can be verified that $u_0 = a\sin(r)/c$ is the steady-state control that is needed to maintain equilibrium at the origin.

The nonlinear general integral controller and the integral observer can be given as,

$$\begin{cases} u = -\mu^{-1}\left(3\hat{x}_1 + 3\sinh(\hat{x}_1) + 3\hat{x}_2 + \tanh(\hat{x}_2) + 4\sigma\right) - 0.3\tanh(\sigma) + 4\sin(\hat{x}_1)/3 \\ \dot{\sigma} = \mu^{-1}\left(3\hat{x}_1 + \sinh(\hat{x}_1) + \hat{x}_2 + 2\tanh(\hat{x}_2)\right) \end{cases}$$

$$\begin{cases} \dot{\hat{\sigma}} = \cosh^{-1}(\hat{\sigma})(x_1 - \hat{x}_1) \\ \dot{\hat{x}}_1 = \hat{x}_2 + \varepsilon^{-1}5(x_1 - \hat{x}_1) \\ \dot{\hat{x}}_2 = -10\sin(\hat{x}_1 + r) - 7.5u + \varepsilon^{-2}20(x_1 - \hat{x}_1) + \varepsilon^{-3}5\sinh(\hat{\sigma}) \end{cases}$$

Thus, it is easy to obtain $6 \le \alpha_1 < 14.1$, $3 \le \alpha_2 \le 4$, $\alpha_\sigma = 4$, $4 \le \beta_1 < 6.68$ and $1 < \beta_2 \le 3$, and then the closed-loop system can be written as,

$$\begin{cases} \dot{z} = A_z z + F_z(z, e) \\ \varepsilon\dot{\eta} = A_\eta \eta + \varepsilon F_\eta(z, e) \end{cases}$$

where

$$z = \begin{bmatrix} x_1 & x_2 & \sigma - \sigma_0 \end{bmatrix}^{\mathrm{T}},$$

$$e_0 = \sinh(\hat{\sigma}) - \sinh(\hat{\sigma}_0),$$

$$e_i = x_i - \hat{x}_i \quad (i = 1, 2),$$

$$\eta_j = \varepsilon^{-2+j} e_j \quad (j = 0, 1, 2),$$

$$A_z = \begin{bmatrix} 0 & 1 & 0 \\ -\mu^{-1}c\alpha_1 & -\mu^{-1}c\left(\alpha_2 + \mu c^{-1}b\right) & -\mu^{-1}c\alpha_\sigma \\ \mu^{-1}\beta_1 & \mu^{-1}\beta_2 & 0 \end{bmatrix},$$

$$A_\eta = \begin{bmatrix} 0 & 1 & 0 \\ 0 & -5 & 1 \\ -5 & -20 & 0 \end{bmatrix},$$

$$F_z(z, e) = \begin{bmatrix} 0 & \delta_1 + \mu^{-1}\delta_2 & -\mu^{-1}\delta_3 \end{bmatrix}^{\mathrm{T}},$$

$$F_\eta(z, e) = \begin{bmatrix} 0 & 0 & \Delta_1 + \mu^{-1}\Delta_2 \end{bmatrix}^{\mathrm{T}},$$

$$\delta_1 = -a\sin(x_1 + r) + a\sin(r) + 4c\sin(\hat{x}_1)/3 - 0.3c(\tanh(\sigma) - \tanh(\sigma_0)),$$

$$\delta_2 = c(\alpha_1 e_1 + \alpha_2 e_2),$$

$$\delta_3 = \beta_1 e_1 + \beta_2 e_2,$$

$$\Delta_1 = -a(\sin(x_1 + r) - \sin(r)) + \hat{a}(\sin(\hat{x}_1 + r) - \sin(r)) - bx_2 + (c - \hat{c})(4\sin(\hat{x}_1)/3 - 0.3\tanh(\sigma) + 0.3\tanh(\sigma_0)),$$

$$\Delta_2 = (c - \hat{c})(\alpha_1 e_1 + \alpha_2 e_2) - (c - \hat{c})(\alpha_1 x_1 + \alpha_2 x_2 + \alpha_\sigma(\sigma - \sigma_0)).$$

The normal parameters are $a = c = 10$ and $b = 2$, and in the perturbed case, b and c are reduced to 1 and 5, respectively, corresponding to double the mass. Thus, with $\alpha_1^m = 6$, $\alpha_2^m = 3$, $\alpha_\sigma = 4$, $\beta_1^M = 6.68$, $\beta_2^m = 1$, $c = 5$ and $b = 1$, the following inequality,

$$c\alpha_2^m \alpha_\sigma \beta_2^m + \mu^2 b\alpha_1^m + \mu(c\alpha_2^m \alpha_1^m + b\alpha_\sigma \beta_2^m - \alpha_\sigma \beta_1^M) > 0$$

holds for all $0 < \mu < \infty$, and then the matrix A_z is Hurwitz for all $6 \leq \alpha_1 < 14.1$, $3 \leq \alpha_2 \leq 4$, $\alpha_\sigma = 4$, $4 \leq \beta_1 < 6.68$, $1 < \beta_2 \leq 3$ and $0 < \mu < \infty$, and A_η is Hurwitz, too.

Now, solving Lyapunov equation, $P_\eta A_\eta + A_\eta^T P_\eta = -I$, obtain $\|P_{\eta n+1}\| \leq 0.57$, and using $\hat{a} = 10$, $\hat{c} = 7.5$, $c = 10$, $b = 2$, obtain,

$$\|\delta_1\| \leq 4.5\|z\| + 13.4\varepsilon\|\eta\|,$$

$$\|\delta_2\| \leq 10\sqrt{\varepsilon^2 \alpha_1^2(t) + \alpha_2^2(t)}\|\eta\|,$$

$$\|\delta_3\| \leq \sqrt{\varepsilon^2 \beta_1^2(t) + \beta_2^2(t)}\|\eta\|,$$

$$\|\Delta_1\| \leq 4.9\|z\| + 13.4\varepsilon\|\eta\|,$$

$$\Delta_2 \leq 2.5\sqrt{\varepsilon^2 \alpha_1^2(t) + \alpha_2^2(t)}\|\eta\| + 2.5\sqrt{\alpha_1^2(t) + \alpha_2^2(t) + \alpha_\sigma^2}\|z\|,$$

and then, we have,

$$\gamma_{\delta_1}^z = 4.5, \quad \gamma_{\delta_2}^\eta(\varepsilon) = 10\sqrt{\varepsilon^2 \alpha_1^2(t) + \alpha_2^2(t)},$$

$$\gamma_{\delta_1}^\eta(\varepsilon) = 13.4\varepsilon, \quad \gamma_{\delta_3}^\eta(\varepsilon) = \sqrt{\varepsilon^2 \beta_1^2(t) + \beta_2^2(t)},$$

$$\gamma_{\Delta_1}^\eta(\varepsilon) = 13.4\varepsilon, \quad \gamma_{\Delta_2}^\eta(\varepsilon) = 2.5\sqrt{\varepsilon^2 \alpha_1^2(t) + \alpha_2^2(t)},$$

$$\gamma_{\Delta_1}^z = 4.9, \quad \gamma_{\Delta_2}^z = 2.5\sqrt{\alpha_1^2(t) + \alpha_2^2(t) + \alpha_\sigma^2}.$$

Thus, using $\alpha_1(t)$, $\alpha_2(t)$, $\beta_1(t)$, $\beta_2(t)$, $\alpha_\sigma = 4$, $c = 5$, $b = 1$ and $\mu = 1$ to solve the equations, $P_z A_z + A_z^T P_z = -I$ and $\varepsilon = \rho_z^z \rho_\eta^\eta / (\rho_z^z \gamma_\eta + 4\rho_\eta^\eta \rho_z^z)$, $\varepsilon^*(t)$ can be obtained.

Now, taking $\mu = 1$ and $\varepsilon(t) = \varepsilon^*(t)$, the simulation is implemented under the normal and perturbed cases, respectively.

Normal case: the initial states are $x_1 = \hat{x}_1 = -3.0$ and $x_2 = \hat{x}_2 = 0$; the system parameters are $a = c = 10$ and $b = 2$.

Perturbed case: the initial states are $x_1 = \hat{x}_1 = -3.0$, $x_2 = -1.5$ and $\hat{x}_2 = 0$; the system parameters are $a = 10$, $b = 1$ and $c = 5$, corresponding to doubling of the mass. Moreover, we consider an additive impulse-like disturbance $d(t)$ of magnitude 60 acting on the system input between 3 s and 3.5 s.

Figure 2 and **Figure 3** showed the simulation results under the normal (solid line) and perturbed (dashed line) cases. The following observations can be made: 1) as $\mu = 1$, there exists $\varepsilon^*(t)$ such that $\rho_z^z > 0$ and $\Lambda > 0$
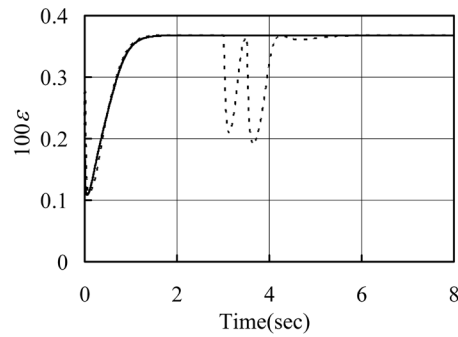
Figure 2. The values of 100ε under normal (solid line) and perturbed case (dashed line).
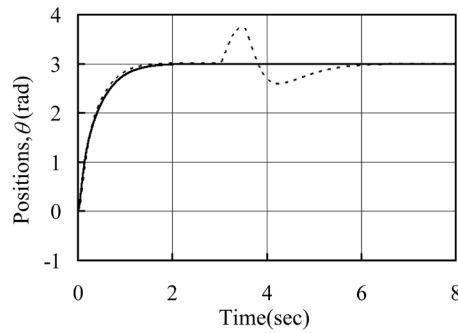
Figure 3. System output under normal (solid line) and perturbed case (dashed line).

hold for all $\alpha_1(t)$, $\alpha_2(t)$, $\beta_1(t)$ and $\beta_2(t)$. This shows that the closed-loop system is uniformly asymptotic stable. 2) the optimum responses are almost identical before the additive impulse-like disturbance appears. This means that by Equal ratio gain technique and Singular perturbation technique, we can tune an output feedback nonlinear general integral controller with good robustness and high control performance. All these demonstrate that output feedback nonlinear general integral control has the striking robustness, that is, so long as the bounded conditions are satisfied, the asymptotically stable control can be achieved, but also the organic combination of Equal ratio gain technique and Singular perturbation technique constitutes a powerful and practical tool to solve the output feedback control design problem of dynamics with the nonlinear and uncertain actions.

6. Conclusions

This paper proposes an output feedback nonlinear general integral controller for a class of uncertain nonlinear system. The main contributions are that: 1) as any row integrator and its controller gains of a canonical interval system matrix tend to infinity with the same ratio, if it is always Hurwitz, and then the same row solutions of Lyapunov equation all tend to zero; 2) theorem to ensure regionally as well as semi-globally exponential stability is established in terms of some bounded information; 3) a real time method to evaluate the ratio coefficients of controller and observer are proposed such that their values can be chosen moderately.

Theoretical analysis and simulation results show that not only output feedback nonlinear general integral control has the striking robustness but also the organic combination of Equal ratio gain technique and Singular perturbation technique constitutes a powerful tool to solve the output feedback control design problem of dynamics with the nonlinear and uncertain actions.

References

[1]   Khalil, H.K. (2007) Nonlinear Systems. 3rd Edition, Electronics Industry Publishing, Beijing, pp. 551, 449-453.

[2]   Liu, B.S. and Tian, B.L. (2012) General Integral Control Design Based on Linear System Theory. *Proceedings of the 3rd International Conference on Mechanic Automation and Control Engineering*, Vol. 5, 3174-3177.

[3]   Liu, B.S. and Tian, B.L. (2012) General Integral Control Design Based on Sliding Mode Technique. *Proceedings of the 3rd International Conference on Mechanic Automation and Control Engineering*, Vol.5, 3178-3181.

[4]   Liu, B.S., Li, J.H. and Luo, X.Q. (2014) General Integral Control Design via Feedback Linearization. *Intelligent Control and Automation*, **5**, 19-23. http://dx.doi.org/10.4236/ica.2014.51003

[5]   Liu, B.S., Luo, X.Q. and Li, J.H. (2014) General Integral Control Design via Singular Perturbation Technique. *International Journal of Modern Nonlinear Theory and Application*, **3**, 173-181. http://dx.doi.org/10.4236/ijmnta.2014.34019

[6]   Liu, B.S., Luo, X.Q. and Li, J.H. (2013) General Concave Integral Control. *Intelligent Control and Automation*, **4**, 356-361. http://dx.doi.org/10.4236/ica.2013.44042

[7]   Liu, B.S., Luo, X.Q. and Li, J.H. (2014) General Convex Integral Control. *International Journal of Automation and Computing*, **11**, 565-570. http://dx.doi.org/10.1007/s11633-014-0813-6

[8]   Liu, B.S. (2014) Constructive General Bounded Integral Control. *Intelligent Control and Automation*, **5**, 146-155. http://dx.doi.org/10.4236/ica.2014.53017

[9]   Liu, B.S. (2014) On the Generalization of Integrator and Integral Control Action. *International Journal of Modern Nonlinear Theory and Application*, **3**, 44-52. http://dx.doi.org/10.4236/ijmnta.2014.32007

[10]   Liu, B.S. (2015) Equal Ratio Gain Technique and Its Application in Linear General Integral Control. *International Journal of Modern Nonlinear Theory and Application*, **4**, 21-36. http://dx.doi.org/10.4236/ijmnta.2015.41003

[11]   Liu, B.S. (2014) Nonlinear General Integral Control Design via Equal Ratio Gain Technique. *International Journal of Modern Nonlinear Theory and Application*, **3**, 256-266. http://dx.doi.org/10.4236/ijmnta.2014.35028

[12]   Liu, B.S., Luo, X.Q. and Li, J.H. (2014) Conventional and Added-Order Proportional Nonlinear Integral Observers. *International Journal of Modern Nonlinear Theory and Application*, **3**, 210-220. http://dx.doi.org/10.4236/ijmnta.2014.35023

[13]   Gajic, Z. (1995) Lyapunov Matrix Equation in System Stability and Control. *Mathematics in Science and Engineering*, **195**, 30-31.

Existence and Smoothness of Solution of Navier-Stokes Equation on R^3

Ognjen Vukovic

Department for Finance, University of Liechtenstein, Vaduz, Liechtenstein
Email: ognjen.vukovic@uni.li, oggyvukovich@gmail.com

Abstract

Navier-Stokes equation has for a long time been considered as one of the greatest unsolved problems in three and more dimensions. This paper proposes a solution to the aforementioned equation on R^3. It introduces results from the previous literature and it proves the existence and uniqueness of smooth solution. Firstly, the concept of turbulent solution is defined. It is proved that turbulent solutions become strong solutions after some time in Navier-Stokes set of equations. However, in order to define the turbulent solution, the decay or blow-up time of solution must be examined. Differential inequality is defined and it is proved that solution of Navier-Stokes equation exists in a finite time although it exhibits blow-up solutions. The equation is introduced that establishes the distance between the strong solutions of Navier-Stokes equation and heat equation. As it is demonstrated, as the time goes to infinity, the distance decreases to zero and the solution of heat equation is identical to the solution of N-S equation. As the solution of heat equation is defined in the heat-sphere, after its analysis, it is proved that as the time goes to infinity, solution converges to the stationary state. The solution has a finite τ time and it exists when $\tau \to \infty$ that implies that it exists and it is periodic. The aforementioned statement proves the existence and smoothness of solution of Navier-Stokes equation on R^3 and represents a major breakthrough in fluid dynamics and turbulence analysis.

Keywords

Navier-Stokes Equation, Millennium Problem, Nonlinear Dynamics, Fluid, Physics

1. Introduction

In this paper, the following form of Navier-Stokes equations in R^3 is studied:

$$\frac{\partial}{\partial t}u_i + \sum_{j=1}^n u_j \cdot y \frac{\partial u_i}{\partial x_j} = \nu \Delta u_i - \frac{\partial p}{\partial x_i} + f_i(x,t) \quad (x \in R^n, t \geq 0) \tag{1}$$

$$div\, u = \sum_{i=1}^{n} \frac{\partial u_i}{\partial x_i} = 0 \ \left(x \in R^n, t \geq 0 \right) \tag{2}$$

With initial conditions

$$u(x,0) = u^0(x) \ \left(x \in R^n \right) \tag{3}$$

Here $u^0 = x$, C^∞ (divergence-free vector field on R^n), $f_i(x,t)$ are the components of a given, externally applied force, v is a positive coefficient (the viscosity) and $\Delta = \sum_{i=1}^{n} \frac{\partial^2}{\partial x_i^2}$ is the Laplacian in space variables. If Euler equations are considered, then the same set of equation must be applied with the condition that viscosity is equal to zero.

The following conditions must be satisfied as it is wanted to make sure that $u(x,t)$ does not grow large as $|x| \to \infty$:

$$\left| \partial_x^\alpha u^o(x) \right| \leq C_{\alpha K} \left(1 + |x| \right)^{-K} \text{ on } R^n \text{ for any } \alpha \text{ and } K \tag{4}$$

And

$$\left| \partial_x^\alpha \partial_t^m f(x,t) \right| \leq C_{\alpha m K} \left(1 + |x| + t \right)^{-K} \text{ on } R^n x[0,\infty[\text{ for any } \alpha, m, K \tag{5}$$

The accepted solution of N-S is physically reasonable if it only satisfies:

$$p, u \in C^\infty \left(R^n x[0,\infty[\right) \tag{6}$$

And

$$\int_{R^n} |u(x,t)| dx < C \text{ for all } t \geq 0 \left(\text{bounded energy} \right) \tag{7}$$

At the same time, it is possible to look at spatially periodic solutions. We can assume the following conditions:

$$u^o(x + e_j) = u^o(x), f(x + e_j, t) = f(x,t) \text{ for } 1 \leq j \leq n \tag{8}$$

Under the condition that $e_j = j^{th}$ is unit vector in R^n. It must be assumed that u^o is smooth and that

$$\left| \partial_x^\alpha \partial_t^m f(x,t) \right| \leq C_{\alpha m K} \left(1 + t \right)^{-K} \text{ on } R^3 x[0,\infty[\text{ for any } \alpha, m, K \tag{9}$$

The solution is then accepted if it satisfies:

$$u(x,t) = u(x + e_j, t) \text{ on } R^3 x[0,\infty[\text{ for } 1 \leq j \leq n \tag{10}$$

And

$$p, u \in C^\infty \left(R^n x[0,\infty[\right)$$

The problem is to find and analyze whether a strong, physically reasonable solution exists for the Navier-Stokes equation.

The statement that will be proved is existence and smoothness of Navier-Stokes solutions on R^3. Take $v > 0$ and $n = 3$. Let $u^o(x)$ be any smooth, divergence-free vector field satisfying (1.4). Take $f(x,t)$ to be identically zero. Then there exist smooth functions $p(x,t)$, $u_i(x,t)$ on $R^3 x[0, \infty]$ and the above conditions and equations are satisfied.

2. Results

Firstly, the definition of turbulent solutions (Oliver and Titti) [1] is provided. We must define the set of all C^∞ real vector functions φ with compact support in R^n such that $div\, \varphi = 0$. We define L_σ^r as the closure of

$C_{0,\sigma}^\infty$ with respect to L^r norm $\|.\|_r$; $(.,.)$ is the inner product in L^2. L^r stands for the usual L^r-space over R^n, $1 \le r \le \infty$. $H_{0,\sigma}^1$ is the closure of $C_{0,\sigma}^\infty$ with respect to the norm $\|\phi\|_{H^1} = \|\phi\|_2 + \|\nabla\phi\|_2$ where $\nabla\varphi = \left(\dfrac{\partial\varphi_i}{\partial x_j}\right)_{i,j=1,\cdots,n}$.

When X is a Banach space, $\|.\|_X$ denotes the norm on X. $C^m\left([t_1,t_2];X\right)$ and $L^r\left([t_1,t_2];X\right)$ are the Banach spaces, where $m = 0,1,\cdots$, and t_1 and t_2 are real numbers such that $t_1 < t_2$. C denotes various constants.

Def 1. (Oliver and Titti) [1] A turbulent solution of Navier-Stokes equation is defined as following:

$$1)\quad u \in L^\infty\left(0,\infty;L_\sigma^2\right)\cap L^2\left(0,T;H_{0,\sigma}^1\right) \text{ for all } 0 < T < \infty \tag{11}$$

The relation

$$2)\quad \int_0^T\left[-(u,\partial\varphi/\partial t)+(\nabla u,\nabla\varphi)+(u\cdot\nabla u,\varphi)\right]dt = \left(a,\varphi(0)\right) \tag{12}$$

Holds for almost all T and all $\varphi \in C^1\left([0,T[\,;H_{0,\sigma}^1 \cap L^n\right)$ such that $\varphi(\cdot,T)=0$

Strong energy inequality

$$3)\quad \|u(t)\|_2^2 + 2\int_s^t\|\nabla u(\tau)\|_2^2 d\tau \le \|u(s)\|_2^2 \tag{13}$$

Holds for almost all $s \ge 0$ including $s = 0$, and all $t > s$.

It is necessary to introduce the Stokes operator A_r in L_σ^r. The following Helmholtz decomposition is obtained:

$$L^r = L_\sigma^r \otimes G^r,\ 1 < r < \infty$$

where $G^r = \left\{\nabla p \in L^r; p \in L_{loc}^r\right\}$. P_σ denotes the projection from L^r onto L_σ^r. A_r defines the Stokes operator with domain $D(A_r) = H^{2,r} \cap L_\sigma^r$. A denotes the Stokes operator A_r. $\{E_\lambda\}_\lambda \ge 0$ denotes the spectral decomposition of self-adjoint operator A.

The existence of turbulent solutions for $n = 3$ and $n = 4$ is given by Leray and Kato. In order to derive the next results, theorem from Takahiro Okabe will be introduced.

Theorem 1. Let $2 \le n \le 4$ and let $r > 1$ and $m \ge 0$ be

For $n = 2$,

$$1 < r < 4/3,\, 0 \le m < 4/r - 3 \text{ and}$$

For $n = 3,4$

$$1 < r < \frac{n}{n-1},\, 0 \le m < \frac{n}{r} - (n-1)$$

Suppose that $K_{m,\alpha}^\delta$ for $K_{m,\alpha}^\delta = \left\{\varphi \in L^2; |\hat{\varphi}(\xi)| \ge \alpha|\xi|^m \text{ for } |\xi| \le \delta\right\}$ for $\alpha,\delta > 0$ and $m \ge 0$. If $a \in L_\sigma^r \cap L_\sigma^2 \cap K_{m,\alpha}^\delta$ for some $\alpha,\delta > 0$ then for every turbulent solution $u(t)$ there exist $T > 0$ and $C(n,r,m,\delta,\alpha,a) > 0$ such that:

$$\left|\frac{\|E_\lambda u(t)\|}{\|u(t)\|_2} - 1\right| \le \frac{C}{\lambda}t^{-(n/r-n+1-m)} \tag{14}$$

holds for all λ and for all $t > T$

Def 2. Let $n < r < \infty$, $a \in L_\sigma^n$. A measurable function u defined on $R^n \times (0,\infty)$ is called a global strong solution of Navier-Stokes equation if:

$$u \in C\left([0,\infty);L_\sigma^n\right)\cap C\left((0,\infty);L^r\right) \tag{15}$$

$\dfrac{\partial u}{\partial t}, Au \in C\left((0,\infty);L_\sigma^n\right)$ and u satisfies:

$$\frac{\partial u}{\partial t} + Au + P_\sigma (u \cdot \nabla u) = 0, \, t > 0 \tag{16}$$

where $P_\sigma (u \cdot \nabla u)$ denotes the projection from L^r onto L^r_σ of the product of the divergence of solution u and the solution itself.

Takahiro Okabe [2], in his paper named "Asymptotic energy concentration in the phase of the weak solutions to the Navier-Stokes equation", proves that turbulent solutions of Navier-Stokes equation become strong solutions after some definite time. So for the turbulent solution of $u(t)$ of Navier-Stokes equation there exists $T_* > 0$ such that $u(t)$ is a strong solution of Navier-Stokes equation on $[T_*, \infty)$, then the energy identity exists:

$$\frac{\mathrm{d}}{\mathrm{d}t} \|u(t)\|_2^2 + 2 \|A^{1/2} u(t)\|_2^2 = 0 \tag{17}$$

For $t \geq T_*$. For any fixed $\lambda > 0$, the second term in (16) is estimated from below as:

$$\|A^{1/2} u(t)\|_2^2 = \int_0^\infty \rho \mathrm{d}\left[E_p u\right]_2^2 \geq \int_\lambda^\infty \rho \mathrm{d}\left[E_p u\right]_2^2 \geq \lambda \int_\lambda^\infty \mathrm{d}\left[E_p u\right]_2^2 \geq \frac{\lambda}{2}\left(\|u(t)\|_2^2 - \|E_\lambda u(t)\|_2^2\right) \tag{18}$$

From (16) to (18), the following is obtained:

$$\frac{\mathrm{d}}{\mathrm{d}t} \|u(t)\|_2^2 + \lambda \|u(t)\|_2^2 \leq \lambda \|E_\chi u(t)\|_2^2 \tag{19}$$

Afted dividing the both sides of (19) by $\lambda \|u(t)\|_2^2$, the following is obtained:

$$\frac{\frac{\mathrm{d}}{\mathrm{d}t}\|u(t)\|_2^2}{\lambda \|u(t)\|_2^2} + 1 \leq \frac{\|E_\chi u(t)\|_2^2}{\|u(t)\|_2^2} \tag{20}$$

By (17), the following is obtained $(\mathrm{d}/\mathrm{d}t)\|u(t)\|_2^2 = -2\|A^{1/2} u(t)\|_2^2 = -2\|\nabla u(t)\|_2^2$ it follows from (17) to (20) that:

$$1 - \frac{\|E_\chi u(t)\|_2^2}{\|u(t)\|_2^2} \leq \frac{2}{\lambda} \frac{\|\nabla u(t)\|_2^2}{\|u(t)\|_2^2} \tag{21}$$

By introducing the new theorem that is proved in Takahiro Okabe's paper [2], the following is obtained.

Theorem 2. Let $2 \leq n \leq 4$. Let r and m be as

1) $n = 2$

$$1 < r < \frac{4}{3}, \, 0 \leq m < \frac{4}{r} - 3$$

2) $n \geq 3$

$$1 < r < \frac{n}{n-1}, \, 0 \leq m < \frac{n}{r} - (n-1)$$

If $a \in L^r_\sigma \cap L^2_\sigma \cap K^\delta_{0,\sigma}$, every turbulent solution of $u(t)$ of Navier-Stokes equation satisfies:

$$\frac{\|\nabla u(t)\|_2^2}{\|u(t)\|_2^2} \leq O\left(t^{-(n/r - n + 1 - m)}\right) \tag{22}$$

As $t \to \infty$.

The following theorem can be proved by using well-known Leray's structure theorem, every turbulent solution of N-S becomes the strong solution after some time. Although Kato proves that the strong solution decays in the same way as the Stokes flow e^{-tA}, we apply different approach by using Oliver and Titti's paper [1] named "Remark on the Rate of Decay of Higher Order Derivatives for solution to the Navier-Stokes equation".

By introducing the above mentioned theorem, the following result is obtained and it proves **Theorem 1**.

$$\left| \frac{\left\| E_\lambda u(t) \right\|_2^2}{\left\| u(t) \right\|_2^2} - 1 \right| \le \frac{C}{\lambda} t^{-(n/r-n+1-m)} \text{ for all } t \ge T$$

This result proves that energy of the molecules of fluid moving is smaller than some value determined by C, n, r, m and it proves asymptotic energy concentration. In order to prove that turbulent solutions are at the same time strong solutions, blow-up time of solutions must be analyzed.

It is demonstrated that Navier-Stokes equation enter some class as it was already proved $D(e^{\tau A}; H^r)$ in arbitrarily short time. Foias and Temam have proved the following solution in the case of periodic boundary condition and for the case of the Navier-Stokes equation on the two-dimensional. Kukavica and Grujic have obtained the given results in L^p spaces. The following lemma must be introduced and it is proved in Oliver and Titi's paper [1]:

Theorem 3. Let $\tau \ge 0$, $r > n/2$ and $s < n/2$. Then there exists a constant $C = C(n, r, s)$ such that any two functions v and w in $D(e^{\tau A}; H^r)$ satisfy the inequality:

$$\left\| A^r e^{\tau A} (vw) \right\|_{L^2} \le C(n, r, s) \left(\left\| A^r e^{\tau A} w \right\|_{H^{r-s}} + \left\| A^s e^{\tau A} v \right\|_{H^{r-s}} \left\| A^r e^{\tau A} w \right\|_{L^2} \right) \quad (23)$$

The theorem is proved by using Plancherel theorem, the triangle inequality, the inequality $(x + y)^r \le 2^{r-1} (x^r + y^r)$ and the convolution estimate $\left\| f * g \right\|_{L^2} \le \left\| f \right\|_{L^1} \left\| g \right\|_{L^2}$. These are the tools used to prove the aforementioned theorem. For further details, look at the aforementioned paper. This theorem demonstrates that the blow-up time is infinite so that the solution is existent. In order to find a solution, it must be captured in some sort of space where the function oscillates. In order to introduce the following solution, a few more results will be introduced.

Firstly, we assume the existence of solutions $u \in L^\infty \left([0, T]; H^r (R^n) \right), r > n/2$ is known for some $T > 0$. In order to simplify the notation, the following is set:

$$J_r = \left\| A^r u \right\|_{L^2}^2 \quad (24)$$

$$G_r = \left\| A^r e^{\tau A} u \right\|_{L^2}^2 \quad (25)$$

where $\tau = \tau(t)$ is to be specified later.

Then the Gevrey norm is used to find the following result:

$$\frac{1}{2} \dot{G}_r = \dot{\tau} G_{r+1/2} - \nu G_{r+1} - \int_{R^n} A^r e^{\tau A} (u \cdot \nabla u) A^r e^{\tau A} u \, dx \quad (26)$$

The contribution of pressure term is zero because A commutes with the Leray projection onto divergence free vector fields. Note that:

$$\left\| A^s e^{\tau A} u \right\|_{H^{r-s}} \le c \left(G_r^{1/2} + G_s^{1/2} \right) \quad (27)$$

By using **Theorem 3** and Cauchy-Schwarz inequality, the following result is obtained.

$$\left| \int_{R^n} A^r e^{\tau A} (u \cdot \nabla u) A^r e^{\tau A} u \, dx \right| \le \left\| A^r e^{\tau A} (u \cdot \nabla u) \right\| \left\| A^r e^{\tau A} u \right\| \le c_1 \left(G_s^{1/2} + G_r^{1/2} \right) G_{r+1}^{1/2} G_r^{1/2} + c_1 \left(G_{s+1}^{1/2} + G_{r+!}^{1/2} \right) G_r \quad (28)$$

In order to proceed, we introduce the **Theorem 4**.

Theorem 4. For all nonnegative p, q and τ we have the following:

$$\left\| A^p e^{\tau A} u \right\|^2 \le e \left\| A^p u \right\|^2 + (2\tau)^{2q} \left\| A^{p+q} e^{\tau A} u \right\|^2 \quad (29)$$

The proof is similar to that in **Theorem 3**, just it should be noted that for every $x \ge 0$, $m > 0$ one has $e^x < e + x^m e^x$ since $e^x < e$ on $[0, 1]$ and $e^x \le x^m e^x$ for $x \ge 1$.

After introducing the theorem and interpolating G_s by using **Theorem 3** and **Theorem 4** with $p = s$, $q = r - s$, the similar thing is done with G_{s-1}. If we apply the Young inequality, the following result is obtained.

$$\left| \int_{R^n} A^r \mathrm{e}^{\tau A} (u \cdot \nabla u) A^r \mathrm{e}^{\tau A} u \mathrm{d}x \right| \leq \left\| A^r \mathrm{e}^{\tau A} (u \cdot \nabla u) \right\| \left\| A^r \mathrm{e}^{\tau A} \right\| \leq c_1 J_s^{1/2} G_r^{1/2} G_{r+1}^{1/2} + c_3 J_{s+1}^{1/2} G_r + c_4 \left(1 + \tau^{r-s}\right) G_r G_{r+1}^{1/2} \qquad (30)$$

where $n/4 < r/2 \leq s < n/2$. After setting $\tau = t$, after interpolating the first term on (26) then use the estimate on (30), the following equation is obtained:

$$\dot{G}_r \leq c\left(\|u\|_{H^1}\right) G_r + c(r,s,t) G_r^2 \qquad (31)$$

This proves that there exists a $\sigma \in (0,T]$ such that $G_r(0) = \|u_0\|_{H^r}^2$ is finite for $t \in [0,\sigma)$. This proves that if space is finite, then Garvey space is finite which demonstrates the existence of stationary solution.

Now the result of differential inequality for longer time will be derived. The radius of uniform analyticity $\rho = \tau/\sqrt{n}$ increases like $\sqrt{t}$ as $t \to \infty$ as the solutions for heat equation. First the optimal decay rate for Gevrey norm is established, the optimal decay rates for norms of finite order derivatives will be established and it will be extended to infinite order.

If first two terms of Equation (26) are considered and it is assumed that only contribution from linear terms is included, interpolation can be used as well as Young inequality while breaking the second term in several fractions. **Theorem 3** provides the following:

$$\frac{G_r - 2J_r}{2\tau^2} \leq G_{r+1} \qquad (32)$$

we all together obtain:

$$\dot{\tau} G_{r+1/2} - v G_{r+1} \leq \frac{1}{2}\frac{\dot{\tau}}{\tau} G_r + \frac{1}{2}\tau\dot{\tau} G_{r+1} - \frac{v}{2} G_{r+1} - \frac{v}{2}\frac{G_r - 2J_r}{2\tau^2}$$
$$= \left(\frac{1}{2}\frac{\dot{\tau}}{\tau} - \frac{v}{8}\frac{1}{\tau^2}\right) G_r + \left(\frac{1}{2}\tau\dot{\tau} - \frac{v}{8}\right) G_{r+1} - \frac{v}{8}\frac{1}{\tau^2} G_r + \frac{v}{2}\frac{1}{\tau^2} J_r - \frac{3v}{8} G_{r+1} \qquad (33)$$

New theorem is introduced, it is already proved by using Plancherel theorem:
Theorem 5. Provided that $2q \geq p \geq 0$ and $\tau > 0$, the following is obtained:

$$\left\| A^q u \right\|^2 \leq c(p,q) \tau^{p-2q} \|u\| \left\| A^p \mathrm{e}^{\tau A} u \right\| \qquad (34)$$

Combining **Theorem 5** with $q = r$ and the Young inequality, the following is obtained.

$$J_r \leq c_3 \frac{1}{\tau^{2r}} J_0 + \frac{1}{8} G_r \qquad (35)$$

If we set $\tau = \sqrt{\left(\tau_0^2 + \alpha t\right)}$ where $\tau_0 > 0$ and $0 < \alpha \leq v/2$. The following is immediately found.

$$\frac{1}{2}\tau\dot{\tau} = \frac{\alpha}{4} \leq \frac{v}{8} \qquad (36)$$

So that the first two terms on the right of equation (33) are nonpositive and can be neglected. The main task is now to analyze the nonlinear terms and if possible prove that these nonlinear solutions do not affect the decay properties of the solution to infinite order. Applying the estimate on nonlinear term and by interpolating J_s by using theorem $p = r$, $q = s$; J_s is interpolated in an analogous manner. By application of Young inequality, the following is found.

$$\left| \int_{R^n} A^r \mathrm{e}^{\tau A} (u \cdot \nabla u) A^r \mathrm{e}^{\tau A} u \mathrm{d}x \right|$$
$$\leq c_5 \tau^{(r/2)-s} J_0^{1/4} G_r^{3/4} G_{r+1}^{1/2} + c_6 \tau^{(r/2)-s-1} J_0^{1/4} G_r^{5/4} + c_4 \left(1 + \tau^{r-s}\right) G_r G_{r+1}^{1/2} \leq c_7 \tau^{r-2s} J_0^{1/2} G_r^{3/2} \qquad (37)$$
$$+ c_6 \tau^{(r/2)-s-1} J_0^{1/4} G_r^{5/4} + C_8 \left(1 + \tau^{2(r-s)}\right) G_r^2 + \frac{3v}{8} G_{r+1}$$

3. Theoretical Findings

The following differential inequality is obtained.

$$\dot{G}_r \le -\frac{v}{8}\frac{1}{\tau^2}G_r + c_3 \frac{v}{\tau^{2(r+1)}}J_0 + 2c_7\tau^{r-2s}J_0^{1/2}G_r^{3/2} + 2c_6\tau^{(r/2)-s-1}J_0^{1/4}G_r^{5/4} + 2c_8\left(1+\tau^{2(r-s)}\right)G_r^2 \tag{38}$$

As we are considering global asymptotics and blow-up profiles, they are only possible in the presence of a critical controlled quantity or the combination of a subcritical and a supercritical controlled quantity. It turns out that the Navier-Stokes equation according to differential inequality tends to contract these quantities, in that way leading to a useful way to force finite time blow-up. The idea of using minimal surface area as controlled quantities originates from Hamilton. In order to discuss the blow-up time, we introduce the following well known proposition:

Assume that $\pi_2(M_t)$ is non-trivial. Let $\beta: S^2 \to M_t$ be any immersed sphere not homotopic to a point. Each such sphere has an energy $E(\beta,t) := \frac{1}{2}\int_{S^2}|d\beta|^2_{g_t}$ using the metric g_t at time t. If we define $W_2(t)$ to be the infimum of $E(\beta,t)$ over all such β. It turns out from standard Sacks-Uhlenbeck minimal surface theory that this infimum is actually attained. The differential inequality is obtained using structure of minimal surfaces and the Gauss-Bonnet formula [3]:

$$\partial_t W_2(t) \le -4\pi - \frac{1}{2}R_{\min}(t)W_2(t) \tag{39}$$

where $R_{\min}$ is the Ricci scalar. It demonstrates that the change of infimum of energy becomes negative in finite which is absurd. Therefore this forces blow-up in finite time. This means that the solution blows up in a finite time, which is why the surgery approach will be used.

If the above mentioned state holds, then the differential inequality, in order to make nonlinear terms of lower order, has to satisfy the following form:

$$\frac{v}{32}\frac{1}{\tau^2} > c_7\tau^{r-2s}J_0^{1/2}G_r^{1/2} + c_6\tau^{(r/2)-s-1}J_0^{1/4}G_r^{1/4} + c_8\left(1+\tau^{2(r-s)}\right)G_r \tag{40}$$

where $s \in \left[(r/2),(r/2)+1\right]$ is fixed. First it must be noted that G_r is an increasing function of τ, so that at the beginning at the initial time $t=0$, G_r is bounded between $\left\|A^r u_0\right\|^2$ when $\tau = \tau_0 = 0$ and $\left\|A^r e^{\sigma A}u_0\right\|^2$ when $\tau = \tau_0 = \sigma$. Thus the left side of equation (39) diverges faster than the right side as $\tau \to 0$, so that we can satisfy condition at $t=0$ by choosing $\tau_0 \in (0,\sigma]$ small enough. However, what happens when τ doesn't converge to 0. Imagine $\tau \to \infty$, then the left part of equation is 0 and the right part is higher than zero, but that is not possible, because it is proved above that the infimum of energy becomes negative, that is absurd. So the solution must blow up in some definite and the equation must hold even for τ as a solution. This proves that the solution is existent and smooth. In order to proceed, we will analyze the nonlinear terms. After having proved that the above equation must hold even for some τ that does not converge to 0, the only equation that must be solved is the following:

$$\dot{G}_r \le -\frac{\delta}{\tau^2}G_r + \frac{c_4}{\tau^{2(r+1)}}J_0 \tag{41}$$

where $\delta = v/16$. According to assumption that there exist positive real numbers M_1 and γ which may depend on u_0 such that $\left\|u(t)\right\|^2 \le \frac{M_1}{(1+t)^\gamma}$ for all $t \ge 0$ where $u(t)$ is a solution to the Navier-Stokes equation $J_0 \le M_1\left(\tau_0/\tau\right)^{2\gamma}$ provided $\tau = \sqrt{\left(\tau_0^2 + \alpha t\right)}$ and $J_0 = \left\|u\right\|^2_{L^2}$, where $\tau_0 > 0$ and $0 < \alpha \le v/2$, a final form of differential inequality is obtained.

$$\dot{G}_r \le -\frac{\delta}{\tau^2}G_r + \frac{k}{\tau^{2(\gamma+r+1)}} \tag{42}$$

The integrating factor for linear differential inequality is:

$$\exp\left(\delta\int_0^t \frac{1}{\tau_0^2 + \alpha t'}dt'\right) = \left(\frac{\tau_0^2 + \alpha t}{\tau_0^2}\right)^{\delta/\alpha} \tag{43}$$

So the following is obtained.

$$\frac{\mathrm{d}}{\mathrm{d}t}\left(\tau^{2\delta/\alpha}G_r\right)\leq k\tau^{2(\delta/\alpha-\gamma-r-1)}$$ (44)

If we fix α small enough so that $\delta>\alpha(\gamma+r)$, the following is concluded:

$$G_r(t)\leq\left(G_r(0)-\frac{k}{\delta-\alpha(\gamma+r)}\frac{1}{\tau_0^{2(\gamma+r)}}\right)\left(\frac{\tau_0^2}{\tau^2}\right)^{\delta/\alpha}+\frac{k}{\delta-\alpha(\gamma+r)}\frac{1}{\tau^{2(\gamma+r)}}$$ (45)

If the condition (39) is satisfied for all t, estimate (44) will be global in time. It is sufficient to show the following:

$$\frac{32}{v}\tau^2\left(c_7\tau^{r-2s}J_0^{1/2}G_r^{1/2}+c_6\tau^{(1/2)-s-1}J_0^{1/4}G_r^{1/4}+c_8\left(1+\tau^{2(r-s)}\right)G_r\right)\leq g(t)$$ (46)

for some non-increasing function $g(t)$. Estimate (44) shows that this is the case whenever $\gamma>0$ and

$$G_r(0)>\frac{k}{\delta-\alpha(\gamma+r)}\frac{1}{\tau_0^{2(\gamma+r)}}$$ (47)

which satisfies the above mentioned conditions and it proves the existence of a solution. As $\tau\to\infty$, G_r converges to zero therefore the solution is existent at the beginning, and if the equations exist, then the solution exists in the time τ.

It is obtained that:

$$G_r(t)\leq\frac{c_6}{\tau^{2(\gamma+r)}}+O\left(\tau^{-2\delta/\alpha}\right)$$ (48)

The upper bound of decay is calculated and given below:

$$\left\|A^m u\right\|^2\leq c(m,r)\tau^{r-2m}J_0^{1/2}G_r^{1/2}\leq c(m,r)\tau^{r-2m}M^{1/2}\left(\frac{\tau_0}{\tau}\right)^\gamma\left(\frac{c_6}{\tau^{2(\gamma+r)}}+O\left(\tau^{-2\delta/\alpha}\right)\right)^{1/2}$$
$$\leq c_9 c(m,r)\frac{1}{\tau^{2(\gamma+m)}}\left(1+O\left(\tau^{\gamma+r-\delta/\alpha}\right)\right)$$ (49)

where $c(m,r)$ is given above according to the following definition and maximum is attained at $|\zeta|=(2q-p)/\tau$ so the following definition demonstrates:

$$c(q,p)=(2q-p)^{2q-p}\mathrm{e}^{-(2q-p)}\text{ for }2q>p$$ (50)

$$c(q,p)=1,\text{ for }2q=p$$ (51)

This proves that solution is existent even when τ does not converge to 0.

Now in order to proceed and analyze the blow-up time, v as the solution of the heat equation will be introduced. It should be proved that the solution $w=u-v$ between Navier-Stokes and heat solution in $\left\|A^m\cdot\right\|$ can be made sufficiently small so that u must decay at the same rate.

First an estimate on the difference w in $D\left(\mathrm{e}^{\tau A};H^r\right)$. Clearly, it satisfies the following equation:

$$\partial_t w=v\Delta w-u\nabla u-\nabla p$$ (52)

$$\nabla\cdot w=0$$ (53)

As the heat equation preserves the divergence condition, the following equation is obtained $\nabla\cdot w=0$ for all $t\geq0$. Setting:

$$\gamma_r=\left\|A^r w\right\|_{L^2}^2$$ (54)

$$\zeta_r=\left\|A^r\mathrm{e}^{\tau A}w\right\|_{L^2}^2$$ (55)

And repeating the steps, the following result is obtained:

$$\frac{1}{2}\dot{\zeta}_r \le \dot{\tau}\zeta_r^{1/2}\zeta_{r+1}^{1/2} - \nu\zeta_{r+1} + c_1\left(G_s^{1/2}+G_r^{1/2}\right)G_{r+1}^{1/2}G_r^{1/2} + c_1\left(G_{s+1}^{1/2}+G_{r+1}^{1/2}\right)G_r$$

$$=\left(\frac{1}{2}\frac{\dot{\tau}}{\tau}-\frac{\nu}{8}\frac{1}{\tau^2}\right)\zeta_r +\left(\frac{1}{2}\tau\dot{\tau}-\frac{\nu}{8}\right)\zeta_{r+1}-\frac{\nu}{16}\frac{1}{\tau^2}\zeta_r+\frac{c_3}{2}\frac{\nu}{\tau^{2(r+1)}}\zeta_0+O\left(\frac{1}{\tau^{3\gamma+5r/2+1}}\right) \tag{56}$$

The second of nonlinear terms arises from (47) by using and choosing the smallest possible $s = r/2$. For $r \le 2$, the following is obtained:

$$\left(G_{s+1}^{1/2}+G_{r+1}^{1/2}\right)G_r = \left(G_{r/2+1}^{1/2}+G_{r+1}^{1/2}\right)G_r = G_{r/2+1}^{1/2}G_r + \text{higher\_order\_terms}$$

$$= O\left(\frac{1}{\tau^{\gamma+r/2+1}}\right)O\left(\frac{1}{\tau^{2(\gamma+r)}}\right)+\text{higher\_order\_terms} \tag{57}$$

The following differential inequality is obtained:

$$\dot{\zeta}_r(t) \le -\frac{\delta}{\tau^2}\zeta_r + \frac{\varepsilon c_8}{\tau^{2(\gamma+r+1)}}+O\left(\frac{1}{\tau^{3\gamma+5r/2+1}}\right) \tag{58}$$

And the following is obtained:

$$\left\|A^m w\right\|^2 \le \frac{\varepsilon c_{11}(m,r)}{\tau^{2(\gamma+m)}}+\text{higher\_order\_terms} \tag{59}$$

After having proved that solution for τ exists and if we examine the equation, as $\tau \to \infty$ the distance between heat equation solution and Navier-Stokes equation demonstrates convergence and if the following heat equation solution is found then the solution for Navier-Stokes equations exist and is in the same range as heat equation solution.

Now the heat solution equation Cannon [4] is analyzed. The solution of heat equation:

$$\left(\partial_t - \Delta\right)u = 0 \tag{60}$$

Satisfies a mean-value property

$$\Delta u = 0, \tag{61}$$

Precisely if u solves

$$\left(\partial_t - \Delta\right)u = 0 \tag{62}$$

And

$$(x,t)+E_\lambda \subset \text{dom}(u) \tag{63}$$

Then

$$u(x,t)=\frac{\lambda}{4}\int_{E_\lambda} u(x-y,t-s)\frac{|y|^2}{s^2}ds dy, \tag{64}$$

where E_λ is a heat ball,

$$E_\lambda := \left\{(y,s):\Phi(y,s)>\lambda\right\}, \tag{65}$$

$$\Phi(x,t):=(4t\pi)^{-\frac{n}{2}}\exp\left(-\frac{|x|^2}{4t}\right). \tag{66}$$

Notice that

$$\text{diam}(E_\lambda)=o(1) \tag{67}$$

So that $\lambda \to \infty$ demonstrates that equation is existent and is captured in the ball if the λ is finite.

The previous assumptions and results prove the existence of smooth and strong Navier-Stokes solution of equation in R^3 and represent the solution of millennium problem in R^3.

4. Conclusion

It is proved that the strong solution of Navier-Stokes equation is smooth, existent and unique. Firstly, turbulent solutions are defined and it is proved that they are strong solution, but as the turbulent solutions are only possible for small time intervals, it is tried to extend the time interval by using the Equation (39) and it is proved that the differential inequality (40) holds at the same time for some τ that does not converge to 0. Then the result is established, it is demonstrated that solutions exhibit possible finite blow-up time, which means that they exist and persist in the system. In order to establish if the solution exists for the finite time, the heat equation solution and Navier-Stokes solution are compared. It is proved that two solutions converge as $\tau \to \infty$ which proves the existence of solution in infinite time. If a surgery procedure is applied, the solution exists for some time, then blows up, then arises again and that process repeats. This statement proves that the solution is either existent or periodic, but it exists all the time. It is possible to introduce a stochastic process in order to explain the existence of the dynamical periodic solution, but this is left for further research. This paper proves the existence of Navier-Stokes solution in R^3 and represents a breakthrough in fluid dynamics analysis.

Acknowledgements

References

[1] Oliver, M. and Titi, E.S. (2000) Remark on the Rate of Decay of Higher Order Derivatives for Solutions to the Navier-Stokes Equations in R^n. *Journal of Functional Analysis*, **172**, 1-18. http://dx.doi.org/10.1006/jfan.1999.3550

[2] Okabe, T. (2009) Asymptotic Energy Concentration in the Phase Space of the Weak Solutions to the Navier-Stokes Equations. *Journal of Differential Equations*, **246**, 895-908. http://dx.doi.org/10.1016/j.jde.2008.07.037

[3] Tao, T. (2006) Perelman's Proof of the Poincaré Conjecture: A Nonlinear PDE Perspective.
http://arxiv.org/abs/math/0610903

[4] Cannon, J.R. (1984) The One-Dimensional Heat Equation. Vol. 23. Cambridge University Press, Cambridge.
http://dx.doi.org/10.1017/CBO9781139086967

Velocity Projection with Upwind Scheme Based on the Discontinuous Galerkin Methods for the Two Phase Flow Problem

Jiangyong Hou[1,2], Wenjing Yan[1,2*], Jie Chen[1,2]

[1]School of Mathematics and Statistics, Xi'an Jiaotong University, Xi'an, China
[2]Center for Computational Geosciences, Xi'an Jiaotong University, Xi'an, China
Email: [*]wenjingyan@mail.xjtu.edu.cn

Abstract

The upwind scheme is very important in the numerical approximation of some problems such as the convection dominated problem, the two-phase flow problem, and so on. For the fractional flow formulation of the two-phase flow problem, the Penalty Discontinuous Galerkin (PDG) methods combined with the upwind scheme are usually used to solve the phase pressure equation. In this case, unless the upwind scheme is taken into consideration in the velocity reconstruction, the local mass balance cannot hold exactly. In this paper, we present a scheme of velocity reconstruction in some H(div) spaces with considering the upwind scheme totally. Furthermore, the different ways to calculate the nonlinear coefficients may have distinct and significant effects, which have been investigated by some authors. We propose a new algorithm to obtain a more effective and stable approximation of the coefficients under the consideration of the upwind scheme.

1. Introduction

In the context of some fields, such as modeling and simulation of fluid flows in petroleum or groundwater reservoirs, the studies of processes of the simultaneous flow of two or more fluid phases within a porous medium are of great significance. In this paper, we consider the cases of two-phase flow where the fluids are immiscible.

[*]Corresponding author.

A large number of methods, which are based on the finite difference (FD), the finite volume (FV) or the finite element (FE) methods, have been developed to deal with the two-phase flow problem. As is well known, no matter which kind of numerical methods is used, the upwind scheme is of great significance in the approximation of some problems such as the convection dominated problem, the two-phase flow problem, and so on.

To achieve stable numerical computations in the simulation of two-phase flow problem, an accurate approximation of the flux is one of the most important and desirable ingredients. If we use Penalty Discontinuous Galerkin (PDG) methods to discretize the pressure equation, like in [1]-[3], both the pressure and saturation equations will be discritized by the PDG methods, and a process of reconstruction of the velocity needs to be done after the pressure equation is solved. In [2], an average total velocity was post processed by substituting the piecewise constants of pressure gradient and saturation gradient into the velocity-pressure expression directly. Actually such reconstructed velocity, on some level, belongs to the lowest order Raviart-Thomas finite element space. In [4], a post-processed total velocity is reconstructed in the Brezzi-Douglas-Marini (BDM) finite element spaces. But it needs that the degree of the polynomial is more than one, that is, using the linear approximation in DG method is not enough to reconstruct a velocity in BDM_1 space. A more stable and accurate reconstruction was developed in [1], in which the velocity reconstructed from the piecewise linear pressures could even belong to the first-order Raviart-Thomas finite element space. However, all the reconstructions mentioned above didn't consider the upwind scheme, which was basically used in the discretization of the equations. The property of the local mass conservation is crucial in porous media flow and transport problems. The upwind scheme has direct effect on the local mass conservation of the reconstructed velocity. We found that unless the upwind scheme and penalty terms which are used in the discretization of the two-phase flow problem are considered together into the velocity reconstruction, the error of the local mass conservation cannot reach a satisfactory level. In this paper, we present a scheme of velocity reconstruction in some H(div) spaces [5] with considering the upwind scheme totally.

The different ways to calculate the nonlinear coefficients may have distinct and significant effects, which have been investigated by some authors. For the approximation of the coefficients, we extend the one used in [6] to that each coefficient in element K is evaluated as the average of the upwind value on ∂K. This improves the stability of the numerical scheme even when an explicit scheme is used. In contrast with the explicit scheme described in [2], our explicit PDG scheme with this special approximation of coefficients can not only get rid of the extra penalties from the pressure equation but also have a robust performance in the heterogeneous media.

The rest of the article is organized as follows: In addition to the introduction and conclusion, we divide the text of this document into four parts. Section 2 is the first part and consists of two subsections, in which we introduce governing equations of two-phase flow problem and the corresponding interface conditions in Subsections 2.1 and 2.2 respectively. The second part, Section 3, comes in four subsections. In Subsection 3.1, the upwind average approximations of coefficients are introduced. In Subsections 3.2 and 3.3, the PDG methods are used for the pressure equation and the velocity reconstruction is presented respectively. In Subsection 3.4, the PDG methods are used for the saturation equation. The third part, Section 4, consists of two subsections. In Subsections 4.1 and 4.2, we introduce all the possible projection schemes with respect to the velocity reconstruction and the scheme without any explicit projections. In the last part, Section 5, several numerical examples in two dimensions are provided.

2. Problem Model

2.1. Mathematical Formulation

We consider two immiscible incompressible fluids in porous media and there is no mass transfer between the phases. Various and alternative model equations for two-phase flow problem can be found in reference [7]. Here we use the phase formulation for which the primary variables are wetting phase pressure and saturation (p_w and S_w), and in the absence of gravity and sink/source term we have:

$$-\nabla \cdot \left(\lambda_t D \nabla p_w + \lambda_n D \nabla p_c \right) = 0, \tag{1}$$

$$\phi \frac{\partial S_w}{\partial t} + \nabla \cdot \left(\lambda_n f_w D \frac{\mathrm{d} p_c}{\mathrm{d} S_w} \nabla S_w \right) + \nabla \cdot \left(f_w u_t \right) = 0, \tag{2}$$

where the denotations and meanings of each coefficient and their relationships are defined as follows: D is the

absolute permeability tensor and is discontinuous in heterogeneous media; ϕ denotes the porosity of the medium; p_c is the capillary pressure; λ_n, λ_w and λ_t are wetting, nonwetting and total mobility respectively; f_w is the fractional flow; ∇ and $\nabla\cdot$ are the gradient operator and divergence operator respectively. We will use the Brooks-Corey model [8] throughout this paper, in which some of these coefficients are non-linear functions defined below:

$$p_c\left(S_w\right)=p_d\overline{S}_w^{-\frac{1}{\theta}}, \tag{3}$$

$$\lambda_n\left(S_w\right)=\frac{\left(1-\overline{S}_w\right)^2\left(1-\overline{S}_w^{\frac{2+\theta}{\theta}}\right)}{\mu_n}, \tag{4}$$

$$\lambda_w\left(S_w\right)=\frac{\overline{S}_w^{\frac{2+3\theta}{\theta}}}{\mu_w}, \tag{5}$$

$$\lambda_t=\lambda_n+\lambda_w, f_w=\frac{\lambda_w}{\lambda_t}, f_n=\frac{\lambda_n}{\lambda_t}, \tag{6}$$

$$\overline{S}_w=\frac{S_w-S_{rw}}{1-S_{rn}-Srw}, \tag{7}$$

where p_d is the entry pressure needed for the wetting phase to enter large pores which are completely filled with the non-wetting phase; μ_n and μ_w are the non-wetting and wetting phase viscosity; θ is the parameter associated with pore size distribution; S_{rn} and S_{rw} are the residual saturation.

Some notations for the mesh are given below: Ω is the domain; $\partial\Omega$ is the boundary of the domain; $\mathcal{T}_h$ is the partition of Ω; K is the finite element in $\mathcal{T}_h$; ∂K is the edges of element K; $\mathcal{E}_h := \{e:$ all edges in $\mathcal{T}_h\}$, is the set of all edges contained in $\mathcal{T}_h$; $\mathcal{E}_h^i$ is the set of all interior edges contained in $\mathcal{T}_h$. The Equations (1) and (2) are subject to appropriate initial and boundary conditions to close the system. Here we give two feasible sets of boundary conditions: one is the Mixed-Neumann boundary condition as in [2],

$$\left(S_w u_t+\lambda_n f_w D\nabla p_c\right)\cdot n=S_{in}u_t\cdot n, \text{ on } \Gamma_{sM}, \tag{8}$$

$$\lambda_n f_w D\nabla p_c\cdot n=g_N, \text{ on } \Gamma_{sN}, \tag{9}$$

$$p_w=g_D, \text{ on } \Gamma_{pD}, \tag{10}$$

$$u_t\cdot n=0, \text{ on } \Gamma_{pN}, \tag{11}$$

and the other is Neumann-Drichlet boundary condition used in [9],

$$u_w\cdot n=\left(\lambda_n f_w D\nabla p_c+f_w u_t\right)\cdot n=g_N^w, \text{ on } \Gamma_{sN}, \tag{12}$$

$$S_n=S_{dir}, \text{ on } \Gamma_{sD}, \tag{13}$$

$$p_w=p_{dir}, \text{ on } \Gamma_{pD}, \tag{14}$$

$$u_t\cdot n=g_N^t\cdot n, \text{ on } \Gamma_{pN}. \tag{15}$$

The whole boundary of the porous medium domain $\partial\Omega$ is divided into three mutually disjoint parts: the inflow, noflow, and outflow boundaries (Γ_{in}, Γ_{no}, Γ_{out}), respectively. In the case of Neumann-Drichlet boundary condition, Γ_{pD} and Γ_{sD} occupy the outflow boundary, Γ_{pN} and Γ_{sN} occupy the inflow and no-flow boundaries such that $g_N<0$ on inflow boundary and $g_N=0$ on no-flow boundary. In the case of mixed-Neumann boundary condition, Γ_{pD} occupies the inflow and outflow boundaries, Γ_{pN} occupies the no-flow boundary, Γ_{sM} occupies the inflow boundary, and Γ_{sN} occupies the no-flow and outflow boundaries.

2.2. Interface Conditions

In order to test the barrier effect phenomenon of two phase flow, the nonlinear interface condition discussed in [1] [6] [10]-[13] will be introduced here. Following [9], we assume an initially fully water saturated domain $\left(\Omega = \Omega_I \bigcup \Omega_{II}\right)$ with an interface Γ_J between two different sands, and the oil is injected from the inflow part of boundary Γ_{in}, see **Figure 1**. In addition, we assume that Ω_I stands the coarse sand and Ω_{II} is the fine sand.

The process of the phenomenon is described briefly below. First, oil approaches the material interface but cannot penetrate it and begin to accumulate. In this case, only water pressure p_w is continuous on the interface, capillary pressure p_c and saturation S_w are discontinuous and satisfy:

$$
\begin{cases}
p_c\big|_{\Omega_I} = p_d^I \overline{S}_w^{-\frac{1}{\theta_I}}, \\
p_c\big|_{\Omega_{II}} = p_d^{II}, \\
S_w^I - S_w^{II} = S_w^I - \left(1 - S_{rn}^{II}\right).
\end{cases}
\tag{16}
$$

Then, when more and more oils accumulate at the interface and the capillary pressure on the coarse side exceeds the entry pressure of the other side $\left(p_c\big|_{\Omega_I} \geq p_d^{II}\right)$, the oils begin to penetrate and enter the fine sand. At this time, both p_w and p_c are continuous, but saturation S_w is still discontinuous and satisfies:

$$
S_w^I - S_w^{II} = S_w^I - \left(1 - S_{rw}^{II} - S_{rn}^{II}\right)\left(\frac{p_d^{II}}{p_d^I}\right)^{\theta_{II}}\left(\frac{S_w^I - S_{rw}^I}{1 - S_{rw}^I - S_{rn}^I}\right)^{\frac{\theta_{II}}{\theta_I}} - S_{rw}^{II}.
\tag{17}
$$

We note that a critical point of saturation can be found when the capillary pressure on coarse side increases to the value equivalent to the threshold pressure on fine side. That is, deducing from $p_c\big|_{\Omega_I} = p_d^{II}$ we have,

$$
S_w^* = \left(1 - S_{rw}^I - S_{rn}^I\right)\left(\frac{p_d^I}{p_d^{II}}\right)^{\theta_I} + S_{rw}^I.
\tag{18}
$$

This point will be used to judge whether the nonwetting phase can or cannot penetrate the material interface. So the interface conditions can be rewritten in the form below. For capillary pressure,

$$
p_c\big|_{\Omega_I} - p_c\big|_{\Omega_{II}} = \begin{cases}
p_d^I \overline{S}_w^{-\frac{1}{\theta_I}} - p_d^{II}, & S_w^I > S_w^*, \\
0, & S_w^I \leq S_w^*,
\end{cases}
\tag{19}
$$

and for wetting phase saturation,

$$
S_w^I - S_w^{II} = \begin{cases}
S_w^I - \left(1 - S_{rn}^{II}\right), & S_w^I > S_w^*, \\
S_w^I - \left(1 - S_{rw}^{II} - S_{rn}^{II}\right)\left(\frac{p_d^{II}}{p_d^I}\right)^{\theta_{II}}\left(\frac{S_w^I - S_{rw}^I}{1 - S_{rw}^I - S_{rn}^I}\right)^{\frac{\theta_{II}}{\theta_I}} - S_{rw}^{II}, & S_w^I \leq S_w^*.
\end{cases}
\tag{20}
$$
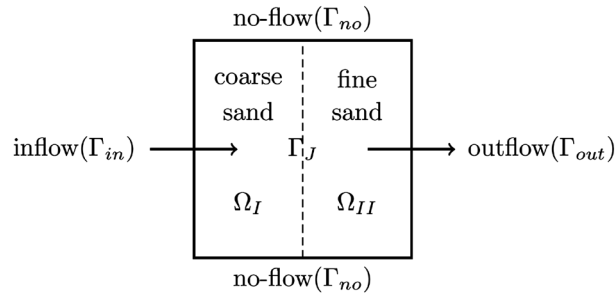
Figure 1. The interface (dashed line) between two subdomains with different rock properties.

Condition (20) is the same as that described in [1] except that the wetting phase (instead of the nonwetting phase) is used as the saturation variable. Moreover, (19) is only written for the capillary pressure and not for the wetting phase pressure, since the variable p_w is always continuous in the problem discussed. Noting that if the sub-domain Ω_I has a finer texture than Ω_{II}, all the relationship above can be treated in a similar manner with superscript I and II reversed.

3. Discrete Schemes

3.1. Approximation of Coefficients

For the approximation of coefficients, we extend the one used in [6]. Let σ denote any coefficients waiting for some proper approximations. Firstly we recall the original way to approximate the coefficients,

$$\begin{cases} \overline{\sigma_e} = \dfrac{1}{|e|}\int_e \sigma, \\ \overline{\sigma_K} = \dfrac{1}{|K|}\int_K \sigma. \end{cases} \tag{21}$$

The approach described in [6] is,

$$\begin{cases} \overline{\sigma_e} = \sigma\left(TS_{K,e}\right), \\ \overline{\sigma_K} = \dfrac{1}{3}\sum_{e \in \partial K}\overline{\sigma_e}\left(TS_{K,e}\right), \end{cases} \tag{22}$$

where $TS_{K,e}$ denotes the mean water saturation on the edge e of the element K, see [6] for more details. Now it is extended to the following one,

$$\begin{cases} \overline{\sigma_e} = \dfrac{1}{|e|}\int_e \sigma, \\ \overline{\sigma_K} = \dfrac{1}{3}\sum_{e \in \partial K}\overline{\sigma_e}^{\uparrow}. \end{cases} \tag{23}$$

where the upwind value of the side average on the interior edge is considered. The quantity $\sigma^{\uparrow}$ is called the upwind flux which is done with respect to the normal component of the total velocity u_t, such that for all

$$e \in \partial K^- \bigcap \partial K^+,$$

$$\sigma^{\uparrow} = \begin{cases} \sigma|_{K^-}, \ u_t \cdot n_e \le 0, \\ \sigma|_{K^+}, \ u_t \cdot n_e > 0. \end{cases} \tag{24}$$

where the normal vector n_e points from K^+ to K^-. Throughout this paper, all the coefficients on element K and edge e are calculated by the upwind averaged constant and the integral average constant which are described in (23).

3.2. Pressure Approximation with PDG

In this section we apply the Penalty Discontinuous Galerkin (PDG) methods [14] such as Nonsymmetric Interior Penalty Galerkin (NIPG) to the pressure Equation (1). Some notations for DG methods are defined:

$$\{v\} := \dfrac{1}{2}\left(v^- + v^+\right), \ [v] := v^- - v^+, \ \forall e \in \mathcal{E}_h, \tag{25}$$

$$\{v\} := v, \ [v] := v, \ \forall e \in \partial\Omega, \tag{26}$$

$$X_h := \left\{w \in L^2\left(\Omega\right)|\ w|_K \in P_1\left(K\right), \forall K \in \mathcal{T}_h\right\}, \tag{27}$$

where $v^{\pm}$ are the restrictions of v on two adjacent elements $K^{\pm}$ respectively.

The pressure Equation (1) discretized by PDG reads as follows.

$$
\text{find } p_w^{k+1} \in X_h, \text{for all } v \in X_h,
$$

$$
\sum_{K \in \mathcal{E}T_h} \int_K \lambda_t^k D_K \nabla p_w^{k+1} \cdot \nabla v_K - \sum_{e \in \mathcal{E}_h^i \cup \Gamma_D} \int_e \left\{ \lambda_t^k D \nabla p_w^{k+1} \cdot n_e \right\} [v]
$$

$$
+ \varepsilon \sum_{e \in \mathcal{E}_h^i \cup \Gamma_D} \int_e \left\{ \lambda_t^k D \nabla v \cdot n_e \right\} \left[p_w^{k+1} \right] + \sum_{e \in \mathcal{E}_h^i \cup \Gamma_D} \int_e \frac{\sigma_e}{|e|^\beta} \left[p_w^{k+1} \right] [v] \tag{28}
$$

$$
= -\sum_{K \in T_h} \int_K \left(\lambda_n \frac{\mathrm{d}p_c}{\mathrm{d}S_w} \right)^k D_K \nabla S_w^k \cdot \nabla v_K + \sum_{e \in \mathcal{E}_h^i \cup \Gamma_D} \int_e \left(\left(\lambda_n \frac{\mathrm{d}p_c}{\mathrm{d}S_w} \right)^k D \nabla S_w^k \cdot n_e \right)^{\uparrow} [v]
$$

$$
+ \varepsilon \sum_{e \in \Gamma_D} \int_e \lambda_t^k D \nabla v \cdot n_e p_{dir} + \sum_{e \in \Gamma_D} \int_e \frac{\sigma_e}{|e|^\beta} p_{dir} v - \sum_{e \in \Gamma_D} \int_e g_N v.
$$

Indeed, the PDG methods are only applied to the wetting-phase pressure term, for the capillary pressure term a traditional DG method with the upwind scheme is used.

3.3. Velocity Reconstruction

After solving the discrete pressure Equation (28), the total velocity will be reconstructed in the lowest-order Raviart-Thomas space (RT_0), the first-order Raviart-Thomas space (RT_1) and the first-order Brezzi-Douglas-Marini space (BDM_1) respectively, refer to [5] for more details about those spaces. The main idea of the reconstruction in the current section follows the one depicted in [1], and we will extend it to the situation that the discretization of the pressure equation contains an upwind scheme.

A proper reconstruction of velocity stems from the local mass conservation law as shown in the following description. Firstly, we recast the variational Equation (28) on element K into two parts as follows,

$$
-\int_K u_t^{k+1} \cdot \nabla v = \int_K \lambda_t^k D_K \nabla p_w^{k+1} \cdot \nabla v + \int_K \left(\lambda_n \frac{\mathrm{d}p_c}{\mathrm{d}S_w} \right)^k D_K \nabla S_w^k \cdot \nabla v + \varepsilon \sum_{e \in \partial K} \int_e \left\{ \lambda_t^k D \nabla v \cdot n_e \right\} \left[p_w^{k+1} \right], \tag{29}
$$

$$
\int_e u_t^{k+1} \cdot n_e v = -\int_e \left\{ \lambda_t^k D \nabla p_w^{k+1} \cdot n_e \right\} [v] - \int_e \left(\left(\lambda_n \frac{\mathrm{d}p_c}{\mathrm{d}S_w} \right)^k D \nabla S_w^k \cdot n_e \right)^{\uparrow} [v] + \int_e \frac{\sigma_e}{|e|^\beta} \left[p_w^{k+1} \right] [v]. \tag{30}
$$

Combing (29) and (30), it is easily seen that the local mass is conserved,

$$
\int_K \left(\nabla \cdot u_t^{k+1} \right) v = -\int_K u_t^{k+1} \cdot \nabla v + \sum_{e \in \partial K} \int_e u_t^{k+1} \cdot n_e v = \int_K \left(q_w^{k+1} + q_n^{k+1} \right) v, \tag{31}
$$

where q_w and q_n are the sink and source terms which are zeros here. Noting that if the edge e belongs to both ∂K and Γ_D on the right hand side of Equations (29) and (30), $\left[p_w^{k+1} \right]$ is equal to $\pm \left(p_w^{k+1} - p_{dir} \right)$ and the sign $\pm$ is determined by the direction of n_e, for example, the sign is positive when n_e is the outer normal vector with respect to ∂K.

Secondly, using (29) and (30) as the degree of freedom for some H(div) spaces, the total velocity will be obtained as some appropriate projections or interpolations in these spaces. In order to have a proper interpolation in RT_0, RT_1 and BDM_1 spaces, we should specify a set of degree of freedom (DOF) for these H(div) spaces and a corresponding set of basis functions. If let v be any constant in the polynomial space of degree zero P_0, (29) will vanish and (30) will become the RT_0 space's DOF which is the integral of the normal component of velocity on each edge. Correspondingly, the set of basis functions for RT_0 on the reference element is,

$$
\hat{\varphi}_i = \frac{1}{2|\hat{K}|} (x - a_i), \quad i = 1, 2, 3, \tag{32}
$$

where $|\hat{K}|$ is the area of the reference element $\hat{K}$ and a_i is one of its the vertices.

Let $v|K$ and $v|e$ be any functions in the space of polynomial of degree one P_1, then (29) and (30) become the DOFs for RT_1. The corresponding basis functions for RT_1 space on the reference elements are,

$$\hat{\varphi}_1 = \begin{pmatrix} 6x - 8xy - 8x^2 \\ 6x + 12y - 8xy - 8y^2 - 4 \end{pmatrix}, \quad \hat{\varphi}_2 = \begin{pmatrix} 8xy - 10x + 16x^2 \\ 16xy - 14y - 12x + 8y^2 + 6 \end{pmatrix},$$

$$\hat{\varphi}_3 = \begin{pmatrix} 8x^2 - 4x \\ 8xy - 2y \end{pmatrix}, \quad \hat{\varphi}_4 = \begin{pmatrix} 2x + 8xy - 8x^2 \\ 8y^2 - 8xy - 2y \end{pmatrix},$$

$$\hat{\varphi}_5 = \begin{pmatrix} 8xy - 6y - 2x + 2 \\ 8y^2 - 4y \end{pmatrix}, \quad \hat{\varphi}_6 = \begin{pmatrix} 14x + 12y - 16xy - 8x^2 - 6 \\ 10y - 8xy - 16y^2 \end{pmatrix},$$

$$\hat{\varphi}_7 = \begin{pmatrix} 16x - 8xy - 16x^2 \\ 8y - 16xy - 8y^2 \end{pmatrix}, \quad \hat{\varphi}_8 = \begin{pmatrix} 8x - 16xy - 8x^2 \\ 16y - 8xy - 16y^2 \end{pmatrix}.$$

Let $v|e$ be any functions in P_1 polynomial space, thus the basis functions of BDM_1 can be obtained in a similar manner except that (29) is not used. All the DOFs for BDM_1 are just defined on the edges of element, so only (30) is used to determine the basis functions. The corresponding basis functions for BDM_1 are,

$$\hat{\varphi}_1 = \begin{pmatrix} -2x \\ 6x + 4y - 4 \end{pmatrix}, \quad \hat{\varphi}_2 = \begin{pmatrix} 6x \\ 6 - 6y - 12x \end{pmatrix},$$

$$\hat{\varphi}_3 = \begin{pmatrix} 4x \\ -2y \end{pmatrix}, \quad \hat{\varphi}_4 = \begin{pmatrix} -6x \\ 6y \end{pmatrix},$$

$$\hat{\varphi}_5 = \begin{pmatrix} 2 - 6y - 2x \\ 4y \end{pmatrix}, \quad \hat{\varphi}_6 = \begin{pmatrix} 6x + 12y - 6 \\ -6y \end{pmatrix}.$$

It is noted that the choice of DOFs for the BDM_1 and RT_1 spaces is not unique, for example, the half-edge integral of the normal components of velocity is also available and applicable.

3.4. Saturation Approximation

The spatial discretization of the saturation equation is similar to that of the pressure equation given in (28). The diffusion term of the saturation equation is discretized by the PDG methods, and the advective term is discretized by a traditional DG method with using the upwind scheme. An Euler scheme in time is used. The saturation Equation (2) equipped with Mixed-Neumann boundary conditions (8)-(11) could be written as:

find $S_w^{k+1} \in X_h$, for all $v \in X_h$,

$$\sum_{K \in \mathcal{T}_h} \int_K \frac{\phi}{\Delta t} S_w^{k+1} v_K - \sum_{K \in \mathcal{T}_h} \int_K \left(\lambda_n f_w \frac{dp_c}{dS_w} \right)^k D_K \nabla S_w^{k+1} \cdot \nabla v_K$$

$$+ \sum_{e \in \mathcal{E}_h} \int_e \left\{ \left(\lambda_n f_w \frac{dp_c}{dS_w} \right)^k D\nabla S_w^{k+1} \cdot n_e \right\} [v] - \varepsilon \sum_{e \in \mathcal{E}_h} \int_e \left\{ \left(\lambda_n f_w \frac{dp_c}{dS_w} \right)^k D\nabla v \cdot n_e \right\} [S_w^{k+1}]$$

$$- \sum_{e \in \Gamma_{sM}} \int_e S_w^{k+1} u_t^k \cdot n_e v + \sum_{e \in \mathcal{E}_h^i} \int_e \frac{\sigma_e}{|e|^\beta} [S_w^{k+1}][v]$$

$$= \sum_{K \in \mathcal{T}_h} \int_K \frac{\phi}{\Delta t} S_w^k v_K + \sum_{K \in \mathcal{T}_h} \int_K (f_w u_t)^k \cdot \nabla v_K - \sum_{e \in \mathcal{E}_h} \int_e (f_w^{\uparrow} u_t \cdot n_e)^k [v]$$

$$- \sum_{e \in \Gamma_{sN}} \int_e g_N v - \sum_{e \in \Gamma_{sM}} \int_e S_{in} u_t^k \cdot n_e v.$$

$$(33)$$

The variational form in terms of Neumann-Dirichlet boundary conditions (12)-(15) reads:

find $S_w^{k+1} \in X_h$, for all $v \in X_h$,

$$\sum_{K \in \mathcal{T}_h} \int_K \frac{\phi}{\Delta t} S_w^{k+1} v_K - \sum_{K \in \mathcal{T}_h} \int_K \left(\lambda_n f_w \frac{\mathrm{d}p_c}{\mathrm{d}S_w} \right)^k D_K \nabla S_w^{k+1} \cdot \nabla v_K$$

$$+ \sum_{e \in \mathcal{E}_h^i \cup \Gamma_D} \int_e \left\{ \left(\lambda_n f_w \frac{\mathrm{d}p_c}{\mathrm{d}S_w} \right)^k D \nabla S_w^{k+1} \cdot n_e \right\} [v]$$

$$- \varepsilon \sum_{e \in \mathcal{E}_h^i \cup \Gamma_D} \int_e \left\{ \left(\lambda_n f_w \frac{\mathrm{d}p_c}{\mathrm{d}S_w} \right)^k D \nabla v \cdot n_e \right\} [S_w^{k+1}] + \sum_{e \in \mathcal{E}_h^i \cup \Gamma_D} \int_e \frac{\sigma_e}{|e|^\beta} [S_w^{k+1}][v] \qquad (34)$$

$$= \sum_{K \in \mathcal{T}_h} \int_K \frac{\phi}{\Delta t} S_w^k v_K + \sum_{K \in \mathcal{T}_h} \int_K (f_w U_t)^k \cdot \nabla v_K - \sum_{e \in \mathcal{E}_h^i \cup \Gamma_D} \int_e (f_w^\uparrow U_t \cdot n_e)^k [v]$$

$$- \sum_{e \in \Gamma_N} \int_e g_N v - \varepsilon \sum_{e \in \Gamma_D} \int_e \left(\lambda_n f_w \frac{\mathrm{d}p_c}{\mathrm{d}S_w} \right)^k D \nabla v \cdot n_e S_{dir} + \sum_{e \in \Gamma_D} \int_e \frac{\sigma_e}{|e|^\beta} S_{dir} v$$

$$- \varepsilon \sum_{e \in \Gamma_h} \int_e \left\{ \left(\lambda_n f_w \frac{\mathrm{d}p_c}{\mathrm{d}S_w} \right)^k D \nabla v \cdot n_e \right\} J(S_w^k) + \sum_{e \in \Gamma_h} \int_e \frac{\sigma_e}{|e|^\beta} [v] J(S_w^k),$$

where $J(S_w)$ is the interface condition of saturation described in (20).

4. Feasible Projections of the Discrete Strategies

4.1. DDG Methods with Some Other Projections

The abbreviation DDG means that DG methods are used for both pressure and saturation equations. For a clear comparison in the numerical experiments, we list all the possible and feasible projections below. Firstly, we denote $RT^{(1)}$ (or $BDM^{(1)}$) as the the velocity space projected into RT (or BDM) space by (29) and (30). Secondly, $RT^{(2)}$ (or $BDM^{(2)}$) means the projection into RT (or BDM) space with considering the upwind scheme but without the penalty term,

$$-\int_K u_t^{k+1} \cdot \nabla v = \int_K \lambda_t^k D_K \nabla p_w^{k+1} \cdot \nabla v + \int_K \left(\lambda_n \frac{\mathrm{d}p_c}{\mathrm{d}S_w} \right)^k D_K \nabla S_w^k \cdot \nabla v, \qquad (35)$$

$$\int_e u_t^{k+1} \cdot n_e v = -\int_e \{ \lambda_t^k D \nabla p_w^{k+1} \cdot n_e \} [v] - \int_e \left(\left(\lambda_n \frac{\mathrm{d}p_c}{\mathrm{d}S_w} \right)^k D \nabla S_w^k \cdot n_e \right)^\uparrow [v]. \qquad (36)$$

Thirdly, for $RT^{(3)}$ (or $BDM^{(3)}$), it means the projection with considering the penalty term but without the upwind scheme,

$$-\int_K u_t^{k+1} \cdot \nabla v = \int_K \lambda_t^k D_K \nabla p_w^{k+1} \cdot \nabla v + \int_K \left(\lambda_n \frac{\mathrm{d}p_c}{\mathrm{d}S_w} \right)^k D_K \nabla S_w^k \cdot \nabla v$$

$$+ \varepsilon \sum_{e \in \partial K} \int_e \{ \lambda_t^k D \nabla v \cdot n_e \} [p_w^{k+1}], \qquad (37)$$

$$\int_e u_t^{k+1} \cdot n_e v = -\int_e \{ \lambda_t^k D \nabla p_w^{k+1} \cdot n_e \} [v] - \int_e \left\{ \left(\lambda_n \frac{\mathrm{d}p_c}{\mathrm{d}S_w} \right)^k D \nabla S_w^k \cdot n_e \right\} [v]$$

$$+ \int_e \frac{\sigma_e}{|e|^\beta} [p_w^{k+1}][v]. \qquad (38)$$

At last, for $RT^{(4)}$ (or $BDM^{(4)}$), it means the projection without considering both the penalty term and the

upwind scheme,

$$-\int_K u_t^{k+1} \cdot \nabla v = \int_K \lambda_t^k D_K \nabla p_w^{k+1} \cdot \nabla v + \int_K \left(\lambda_n \frac{\mathrm{d}p_c}{\mathrm{d}S_w} \right)^k D_K \nabla S_w^k \cdot \nabla v, \tag{39}$$

$$\int_e u_t^{k+1} \cdot n_e v = -\int_e \left\{ \lambda_t^k D \nabla p_w^{k+1} \cdot n_e \right\} [v] - \int_e \left\{ \left(\lambda_n \frac{\mathrm{d}p_c}{\mathrm{d}S_w} \right)^k D \nabla S_w^k \cdot n_e \right\} [v]. \tag{40}$$

As indicated in introduction, for all DDG methods the velocity derived by the projection $RT^{(1)}$ (or $BDM_1^{(1)}$) preserves the local mass conservation property best, which will shown in the numerical examples.

4.2. DDG Method without Explicit Projections

In [2] the velocity is used directly as the combination of the gradient of the solutions and coefficients, as follows,

$$u_t^{k+1} \cdot n_e = -\left\{ \lambda_t^k D \nabla p_w^{k+1} \cdot n_e \right\} - \left\{ \left(\lambda_n \frac{\mathrm{d}p_c}{\mathrm{d}S_w} \right)^k D \nabla S_w^k \cdot n_e \right\}, \tag{41}$$

$$u_t^{k+1} \mid K = -\lambda_t^k D_K \nabla p_w^{k+1} \mid_K - \left(\lambda_n \frac{\mathrm{d}p_c}{\mathrm{d}S_w} \right)^k D_K \nabla S_w^k \mid_K, \tag{42}$$

where the average of the total velocity is used in the interior edges. Although it doesn't use any projections explicitly, the velocities constructed from (41) and (42) are some kind of implicit projections into RT_0 space. The velocity derived from (41) and (42) is close to the velocity projection in $RT_0^{(4)}$ space which is constructed by (39) and (40). But their value in each element is different. Furthermore, the DDG method with using the velocity reconstruction presented in this subsection has certain differences in contrast to what proposed in [2], which are reflected in two aspects below:

1) The variational form of the saturation equation doesn't incorporate any additional penalties from the pressure equation.

2) The approximations of the coefficients are totally different.

5. Numerical Examples

In this section, we present some computer experiments to examine the proposed methods on two dimensional spaces. Both two boundary conditions with different types are used in the examination of all the methods. In tests 1 and 2 we consider the displacement of the non-wetting phase by the wetting phase, which is similar to the so called quarter-five spot problem introduced in [2]. In test 3 we consider the displacement of the wetting phase by the non-wetting phase which is used to simulate the barrier effect in [9]. The domains used in the experiments are the square $(0,2)^2$ with two corners be cut off, and for the mesh used in the discontinuous problem a small square with different rock property is fixed inside the domain, see **Figure 2(a)** and **Figure 2(b)**. In each test, we use the Nonsymmetric Interior Penalty Galerkin (NIPG) method with the penalty parameters $\varepsilon = 1$, $\sigma = 1$ and $\beta = 1$. In order to prevent the oscillations, a slope limiter procedure described in [15] is used.

If considering the mixed-Neumann type boundary (8)-(9) for the saturation equation, the following initial and boundary conditions are used:

$$S_w (t = 0) = 0.2, \tag{43}$$

$$S_{in} = 0.9 \quad \text{on} \quad \Gamma_{sM} (\Gamma_{in}), \tag{44}$$

$$g_N = 0 \, \mathrm{m/s} \quad \text{on} \quad \Gamma_{sN} (\Gamma_{no} \cup \Gamma_{out}), \tag{45}$$

$$p_{dir} = 3.45 \times 10^6 \, \mathrm{Pa} \quad \text{on} \quad \Gamma_{pD} (\Gamma_{in}), \tag{46}$$
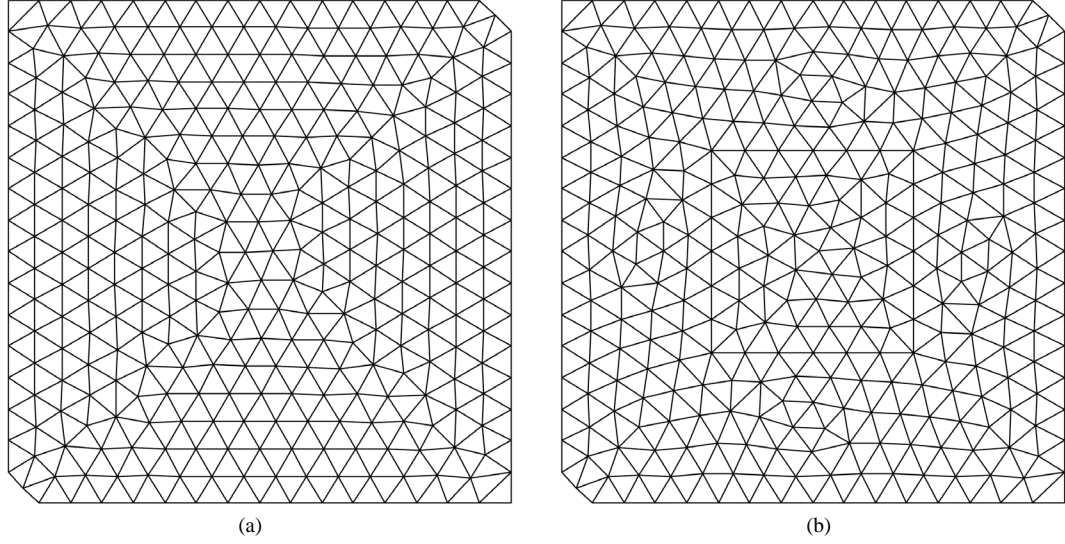
Figure 2. Meshes used in the experiments. (a) quarter-five spot mesh used in homogeneous medium; (b) quarter- five spot mesh used in discontinuous media.

$$p_{dir} = 2.41 \times 10^6 \text{ Pa} \quad \text{on } \Gamma_{pD}\left(\Gamma_{out}\right), \tag{47}$$

$$u_t \cdot n_e = 0 \text{ m/s} \quad \text{on } \Gamma_{pN}\left(\Gamma_{no}\right). \tag{48}$$

When the Neumann-Dirichlet type boundary (12)-(13) is used for the saturation equation, the following initial and boundary conditions are considered:

$$S_w\left(t=0\right)=1, \tag{49}$$

$$u_n \cdot n_e = 0 \text{ m} \cdot \text{s}^{-1} \quad \text{on } \Gamma_{sN}\left(\Gamma_{in}\right), \tag{50}$$

$$u_w \cdot n_e = 0 \text{ m} \cdot \text{s}^{-1} \quad \text{on } \Gamma_{sN}\left(\Gamma_{no}\right), \tag{51}$$

$$S_{dir} = 1 \quad \text{on } \Gamma_{sD}\left(\Gamma_{out}\right), \tag{52}$$

$$u_t \cdot n_e = 2.05 \times 10^{-2} \text{ m} \cdot \text{s}^{-1} \quad \text{on } \Gamma_{pN}\left(\Gamma_{in}\right), \tag{53}$$

$$u_t \cdot n_e = 0 \text{ m} \cdot \text{s}^{-1} \quad \text{on } \Gamma_{pN}\left(\Gamma_{no}\right) \tag{54}$$

$$p_{dir} = 2.01 \times 10^5 \text{ Pa} \quad \text{on } \Gamma_{pD}\left(\Gamma_{out}\right). \tag{55}$$

The parameters including rock and fluid properties used in the simulation are summarized in **Table 1**.

5.1. Test 1

In test 1, we examine the property of the local mass conservation law. For this purpose, we solve the so-called quarter-five spot problem on a homogeneous medium and check the numerical local mass of the reconstructed velocity. All the projection methods discussed above will be used and compared. The domain used in the experiment is the square $(0,2)^2$ with two corners be cut off, see **Figure 2(a)**. The initial and boundary conditions (43)-(48) is used. The parameters with respect to the rock property and Brooks-Corey model are listed in **Table 1**, Test 1. In **Figure 2(a)**, the spot at the left bottom is the inflow boundary Γ_{in}, the outflow boundary Γ_{out} is located at the right top corner, the rest of the boundary is the noflow boundary Γ_{no}. To make sure that the water front stays inside the domain, the final time is set to $T = 160$ s. We use a constant time step, and the ratio of the time step to the space step's square is about $dt/h^2 \sim 4.5$. We use $DDG^{(0)}$ to denote the DDG method without

Table 1. Parameters used in the numerical simulations.

Test 1	
porosity	$\phi = 0.4$
permeability [m²]	$D = [50.4, 0; 0, 1] \times 10^{-11}$
viscosity[kg/(ms)]	$\mu_n = 1.0 \times 10^{-3}$, $\mu_w = 1.0 \times 10^{-4}$
residual saturation	$S_{rw} = 0.05$, $S_{rn} = 0.1$
Brooks-Corey	$p_d = 3 \times 10^3$ Pa , $\theta = 3$
Test 2	
porosity	$\phi = 0.2$
permeability [m²]	$D = [1, 0; 0, 1] \times 10^{-11}$
viscosity[kg/(ms)]	$\mu_n = 2.0 \times 10^{-3}$, $\mu_w = 5.0 \times 10^{-4}$
residual saturation	$S_{rw} = 0.05, S_{rn} = 0.01$
Brooks-Corey	$p_d = 5 \times 10^3$ Pa , $\theta = 2$
Test 3	
porosity	$\phi_I = 0.2$, $\phi_{II} = 0.2$
permeability [m²]	$D^I = [10, 0; 0, 1] \times 10^{-11}$, $D^{II} = [1, 0; 0, 1] \times 10^{-11}$
viscosity[kg/(ms)]	$\mu_n = 1.0 \times 10^{-2}$, $\mu_w = 1.0 \times 10^{-3}$
residual saturation	$S_{rw}^I = S_{rw}^{II} = 0$, $S_{rw}^I = S_{rn}^{II} = 0$
Brooks-Corey	$p_d^I = 1 \times 10^4$ Pa , $p_d^{II} = 1.5 \times 10^4$ Pa , $\theta^I = 2$, $\theta^{II} = 2$

explicit projections. Since there is no sink and source terms the exact local mass is zero on each elements, that is, $\forall K \in \mathcal{T}_h, \sum_{e \in \partial K} \int_e u_t \cdot n_e = 0,$ where n_e is the outward unit normal vector to ∂K. Thus we can easily define the errors of the local mass conservation under the vector norms l^∞ and l^2 which are respectively

$$\max_{K \in \mathcal{T}_h} \left\{ \left| \sum_{e \in \partial K} \int_e u_t \cdot n_e \right| \right\} \text{ and } \left(\sum_{K \in \mathcal{T}_h} \left| \sum_{e \in \partial K} \int_e u_t \cdot n_e \right|^2 \right)^{\frac{1}{2}}. \tag{56}$$

The errors of the local mass conservation at selected times are listed in **Table 2** and **Table 3**.

5.2. Test 2

In this test, we show the numerical solutions solved by our scheme with using projection $RT_0^{(1)}$ in a homogeneous media. For the results with using projection $BDM_1^{(1)}$ and $RT_1^{(1)}$, they are similar with using $RT_0^{(1)}$ so are omitted. The mesh used in test 2 is the same as the previous test. The initial and boundary conditions (43)-(48) are used in this test. To make sure that the water front stays inside the domain, the final time is set to $T = 180$ s. A constant time step is used, and the ratio of the time step to the space step's square is about $dt/h^2 \sim 4.5$. The parameters of rock property and Brooks-Corey model are listed in **Table 1**, Test 2. The contours of wetting phase saturation in the homogeneous medium at selected times are presented in **Figure 3**.

5.3. Test 3

In the last test, we examine our scheme in a discontinuous media. We assume that the domain used here is initially fully water saturated and with the interfaces between two different sands, see **Figure 4**. Ω_{II} is the fine sand and Ω_I is the coarse sand, so the oil-trapped phenomenon will appear on the interfaces Γ_J^+ see **Figure 4**. The critical point in (19) is $S_w^* \approx 0.44$, and the oil will penetrate the interface Γ_J^+ when $S_w^I \leq S_w^*$. The mesh

Table 2. Numerical errors of the local mass conservation in test 1 at times $t = 40$ s and $t = 80$ s.

	$t = 40$ s		$t = 80$ s	
	l^∞	l^2	l^∞	l^2
$DDG^{(0)}$	2.2913e−04	5.7110e−04	2.3767e−04	5.8819e−04
$RT_0^{(1)}$	2.8284e−09	1.6994e−08	2.2655e−09	1.6564e−08
$RT_0^{(2)}$	2.2117e−04	5.2564e−04	2.2860e−04	5.3194e−04
$RT_0^{(3)}$	2.0947e−05	7.6105e−05	1.8192e−05	6.8195e−05
$RT_0^{(4)}$	2.2087e−04	5.2553e−04	2.2808e−04	5.3135e−04
$BDM_1^{(1)}$	2.6577e−09	1.6747e−08	2.1773e−09	1.5875e−08
$BDM_1^{(2)}$	2.2117e−04	5.2564e−04	2.2860e−04	5.3194e−04
$BDM_1^{(3)}$	2.1408e−05	7.8417e−05	1.7849e−05	6.9403e−05
$BDM_1^{(4)}$	2.2086e−04	5.2552e−04	2.2808e−04	5.3135e−04
$RT_1^{(1)}$	2.0632e−09	1.6436e−08	2.5179e−09	1.7404e−06
$RT_1^{(2)}$	2.2933e−04	5.7035e−04	2.3798e−04	5.8939e−04
$RT_1^{(3)}$	2.1631e−05	7.9100e−05	1.7994e−05	7.0000e−05
$RT_1^{(4)}$	2.2913e−04	5.7110e−04	2.3766e−04	5.8819e−04

Table 3. Numerical errors of the local mass balance in test 1 at times $t = 120$ s and $t = 160$ s.

	$t = 120$ s		$t = 160$ s	
	l^∞	l^2	l^∞	l^2
$DDG^{(0)}$	2.4309e−04	5.9636e−04	2.4690e−04	6.0363e−04
$RT_0^{(1)}$	2.4551e−09	1.7281e−08	2.3734e−09	1.8916e−08
$RT_0^{(2)}$	2.3367e−04	5.4152e−04	2.3644e−04	5.4898e−04
$RT_0^{(3)}$	2.1099e−05	7.1351e−05	1.4933e−05	6.7183e−05
$RT_0^{(4)}$	2.3305e−04	5.3781e−04	2.3576e−04	5.4316e−04
$BDM_1^{(1)}$	2.4264e−09	1.7214e−08	2.4283e−09	1.7782e−08
$BDM_1^{(2)}$	2.3368e−04	5.4152e−04	2.3644e−04	5.4898e−04
$BDM_1^{(3)}$	2.1464e−05	7.2709e−05	1.5027e−05	6.7311e−05
$BDM_1^{(4)}$	2.3305e−04	5.3780e−04	2.3576e−04	5.4316e−04
$RT_1^{(1)}$	2.0203e−09	1.6556e−08	2.4811e−09	1.8123e−08
$RT_1^{(2)}$	1.5926e−04	5.9819e−04	2.4740e−04	6.0948e−04
$RT_1^{(3)}$	2.1777e−05	7.3186e−05	1.5423e−05	6.6493e−05
$RT_1^{(4)}$	2.4309e−04	5.9636e−04	2.4691e−04	6.0363e−04
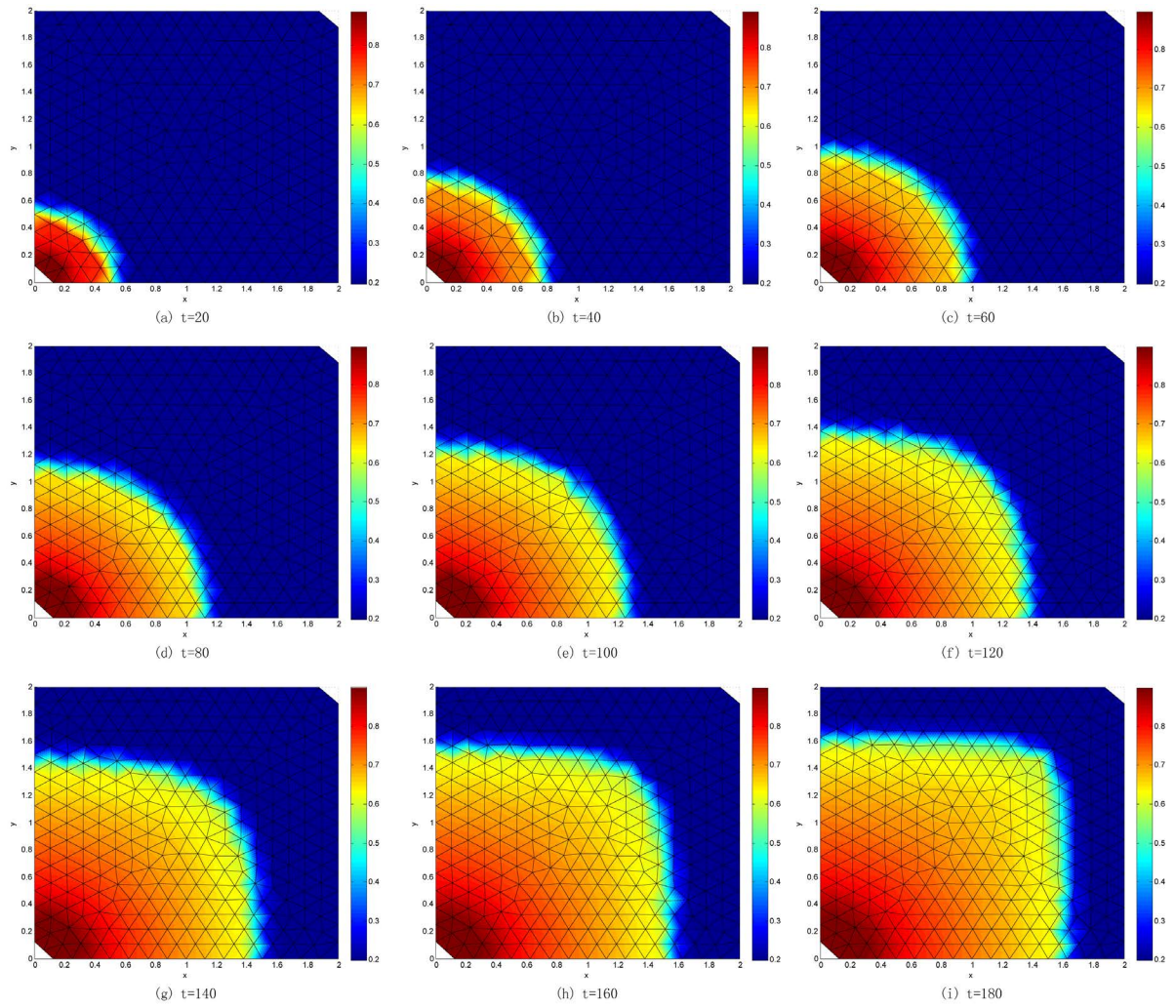
Figure 3. The contours of wetting phase saturation in the homogeneous medium at selected times in the Test 2.
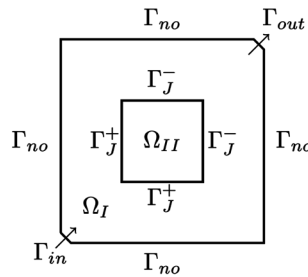
Figure 4. Discontinuous quarter-five spot problem.

used in this test is **Figure 2(b)**. The initial and boundary conditions (49)-(55) are used in this test. The initial and boundary conditions (49)-(55) are used in this test. To make sure that the water front stays inside the domain, the final time is set to $T = 200$ s. A constant time step is used, and the ratio of the time step to the space step's square is about $dt/h^2 \sim 4.5$. The parameters of rock property and Brooks-Corey model are listed in **Table 1**, Test 3. When the oil flows from coarse sand to fine sand with the injection of oil from the inflow boundary Γ_{in}, more and more oil approaches and accumulates at the front of the interface of the fine sand. When the accumulation reaches a critical point, that is, when the capillary pressure at the coarse side of the interface is greater than at the fine side, the accumulated oil will penetrate the interface and enter the fine sand area. By contrast, in
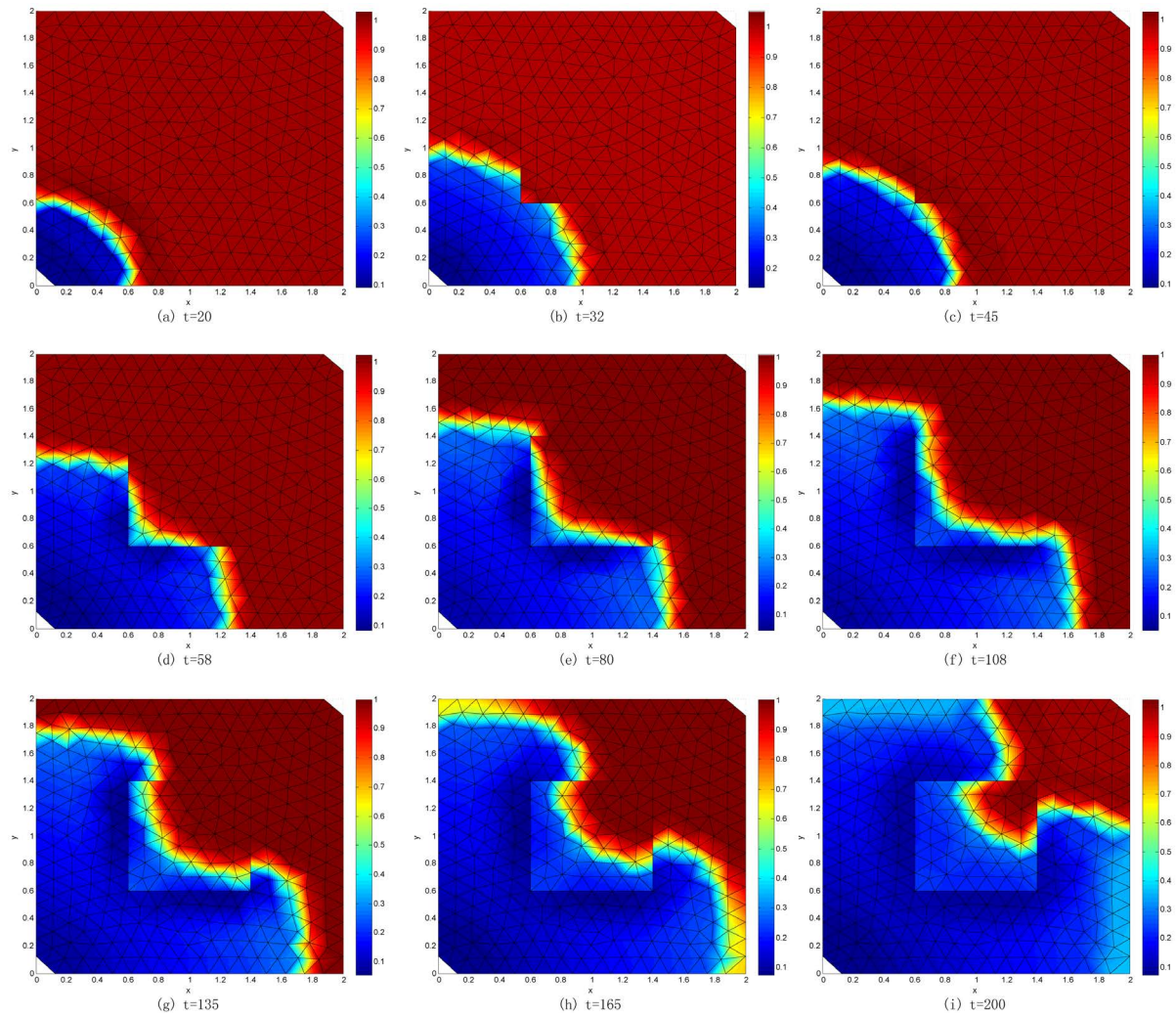
Figure 5. The contours of wetting phase saturation in the discontinuous media at selected times in the Test 3.

the reversed direction the oil immediately penetrate the interface, that is, the oil-trapped phenomenon will not happen if the oil flows from fine sand to coarse sand. The contours of wetting phase saturation in the discontinuous media at selected times are presented in **Figure 5**.

6. Conclusion

The velocities reconstructed from projections $RT_0^{(1)}$ $BDM_1^{(1)}$ and $RT_1^{(1)}$ are much better to preserve the local mass conservation property than the others. That is, the velocity reconstruction with the projection that considers both the upwind scheme and penalty term can best preserve the local mass conservation property. The approximation of the coefficient (23) is very essential to the stability of all the DDG methods. Instead of (23), if the approximation of coefficient (21) is used, the variational form of the saturation equation has to incorporate additional penalties from the pressure equation; otherwise the scheme will be unstable.

Funding

References

[1] Ern, A., Mozolevski, I. and Schuh, L. (2010) Discontinuous Galerkin Approximation of Two-Phase Flows in Hetero-

geneous Porous Media with Discontinuous Capillary Pressures. *Computer Methods in Applied Mechanics and Engineering*, **199**, 1491-1501. http://dx.doi.org/10.1016/j.cma.2009.12.014

[2] Klieber, W. and Rivière, B. (2006) Adaptive Simulations of Two-Phase Flow by Discontinuous Galerkin Methods. *Computer Methods in Applied Mechanics and Engineering*, **196**, 404-419. http://dx.doi.org/10.1016/j.cma.2006.05.007

[3] Mozolevski, I. and Schuh, L. (2013) Numerical Simulation of Two-Phase Immiscible Incompressible Flows in Heterogeneous Porous Media with Capillary Barriers. *Journal of Computational and Applied Mathematics*, **242**, 12-27. http://dx.doi.org/10.1016/j.cam.2012.09.045

[4] Bastian, P. and Rivière, B. (2003) Superconvergence and H(div) Projection for Discontinuous Galerkin Methods. *International Journal for Numerical Methods in Fluids*, **42**, 1043-1057. http://dx.doi.org/10.1002/fld.562

[5] Brezzi, F. and Fortin, M. (1991) Mixed and hybrid finite element methods. Springer, New York. http://dx.doi.org/10.1007/978-1-4612-3172-1

[6] Nayagum, D., Schäfer, G. and Mosé, R. (2004) Modelling Two-Phase Incompressible Flow in Porous Media Using Mixed Hybrid and Discontinuous Finite Elements. *Computational Geosciences*, **8**, 49-73. http://dx.doi.org/10.1023/B:COMG.0000024446.98662.36

[7] Chen, Z.X., Huan, G.R. and Ma, Y.L. (2006) Computational Methods for Multiphase Flows in Porous Media. SIAM, Philadelphia. http://dx.doi.org/10.1137/1.9780898718942

[8] Brooks, R.H. and Corey, A.T. (1964) Hydraulic Properties of Porous Media. Colorado State University, Fort Collins.

[9] Fučk, R. and Mikyška, J. (2011) Mixed-Hybrid Finite Element Method for Modelling Two-Phase Flow in Porous Media. *Journal of Math-for-Industry*, **3**, 9-19.

[10] Hoteit, H. and Firoozabadi, A. (2008) Numerical Modeling of Two-Phase Flow in Heterogeneous Permeable Media with Different Capillarity Pressures. *Advances in Water Resources*, **31**, 56-73. http://dx.doi.org/10.1016/j.advwatres.2007.06.006

[11] Enchéry, G., Eymard, R. and Michel, A. (2006) Numerical Approximation of a Two-Phase Flow Problem in a Porous Medium with Discontinuous Capillary Forces. *SIAM Journal on Numerical Analysis*, **43**, 2402-2422. http://dx.doi.org/10.1137/040602936

[12] Cancès, C. (2009) Finite Volume Scheme for Two-Phase Flow in Heterogeneous Porous Media Involving Capillary Pressure Discontinuities. *ESAIM*: *Mathematical Modelling and Numerical Analysis*, **43**, 973-1001. http://dx.doi.org/10.1051/m2an/2009032

[13] Cancès, C., Gallouët, T. and Porretta, A. (2009) Two-Phase Flows Involving Capillary Barriers in Heterogeneous Porous Media. *Interfaces and Free Boundaries*, **11**, 239-258. http://dx.doi.org/10.4171/IFB/210

[14] Rivière, B. (2008) Discontinuous Galerkin Methods for Solving Elliptic and Parabolic Equations: Theory and Implementation. SIAM, Philadelphia. http://dx.doi.org/10.1137/1.9780898717440

[15] Chavent, G. and Jaffré, J. (1986) Mathematical Models and Finite Elements for Reservoir Simulation. Studies in Mathematics and Its Applications. North-Holland, Amsterdam.

The Global Attractors for a Nonlinear Viscoelastic Wave Equation with Strong Damping and Linear Damping and Source Terms

Liang Guo, Zhaoqin Yuan, Guoguang Lin

Department of Mathematics, Yunnan University, Kunming, China
Email: guoliang142857@163.com, yuanzq091@163.com, gglin@ynu.edu.cn

Abstract

In this paper, firstly, some priori estimates are obtained for the existence and uniqueness of solutions of a nonlinear viscoelastic wave equation with strong damping, linear damping and source terms. Then we study the global attractors of the equation.

Keywords

Global Attractors, Viscoelastic Equation, Priori Estimates

1. Introduction

We know that viscoelastic materials have memory effects. These properties are due to the mechanical response influenced by the history of the materials. As these materials have a wide application in the natural science, their dynamics are of great importance and interest. The memory effects can be modeled by a partial differential equation. In recent years, the behaviors of solutions for the PDE system have been studied extensively, and many achievements have been obtained. Many authors have focused on the problem of existence, decay and blow-up for the last two decades, see [1]-[5]. And the attractors are still important contents that are studied.

In [6], R.O. Araújo, T. Ma and Y.M. Qin studied the following equation

$$\left| u_t \right|^\rho u_{tt} - \Delta u - \Delta u_{tt} + \int_0^{+\infty} g(s) \Delta u(t-s) \mathrm{d}s + f(u) = h(x) \tag{1.1}$$

and they proved the global existence, uniqueness and exponential stability of solutions and existence of the

global attractor.

In [7], Y.M. Qin, B.W. Feng and M. Zhang considered the following initial-boundary value problem:

$$\begin{cases} \left|u_t\right|^\rho u_{tt} - \Delta u - \Delta u_{tt} + \int_0^{+\infty} g(s)\Delta u(t-s)\mathrm{d}s + u_t = \sigma(x,t), \ x \in \Omega, t > \tau \\ u(x,t) = 0, \ x \in \partial\Omega, t \geq \tau \\ u(x,\tau) = u_0^\tau(x), \ u_t(x,\tau) = u_1^\tau(x), \ u(x,t) = u_\tau(x,t), \ x \in \Omega, \tau \in R^+ \end{cases} \tag{1.2}$$

where Ω is a bounded domain of R^n $(n \geq 1)$ with a smooth boundary $\partial\Omega$, $u_\tau(x,t)$ (the past history of u) is a given datum which has to be known for all $t \leq \tau$, the function g represents the kernel of a memory, $\sigma = \sigma(x,t)$ is a non-autonomous term, called a symbol, and ρ is a real number such that $1 < \rho \leq \dfrac{2}{n-2}$ if $n \geq 3$; $\rho > 1$ if $n = 1, 2$. They proved the existence of uniform attractors for a non-autonomous viscoelastic equation with a past history. For more related results, we refer the reader to [8]-[14].

In this work, we intend to study the following initial-boundary problem:

$$\begin{cases} u_{tt} - \Delta u + \int_0^{+\infty} g(s)\Delta u(t-s)\mathrm{d}s - \varepsilon_1 \Delta u_t + \varepsilon_2 u_t + \varepsilon_3 \left|u\right|^{p-2} u = f(x), \quad x \in \Omega, t > 0 \\ u(x,t) = 0, \quad x \in \partial\Omega, t \geq 0 \\ u(x,0) = u_0(x), \quad u_t(x,0) = u_1(x), \quad x \in \Omega \end{cases} \tag{1.3}$$

where $\varepsilon_1, \varepsilon_2, \varepsilon_3 \geq 0$, and $\Omega \subset R^n$ $(n \geq 1)$ is a bounded domain with smooth boundary $\partial\Omega$, $2 < p < \min\left\{\dfrac{2n}{n-2}, \dfrac{2n+4}{n}\right\}$ if $n \geq 3$; $p > 2$ if $n = 1, 2$, for the problem (1.3), the memory term $\int_0^{+\infty} g(s)\Delta u(t-s)\mathrm{d}s$ replaces $\int_0^t g(t-s)\Delta u(s)\mathrm{d}s$, and we consider the strong damping term $-\varepsilon_1 \Delta u_t$, the linear damping term $\varepsilon_2 u_t$ and source terms $\varepsilon_3 \left|u\right|^{p-2} u$. We define

$$\eta = \eta(s) = \eta^t(x,s) = u(x,t) - u(x,t-s)$$

A direct computation yields

$$\eta_t(s) = -\eta_s(s) + u_t(t)$$

Thus, the original memory term can be written as

$$\int_0^{+\infty} g(s)\Delta u(t-s)\mathrm{d}s = \int_0^{+\infty} g(s)\mathrm{d}s \cdot \Delta u - \int_0^{+\infty} g(s)\Delta\eta(s)\mathrm{d}s$$

and we get a new system

$$u_{tt} - \left(1 - \int_0^{+\infty} g(s)\mathrm{d}s\right)\Delta u - \varepsilon_1 \Delta u_t - \int_0^{+\infty} g(s)\Delta\eta(s)\mathrm{d}s + \varepsilon_2 u_t + \varepsilon_3 \left|u\right|^{p-2} u = f(x) \tag{1.4}$$

$$\eta_t = -\eta_s + u_t \tag{1.5}$$

with the initial conditions

$$u(x,0) = u_0(x), \ u_t(x,0) = u_1(x), \ \eta(0) = \eta^t(x,0) = 0, \ x \in \Omega \tag{1.6}$$

and the boundary conditions

$$u(x,t) = 0, \ x \in \partial\Omega, t \geq 0 \tag{1.7}$$

The rest of this paper is organized as follows. In Section 2, we first obtain the priori estimates, then in Section 3, we prove the existence of the global attractors.

For convenience, we denote the norm and scalar product in $L^2(\Omega)$ by $\|\cdot\|$ and $(\cdot,\cdot)$, let $V = H^1(\Omega)$, $D(A) = H^2(\Omega)$.

2. The Priori Estimates of Solution of Equation

In this section, we present some materials needed in the proof of our results, state a global existence result, and prove our main result. For this reason, we assume that

(G1) $g: R^+ \to R^+$ is a differentiable function satisfying $1 - \int_0^{+\infty} g(s) \, \mathrm{d}s = l > 0$;

(G2) $g(s) \geq 0, g'(s) \leq 0, \forall s \in R^+$;

(G3) There exists a constant $\xi > 0$ such that $g'(s) + \xi g(s) \leq 0$, $\forall s \in R^+$;

Lemma 1. Assume (G1), (G2) and (G3) hold, let

$$
\begin{cases}
2 < p < \dfrac{2n}{n-2}, & n \geq 3 \\
p \geq 2, & n = 1, 2
\end{cases}
$$

and $(u_0, u_1) \in H_0^1(\Omega) \times L^2(\Omega)$, $f \in L^2(\Omega)$, $v = u_t + \varepsilon u$, then the solution (u, v) of Equation (1.3) satisfies $(u, v) \in H_0^1(\Omega) \times L^2(\Omega)$ and

$$
\|(u,v)\|_{H_0^1 \times L^2}^2 = \|\nabla u\|^2 + \|v\|_2^2 \leq \frac{W(0)}{k} e^{-\alpha_1 t} + \frac{C_1}{\alpha_1 k} \left(1 - e^{-\alpha_1 t} \right) \tag{2.1}
$$

here $W(0) = \|v_0\|_2^2 + (l - \varepsilon_1 \varepsilon) \|\nabla u_0\|_2^2 + \dfrac{2\varepsilon_3}{p} \|u_0\|_p^p$, thus there exists E_0 and $t_1 = t_1(\Omega) > 0$, such that

$$
\|(u,v)\|_{H_0^1 \times L^2}^2 = \|\nabla u(t)\|_2^2 + \|v(t)\|_2^2 \leq E_0 \, (t > t_1) \tag{2.2}
$$

Proof. We multiply $v = u_t + \varepsilon u$ with both sides of equation and obtain

$$
\left(u_{tt} - \left(1 - \int_0^{+\infty} g(s) \, \mathrm{d}s \right) \Delta u - \varepsilon_1 \Delta u_t - \int_0^{+\infty} g(s) \Delta \eta(s) \, \mathrm{d}s + \varepsilon_2 u_t + \varepsilon_3 |u|^{p-2} u, v \right) = (f, v)
$$

By using Holder inequality, Young's inequality and Poincare inequality, we get

$$
(u_{tt}, v) = (v_t - \varepsilon u_t, v) = \frac{1}{2} \frac{\mathrm{d}}{\mathrm{d}t} \|v\|_2^2 - \varepsilon(u_t, v) = \frac{1}{2} \frac{\mathrm{d}}{\mathrm{d}t} \|v\|_2^2 - \varepsilon(v - \varepsilon u, v)
$$

$$
= \frac{1}{2} \frac{\mathrm{d}}{\mathrm{d}t} \|v\|_2^2 - \varepsilon \|v\|_2^2 + \varepsilon^2 (u, v) \geq \frac{1}{2} \frac{\mathrm{d}}{\mathrm{d}t} \|v\|_2^2 - \varepsilon \|v\|_2^2 - \frac{\varepsilon^2}{2} \|u\|_2^2 - \frac{\varepsilon^2}{2} \|v\|_2^2 \tag{2.3}
$$

$$
\geq \frac{1}{2} \frac{\mathrm{d}}{\mathrm{d}t} \|v\|_2^2 - \varepsilon \|v\|_2^2 - \frac{\varepsilon^2}{2\lambda_1} \|\nabla u\|_2^2 - \frac{\varepsilon^2}{2} \|v\|_2^2,
$$

and

$$
\left(-\left(1 - \int_0^{+\infty} g(s) \, \mathrm{d}s \right) \Delta u, v \right) = -l(\Delta u, u_t + \varepsilon u) = \frac{l}{2} \frac{\mathrm{d}}{\mathrm{d}t} \|\nabla u\|_2^2 + l\varepsilon \|\nabla u\|_2^2 \tag{2.4}
$$

and

$$
\left(-\int_0^{+\infty} g(s) \Delta \eta(s) \, \mathrm{d}s, v \right) = \left(-\int_0^{+\infty} g(s) \Delta \eta(s) \, \mathrm{d}s, u_t \right) + \left(-\int_0^{+\infty} g(s) \Delta \eta(s) \, \mathrm{d}s, \varepsilon u \right) \tag{2.5}
$$

For the first term on the right side (2.5), by using (G1), (G2) and (G3), we have

$$
\int_0^{+\infty} g(s) \int_\Omega \nabla \eta(s) \cdot \nabla u_t \, \mathrm{d}x \mathrm{d}s = \int_0^{+\infty} g(s) \int_\Omega \nabla \eta(s) \cdot (\nabla \eta_t + \nabla \eta_s) \, \mathrm{d}x \mathrm{d}s
$$

$$
= \int_0^{+\infty} g(s) \frac{1}{2} \frac{\mathrm{d}}{\mathrm{d}t} \|\nabla \eta\|_2^2 \, \mathrm{d}s + \int_0^{+\infty} g(s) \mathrm{d} \frac{1}{2} \|\nabla \eta\|_2^2 \tag{2.6}
$$

$$
\geq \frac{1}{2} \frac{\mathrm{d}}{\mathrm{d}t} \|\eta\|_{g,V}^2 + \frac{\xi}{2} \|\eta\|_{g,V}^2,
$$

where

$$\|\eta\|_{g,V}^2 = \int_0^{+\infty} g(s)\|\nabla\eta(s)\|_2^2\,\mathrm{d}s \tag{2.7}$$

For the second term on the right side (2.5), by using Holder inequality and Young's inequality, we get

$$\left(-\int_0^{+\infty} g(s)\Delta\eta(s)\,\mathrm{d}s,\varepsilon u\right) = \varepsilon\int_0^{+\infty} g(s)\int_\Omega \nabla\eta(s)\nabla u\,\mathrm{d}x\mathrm{d}s$$
$$\geq -\frac{\xi}{4}\|\eta\|_{g,V}^2 - \frac{\varepsilon^2}{\xi}\int_0^{+\infty} g(s)\,\mathrm{d}s\|\nabla u\|_2^2 \tag{2.8}$$

So, we have

$$\left(-\int_0^{+\infty} g(s)\Delta\eta(s)\,\mathrm{d}s,v\right) = \left(-\int_0^{+\infty} g(s)\Delta\eta(s)\,\mathrm{d}s,u_t\right) + \left(-\int_0^{+\infty} g(s)\Delta\eta(s)\,\mathrm{d}s,\varepsilon u\right)$$
$$\geq \frac{1}{2}\frac{\mathrm{d}}{\mathrm{d}t}\|\eta\|_{g,V}^2 + \frac{\xi}{4}\|\eta\|_{g,V}^2 - \frac{\varepsilon^2}{\xi}\int_0^{+\infty} g(s)\,\mathrm{d}s\|\nabla u\|_2^2 \tag{2.9}$$

By using Poincare inequality, we obtain

$$(-\varepsilon_1\Delta u_t,v) = \varepsilon_1\left(-\Delta v + \varepsilon\Delta u,v\right) = \varepsilon_1\|\nabla v\|_2^2 + \varepsilon_1\varepsilon\left(\Delta u,u_t+\varepsilon u\right)$$
$$= \varepsilon_1\|\nabla v\|_2^2 - \frac{\varepsilon_1\varepsilon}{2}\frac{\mathrm{d}}{\mathrm{d}t}\|\nabla u\|_2^2 - \varepsilon_1\varepsilon^2\|\nabla u\|_2^2 \tag{2.10}$$
$$\geq \varepsilon_1\lambda_1\|v\|_2^2 - \frac{\varepsilon_1\varepsilon}{2}\frac{\mathrm{d}}{\mathrm{d}t}\|\nabla u\|_2^2 - \varepsilon_1\varepsilon^2\|\nabla u\|_2^2$$

and

$$(\varepsilon_2 u_t,v) = \varepsilon_2\left(u_t,u_t+\varepsilon u\right) = \varepsilon_2\|u_t\|_2^2 - \varepsilon_2\varepsilon\|u\|_2\|u_t\|_2$$
$$\geq \varepsilon_2\|u_t\|_2^2 - \frac{\varepsilon_2\varepsilon}{2}\|u\|_2^2 - \frac{\varepsilon_2\varepsilon}{2}\|u_t\|_2^2 \tag{2.11}$$
$$\geq \varepsilon_2\left(1-\frac{\varepsilon}{2}\right)\|u_t\|_2^2 - \frac{\varepsilon_2\varepsilon}{2\lambda_1}\|\nabla u\|_2^2$$

and

$$\left(\varepsilon_3|u|^{p-2}u,v\right) = \varepsilon_3\left(|u|^{p-2}u,u_t+\varepsilon u\right) = \frac{\varepsilon_3}{p}\frac{\mathrm{d}}{\mathrm{d}t}\|u\|_p^p + \varepsilon_3\varepsilon\|u\|_p^p \tag{2.12}$$

By using Holder inequality and Young's inequality, we obtain

$$(f(x),v) \leq \|f\|\cdot\|v\| \leq \frac{\lambda_1}{2}\|v\|_2^2 + \frac{1}{2\lambda_1}\|f\|_2^2 \tag{2.13}$$

Then, we have

$$\frac{1}{2}\frac{\mathrm{d}}{\mathrm{d}t}\|v\|_2^2 - \varepsilon\|v\|_2^2 - \frac{\varepsilon^2}{2\lambda_1}\|\nabla u\|_2^2 - \frac{\varepsilon^2}{2}\|v\|_2^2 + \frac{l}{2}\frac{\mathrm{d}}{\mathrm{d}t}\|\nabla u\|_2^2 + l\varepsilon\|\nabla u\|_2^2 + \frac{1}{2}\frac{\mathrm{d}}{\mathrm{d}t}\|\eta\|_{g,V}^2$$
$$+ \frac{\xi}{4}\|\eta\|_{g,V}^2 - \frac{\varepsilon^2}{\xi}\int_0^{+\infty} g(s)\,\mathrm{d}s\|\nabla u\|_2^2 + \varepsilon_1\lambda_1\|v\|_2^2 - \frac{\varepsilon_1\varepsilon}{2}\frac{\mathrm{d}}{\mathrm{d}t}\|\nabla u\|_2^2 - \varepsilon_1\varepsilon^2\|\nabla u\|_2^2$$
$$+ \varepsilon_2\left(1-\frac{\varepsilon}{2}\right)\|u_t\|_2^2 - \frac{\varepsilon_2\varepsilon}{2\lambda_1}\|\nabla u\|_2^2 + \frac{\varepsilon_3}{p}\frac{\mathrm{d}}{\mathrm{d}t}\|u\|_p^p + \varepsilon_3\varepsilon\|u\|_p^p$$
$$\leq \frac{\lambda_1}{2}\|v\|_2^2 + \frac{1}{2\lambda_1}\|f\|_2^2 \tag{2.14}$$

That is

$$
\frac{\mathrm{d}}{\mathrm{d}t}\left[\|v\|_2^2+(l-\varepsilon_1\varepsilon)\|\nabla u\|_2^2+\|\eta\|_{g,V}^2+\frac{2\varepsilon_3}{p}\|u\|_p^p\right]+\left(2\varepsilon_1\lambda_1-2\varepsilon-\varepsilon^2-\lambda_1\right)\|v\|_2^2
$$

$$
+2\varepsilon\left(l-\varepsilon_1\varepsilon-\frac{\varepsilon}{2\lambda_1}-\frac{\varepsilon}{\xi}\int_0^{+\infty}g(s)\mathrm{d}s-\frac{\varepsilon_2}{2\lambda_1}\right)\|\nabla u\|_2^2+\frac{\xi}{2}\|\eta\|_{g,V}^2+2\varepsilon_3\varepsilon\|u\|_p^p \tag{2.15}
$$

$$
+2\varepsilon_2\left[1-\frac{\varepsilon}{2}\right]\|u_t\|_2^2\leq\frac{1}{\lambda_1}\|f\|_2^2
$$

Next, we take proper $\varepsilon,\varepsilon_1,\varepsilon_2,\varepsilon_3$, such that

$$
\begin{cases}
a_1=2\varepsilon_1\lambda_1-2\varepsilon-\varepsilon^2-\lambda_1\geq 0 \\
a_2=2\varepsilon\left(l-\varepsilon_1\varepsilon-\dfrac{\varepsilon}{2\lambda_1}-\dfrac{\varepsilon}{\xi}\int_0^{+\infty}g(s)\mathrm{d}s-\dfrac{\varepsilon_2}{2\lambda_1}\right)\geq 0 \\
a_3=2\varepsilon_2\left(1-\dfrac{\varepsilon}{2}\right)\geq 0
\end{cases} \tag{2.16}
$$

Taking $\alpha_1=\min\left\{a_1,\dfrac{a_2}{l-\varepsilon_1\varepsilon},\dfrac{\xi}{2},p\varepsilon\right\}$, then

$$
\frac{\mathrm{d}}{\mathrm{d}t}W(t)+\alpha_1 W(t)\leq\frac{1}{\lambda_1}\|f\|_2^2:=C_1 \tag{2.17}
$$

where $W(t)=\|v\|_2^2+(l-\varepsilon_1\varepsilon)\|\nabla u\|_2^2+\|\eta\|_{g,V}^2+\dfrac{2\varepsilon_3}{p}\|u\|_p^p$, by using Gronwall inequality, we obtain

$$
W(t)\leq W(0)\mathrm{e}^{-\alpha_1 t}+\frac{C_1}{\alpha_1}\left(1-\mathrm{e}^{-\alpha_1 t}\right) \tag{2.18}
$$

From $2<p<\dfrac{2n}{n-2},n\geq 3$, according to Embedding Theorem then $H_0^1(\Omega)\subset L^p(\Omega)$, let $k=\min\left\{1,(l-\varepsilon_1\varepsilon)\right\}$, so we have

$$
\|(u,v)\|_{H_0^1\times L^2}^2=\|\nabla u\|^2+\|v\|_2^2\leq\frac{W(0)}{k}\mathrm{e}^{-\alpha_1 t}+\frac{C_1}{\alpha_1 k}\left(1-\mathrm{e}^{-\alpha_1 t}\right)
$$

Then

$$
\varlimsup_{t\to\infty}\|(u,v)\|_{H_0^1\times L^2}^2\leq\frac{C_1}{\alpha_1 k}
$$

So, there exists E_0 and $t_1=t_1(\Omega)>0$, such that

$$
\|(u,v)\|_{H_0^1\times L^2}^2=\|\nabla u(t)\|_2^2+\|v\|_2^2\leq E_0\ (t>t_1)
$$

Lemma 2. Assume (G1), (G2) and (G3) hold, let

$$
\begin{cases}
2<p<\dfrac{2n+4}{n}, & n\geq 3 \\
p\geq 2, & n=1,2
\end{cases}
$$

and $(u_0, u_1) \in H^2(\Omega) \times H^1(\Omega)$, $f \in H^1(\Omega)$, $v = u_t + \varepsilon u$, then the solution (u, v) of Equation (1.3) satisfies $(u, v) \in H^2(\Omega) \times H^1(\Omega)$ and

$$\|(u,v)\|_{H_0^2 \times H^1}^2 = \|\Delta u\|_2^2 + \|\nabla v\|_2^2 \leq \frac{W(0)}{k} e^{-\alpha_2 t} + \frac{C_2}{\alpha_2 k} \left(1 - e^{-\alpha_2 t}\right) \tag{2.19}$$

Here $V(0) = \|\nabla u_1 + \nabla u_0\|_2^2 + (l - \varepsilon_1 \varepsilon) \|\Delta u_0\|_2^2$, thus there exists E_1 and $t_2 = t_2(\Omega) > 0$, such that

$$\|(u,v)\|_{H^2 \times H^1}^2 = \|\Delta u(t)\|_2^2 + \|\nabla v(t)\|_2^2 \leq E_1 \quad (t > t_2) \tag{2.20}$$

Proof. We multiply $-\Delta v = -\Delta u_t - \varepsilon \Delta u$ with both sides of equation and obtain

$$\left(u_{tt} - \left(1 - \int_0^{+\infty} g(s) \mathrm{d}s\right) \Delta u - \varepsilon_1 \Delta u_t - \int_0^{+\infty} g(s) \Delta \eta(s) \mathrm{d}s + \varepsilon_2 u_t + \varepsilon_3 |u|^{p-2} u, -\Delta v\right) = (f, -\Delta v) \tag{2.21}$$

By using Holder inequality, Young's inequality and Poincare inequality, we get

$$\begin{aligned}
(u_{tt}, -\Delta v) &= (v_t - \varepsilon u_t, -\Delta v) = \frac{1}{2} \frac{\mathrm{d}}{\mathrm{d}t} \|\nabla v\|_2^2 - \varepsilon (u_t, -\Delta v) \\
&= \frac{1}{2} \frac{\mathrm{d}}{\mathrm{d}t} \|\nabla v\|_2^2 - \varepsilon (v - \varepsilon u, -\Delta v) \\
&= \frac{1}{2} \frac{\mathrm{d}}{\mathrm{d}t} \|\nabla v\|_2^2 - \varepsilon \|\nabla v\|_2^2 + \varepsilon^2 (\nabla u, \nabla v) \\
&\geq \frac{1}{2} \frac{\mathrm{d}}{\mathrm{d}t} \|\nabla v\|_2^2 - \varepsilon \|\nabla v\|_2^2 - \frac{\varepsilon^2}{2} \|\nabla u\|_2^2 - \frac{\varepsilon^2}{2} \|\nabla v\|_2^2 \\
&\geq \frac{1}{2} \frac{\mathrm{d}}{\mathrm{d}t} \|\nabla v\|_2^2 - \varepsilon \|\nabla v\|_2^2 - \frac{\varepsilon^2}{2\lambda_1} \|\Delta u\|_2^2 - \frac{\varepsilon^2}{2} \|\nabla v\|_2^2
\end{aligned}$$

and

$$\left(-\left(1 - \int_0^{+\infty} g(s) \mathrm{d}s\right) \Delta u, -\Delta v\right) = -l(\Delta u, -\Delta u_t - \varepsilon \Delta u) = \frac{l}{2} \frac{\mathrm{d}}{\mathrm{d}t} \|\Delta u\|_2^2 + l\varepsilon \|\Delta u\|_2^2 \tag{2.22}$$

and

$$\left(-\int_0^{+\infty} g(s) \Delta \eta(s) \mathrm{d}s, -\Delta v\right) = \left(-\int_0^{+\infty} g(s) \Delta \eta(s) \mathrm{d}s, -\Delta u_t\right) + \left(-\int_0^{+\infty} g(s) \Delta \eta(s) \mathrm{d}s, -\varepsilon \Delta u\right) \tag{2.23}$$

For the first term on the right side (2.23), by using (G1), (G2) and (G3), we have

$$\begin{aligned}
\int_0^{+\infty} g(s) \int_\Omega \Delta \eta(s) \cdot \Delta u_t \mathrm{d}x \mathrm{d}s &= \int_0^{+\infty} g(s) \int_\Omega \Delta \eta(s) \cdot (\Delta \eta_t + \Delta \eta_s) \mathrm{d}x \mathrm{d}s \\
&= \int_0^{+\infty} g(s) \frac{1}{2} \frac{\mathrm{d}}{\mathrm{d}t} \|\Delta \eta\|_2^2 \mathrm{d}s + \int_0^{+\infty} g(s) \mathrm{d} \frac{1}{2} \|\Delta \eta\|_2^2 \\
&\geq \frac{1}{2} \frac{\mathrm{d}}{\mathrm{d}t} \|\eta\|_{g, D(A)}^2 + \frac{\xi}{2} \|\eta\|_{g, D(A)}^2
\end{aligned} \tag{2.24}$$

where

$$\|\eta\|_{g, D(A)}^2 = \int_0^{+\infty} g(s) \|\Delta \eta(s)\|_2^2 \mathrm{d}s \tag{2.25}$$

For the second term on the right side (2.23), by using Holder inequality and Young's inequality, we get

$$\begin{aligned}
\left(-\int_0^{+\infty} g(s) \Delta \eta(s) \mathrm{d}s, -\varepsilon \Delta u\right) &= \varepsilon \int_0^{+\infty} g(s) \int_\Omega \Delta \eta(s) \Delta u \mathrm{d}x \mathrm{d}s \\
&\geq -\frac{\xi}{4} \|\eta\|_{g, D(A)}^2 - \frac{\varepsilon^2}{\xi} \int_0^{+\infty} g(s) \mathrm{d}s \|\Delta u\|_2^2
\end{aligned} \tag{2.26}$$

so, we have

$$\left(-\int_0^{+\infty} g(s)\Delta\eta(s)\,\mathrm{d}s, -\Delta v\right)$$

$$=\left(-\int_0^{+\infty} g(s)\Delta\eta(s)\,\mathrm{d}s, -\Delta u_t\right)+\left(-\int_0^{+\infty} g(s)\Delta\eta(s)\,\mathrm{d}s, -\varepsilon\Delta u\right)$$

$$=\frac{1}{2}\frac{\mathrm{d}}{\mathrm{d}t}\|\eta\|_{g,D(A)}^2+\frac{\xi}{4}\|\eta\|_{g,D(A)}^2-\frac{\varepsilon^2}{\xi}\int_0^{+\infty} g(s)\,\mathrm{d}s\|\Delta u\|_2^2$$

By using Poincare inequality, we have

$$\left(-\varepsilon_1\Delta u_t, -\Delta v\right)=\varepsilon_1\left(-\Delta v+\varepsilon\Delta u, -\Delta v\right)=\varepsilon_1\|\Delta v\|_2^2+\varepsilon_1\varepsilon\left(\Delta u, -\Delta u_t-\varepsilon\Delta u\right)$$

$$=\varepsilon_1\|\Delta v\|_2^2-\frac{\varepsilon_1\varepsilon}{2}\frac{\mathrm{d}}{\mathrm{d}t}\|\Delta u\|_2^2-\varepsilon_1\varepsilon^2\|\Delta u\|_2^2, \tag{2.27}$$

and

$$\left(\varepsilon_2 u_t, -\Delta v\right)=\varepsilon_2\left(u_t, -\Delta u_t-\varepsilon\Delta u\right)=\varepsilon_2\|\nabla u_t\|_2^2-\varepsilon_2\varepsilon\|\nabla u\|_2\|\nabla u_t\|_2$$

$$\geq\varepsilon_2\left(1-\frac{\varepsilon}{2}\right)\|\nabla u_t\|_2^2-\frac{\varepsilon_2\varepsilon}{2\lambda_1}\|\Delta u\|_2^2 \tag{2.28}$$

And using Interpolation Theorem, we have

$$\left(\varepsilon_3|u|^{p-2}u, -\Delta v\right)\leq\varepsilon_3\|u\|_{2p-2}^{p-1}\|\Delta v\|_2\leq\varepsilon_3 C_0\left(\|u\|_2\right)\|\Delta u\|_2^{\frac{n(p-2)}{4}}\|\Delta v\|_2$$

$$\leq\frac{\varepsilon_1}{2}\|\Delta v\|_2^2+\frac{\varepsilon_3^2 C_0^2\left(\|u\|_2\right)}{2\varepsilon_1}\|\Delta u\|_2^{\frac{n(p-2)}{2}} \tag{2.29}$$

$$\leq\frac{\varepsilon_1}{2}\|\Delta v\|_2^2+\frac{l\varepsilon}{2}\|\Delta u\|_2^2+C_0\left(\|u\|_2, \varepsilon_1, \varepsilon_3, l, \varepsilon\right).$$

By using Holder inequality and Young's inequality, we have

$$\left(f(x), -\Delta v\right)\leq\|\nabla f\|\cdot\|\nabla v\|\leq\frac{\lambda_1\varepsilon_1}{4}\|\nabla v\|_2^2+\frac{1}{\lambda_1\varepsilon_1}\|\nabla f\|_2^2, \tag{2.30}$$

Then, we have

$$\frac{1}{2}\frac{\mathrm{d}}{\mathrm{d}t}\|\nabla v\|_2^2-\varepsilon\|\nabla v\|_2^2-\frac{\varepsilon^2}{2\lambda_1}\|\Delta u\|_2^2-\frac{\varepsilon^2}{2}\|\nabla v\|_2^2+\frac{l}{2}\frac{\mathrm{d}}{\mathrm{d}t}\|\Delta u\|_2^2+l\varepsilon\|\Delta u\|_2^2$$

$$+\frac{1}{2}\frac{\mathrm{d}}{\mathrm{d}t}\|\eta\|_{g,D(A)}^2+\frac{\xi}{4}\|\eta\|_{g,D(A)}^2-\frac{\varepsilon^2}{\xi}\int_0^{+\infty} g(s)\,\mathrm{d}s\|\Delta u\|_2^2+\varepsilon_1\|\Delta v\|_2^2$$

$$-\frac{\varepsilon_1\varepsilon}{2}\frac{\mathrm{d}}{\mathrm{d}t}\|\Delta u\|_2^2-\varepsilon_1\varepsilon^2\|\Delta u\|_2^2+\varepsilon_2\left(1-\frac{\varepsilon}{2}\right)\|\nabla u_t\|_2^2-\frac{\varepsilon_2\varepsilon}{2\lambda_1}\|\Delta u\|_2^2$$

$$\leq\frac{\varepsilon_1}{2}\|\Delta v\|_2^2+\frac{l\varepsilon}{2}\|\Delta u\|_2^2+C_0\left(\|u\|_2, \varepsilon_1, \varepsilon_3, l, \varepsilon\right)+\frac{\lambda_1\varepsilon_1}{4}\|\nabla v\|_2^2+\frac{1}{\lambda_1\varepsilon_1}\|\nabla f\|_2^2$$

That is

$$\frac{\mathrm{d}}{\mathrm{d}t}\left[\|\nabla v\|_2^2+(l-\varepsilon_1\varepsilon)\|\Delta u\|_2^2+\|\eta\|_{g,D(A)}^2\right]+\left(\frac{\varepsilon_1\lambda_1}{2}-2\varepsilon-\varepsilon^2\right)\|\nabla v\|_2^2$$

$$+2\varepsilon\left(\frac{l}{2}-\varepsilon_1\varepsilon-\frac{\varepsilon}{2\lambda_1}-\frac{\varepsilon}{\xi}\int_0^{+\infty} g(s)\,\mathrm{d}s-\frac{\varepsilon_2}{2\lambda_1}\right)\|\Delta u\|_2^2+\frac{\xi}{2}\|\eta\|_{g,D(A)}^2 \tag{2.31}$$

$$+2\varepsilon_2\left[1-\frac{\varepsilon}{2}\right]\|\nabla u_t\|_2^2\leq\frac{2}{\lambda_1\varepsilon_1}\|\nabla f\|_2^2+2C_0\left(\|u\|_2, \varepsilon_1, \varepsilon_3, l, \varepsilon\right).$$

Next, we take proper $\varepsilon, \varepsilon_1, \varepsilon_2, \varepsilon_3$, such that

$$\begin{cases} b_1 = \dfrac{\varepsilon_1 \lambda_1}{2} - 2\varepsilon - \varepsilon^2 \geq 0 \\[2mm] b_2 = 2\varepsilon \left(\dfrac{l}{2} - \varepsilon_1 \varepsilon - \dfrac{\varepsilon}{2\lambda_1} - \dfrac{\varepsilon}{\xi} \int_0^{+\infty} g(s) \mathrm{d}s - \dfrac{\varepsilon_2}{2\lambda_1} \right) \geq 0 \\[2mm] b_3 = 2\varepsilon_2 \left(1 - \dfrac{\varepsilon}{2} \right) \geq 0 \end{cases} \qquad (2.32)$$

Taking $\alpha_2 = \min \left\{ b_1, \dfrac{b_2}{l - \varepsilon_1 \varepsilon}, \dfrac{\xi}{2} \right\}$, then

$$\frac{\mathrm{d}}{\mathrm{d}t} V(t) + \alpha_2 V(t) \leq \frac{2}{\lambda_1 \varepsilon_1} \|\nabla f\|_2^2 + 2C_0 \left(\|u\|_2, \varepsilon_1, \varepsilon_3, l, \varepsilon \right) := C_2, \qquad (2.33)$$

where $V(t) = \|\nabla v\|_2^2 + (l - \varepsilon_1 \varepsilon) \|\Delta u\|_2^2 + \|\eta\|_{g,D(A)}^2$, by Gronwall inequality, we have

$$V(t) \leq V(0) \mathrm{e}^{-\alpha_2 t} + \frac{C_2}{\alpha_2} \left(1 - \mathrm{e}^{-\alpha_2 t} \right) \qquad (2.34)$$

From $2 < p \leq \dfrac{2n}{n-2}$, according to Embedding Theorem, then $H^2(\Omega) \subset W^{1,p}(\Omega)$, let $k = \min \left\{ 1, (l - \varepsilon_1 \varepsilon) \right\}$, so, we have

$$\|(u,v)\|_{H^2 \times H^1}^2 = \|\Delta u\|_2^2 + \|\nabla v\|_2^2 \leq \frac{V(0)}{k} \mathrm{e}^{-\alpha_2 t} + \frac{C_2}{\alpha_2 k} \left(1 - \mathrm{e}^{-\alpha_2 t} \right)$$

then

$$\overline{\lim_{t \to \infty}} \|(u,v)\|_{H^2 \times H^1}^2 \leq \frac{C_2}{\alpha_2 k}$$

So, there exists $E_1 > 0$ and $t_2 = t_2(\Omega) > 0$, such that

$$\|(u,v)\|_{H^2 \times H^1}^2 = \|\Delta u(t)\|_2^2 + \|\nabla v(t)\|_2^2 \leq E_1 \quad (t > t_2).$$

3. Global Attractors

Theorem 1. Assume (G1), (G2) and (G3) hold, let

$$\begin{cases} 2 < p < \min \left\{ \dfrac{2n}{n-2}, \dfrac{2n+4}{n} \right\}, & n \geq 3 \\[2mm] p \geq 2, & n = 1, 2 \end{cases}$$

and $(u_0, u_1) \in H^2(\Omega) \times H^1(\Omega)$, $f \in H^1(\Omega)$, $v = u_t + \varepsilon u$, so Equation (1.3) exists a unique smooth solution

$$(u,v) \in L^{\infty} \left([0, +\infty); H^2(\Omega) \times H^1(\Omega) \right)$$

Proof. By the method of Galerkin and **Lemma 1** and **Lemma 2**, we can easily obtain the existence of solutions. Next, we prove the uniqueness of solutions in detail.

Assume that u, v are two solutions of equation, let $w = u - v$, then, the two equations subtract and obtain

$$w'' - \left(1 - \int_0^{+\infty} g(s) \mathrm{d}s \right) \Delta w - \int_0^{+\infty} g(s) (\Delta \eta_1 - \Delta \eta_2) \mathrm{d}s - \varepsilon_1 \Delta w' + \varepsilon_2 w'$$
$$= \varepsilon_3 \left(|v|^{p-2} v - |u|^{p-2} u \right) \qquad (3.1)$$

where

$$\eta_1 = u(x,t) - u(x,t-s), \; \eta_2 = v(x,t) - v(x,t-s) \tag{3.2}$$

By multiplying the equation by w' and integrating over Ω, we get

$$\left(w'' - \left(1 - \int_0^{+\infty} g(s) \, ds\right) \Delta w - \int_0^{+\infty} g(s)(\Delta \eta_1 - \Delta \eta_2) \, ds - \varepsilon_1 \Delta w' + \varepsilon_2 w', w' \right)$$
$$= \left(\varepsilon_3 \left(|v|^{p-2} v - |u|^{p-2} u \right), w' \right) \tag{3.3}$$

here

$$(w'', w') = \frac{1}{2} \frac{d}{dt} \|w'\|_2^2 \tag{3.4}$$

and

$$\left(-\left(1 - \int_0^{+\infty} g(s) \, ds\right) \Delta w, w' \right) = \frac{l}{2} \frac{d}{dt} \|\nabla w\|_2^2 \tag{3.5}$$

by using (G1), (G2) and (G3), we have

$$\left(-\int_0^{+\infty} g(s)(\Delta \eta_1 - \Delta \eta_2) \, ds, w' \right) = \left(-\int_0^{+\infty} g(s)(\Delta \eta_1 - \Delta \eta_2) \, ds, (\eta_1 - \eta_2)_t + (\eta_1 - \eta_2)_s \right)$$
$$\geq \frac{1}{2} \frac{d}{dt} \|\eta_1 - \eta_2\|_{g,V}^2 + \frac{\xi}{2} \|\eta_1 - \eta_2\|_{g,V}^2 \tag{3.6}$$

By using Poincare inequality, we have

$$\left(-\varepsilon_1 \Delta w', w' \right) = \varepsilon_1 \|\nabla w'\|_2^2 \geq \varepsilon_1 \lambda_1 \|w'\|_2^2 \tag{3.7}$$

and

$$\left(\varepsilon_2 w', w' \right) = \varepsilon_2 \|w'\|_2^2 \tag{3.8}$$

By using Holder inequality, Young's inequality and Poincare inequality, we have

$$\varepsilon_3 \left(|u|^{p-2} u - |v|^{p-2} v, w' \right) = \varepsilon_2 \int \left(|u|^{p-2} u - |v|^{p-2} v \right) w' \, dx$$
$$\leq \varepsilon_2 p \int \left(|u|^{p-1} + |v|^{p-1} \right) |w| |w'| \, dx \leq \varepsilon_3 C_0 \|w\| \|w'\| \tag{3.9}$$
$$\leq 2\varepsilon_3 \lambda_1 \|w'\|_2^2 + \frac{\varepsilon_3 C_0^2}{8\lambda_1} \|w\|_2^2 \leq 2\varepsilon_3 \lambda_1 \|w'\|_2^2 + \frac{\varepsilon_3 C_0^2}{8\lambda_1^2} \|\nabla w\|_2^2$$

then, we have

$$\frac{1}{2} \frac{d}{dt} \|w'\|_2^2 + \frac{l}{2} \frac{d}{dt} \|\nabla w\|_2^2 + \frac{1}{2} \frac{d}{dt} \|\eta_1 - \eta_2\|_{g,V}^2 + \frac{\xi}{2} \|\eta_1 - \eta_2\|_{g,V}^2 + \varepsilon_1 \lambda_1 \|w'\|_2^2 + \varepsilon_2 \|w'\|_2^2$$
$$\leq 2\varepsilon_3 \lambda_1 \|w'\|_2^2 + \frac{\varepsilon_3 C_0^2}{8\lambda_1^2} \|\nabla w\|_2^2 \tag{3.10}$$

That is

$$\frac{d}{dt} \left[\|w'\|_2^2 + l \|\nabla w\|_2^2 + \|\eta_1 - \eta_2\|_{g,V}^2 \right] \leq 4\varepsilon_3 \lambda_1 \|w'\|_2^2 + \frac{\varepsilon_3 C_0^2}{4\lambda_1^2} \|\nabla w\|_2^2 + \|\eta_1 - \eta_2\|_{g,V}^2 \tag{3.11}$$

Taking $m = \max \left\{ 4\varepsilon_3 \lambda_1, \frac{\varepsilon_3 C_0^2}{4\lambda_1^2 l}, 1 \right\}$, then

$$\frac{\mathrm{d}}{\mathrm{d}t}\left[\left\|w'\right\|_2^2 + l\left\|\nabla w\right\|_2^2 + \left\|\eta_1 - \eta_2\right\|_{g,V}^2\right] \le m\left(\left\|w'\right\|_2^2 + l\left\|\nabla w\right\|_2^2 + \left\|\eta_1 - \eta_2\right\|_{g,V}^2\right) \tag{3.12}$$

By using Gronwall inequality, we have

$$\left\|w'\right\|_2^2 + l\left\|\nabla w\right\|_2^2 + \left\|\eta_1 - \eta_2\right\|_{g,V}^2 \le \left[\left\|w'(0)\right\|_2^2 + l\left\|\nabla w(0)\right\|_2^2 + \left\|\eta_1(0) - \eta_2(0)\right\|_{g,V}^2\right]\mathrm{e}^{mt} \tag{3.13}$$

So we get $w(t) \equiv 0$, the uniqueness is proved.

Theorem 2. Let X be a Banach space, and $\{S(t)\}\,(t \ge 0)$ are the semigroup operator on X. $S(t): X \to X$, $S(t)S(\tau) = S(t+\tau)$, $S(0) = I$, here I is a unit operator. Set $S(t)$ satisfy the follow conditions.

1) $S(t)$ is bounded, namely $\forall R > 0$, $\left\|u\right\|_X \le R$, it exists a constant $C(R)$, so that

$$\left\|S(t)u\right\|_X \le C(R)\ \left(t \in [0,+\infty)\right)$$

2) It exists a bounded absorbing set $B_0 \subset X$, namely, $\forall B \subset B_0$, it exists a constant t_0, so that

$$S(t)B \subset B_0\ (t \ge t_0)$$

3) When $t > 0$, $S(t)$ is a completely continuous operator A.

Therefore, the semigroup operators $S(t)$ exist a compact global attractor.

Theorem 3. Under the assume of **Theorem 1**, equations have global attractor

$$A = \omega(B_0) = \bigcap_{s \ge 0}\overline{\bigcup_{t \ge s} S(t)B_0}$$

where $B_0 = \left\{(u,v) \in H_0^2 \times H^1 : \left\|(u,v)\right\|_{H_0^2 \times H^1}^2 = \left\|u\right\|_{H_0^2}^2 + \left\|v\right\|_{H^1}^2 \le E_0 + E_1\right\}$, B_0 is the bounded absorbing set of $H^2(\Omega) \times H_0^1(\Omega)$ and satisfies

1) $S(t)A = A$, $t > 0$;
2) $\lim_{t \to \infty} dist\left(S(t)B_0, A\right) = 0$, here $B \subset H_0^2(\Omega) \times H^1(\Omega)$ and it is a bounded set,

$$dist(X,Y) = \sup_{x \in X}\inf_{y \in Y}\left\|x - y\right\|_{H^2 \times H^1}$$

Proof. Under the conditions of **Theorem 1**, it exists the solution semigroup $S(t)$, here $X = H_0^2(\Omega) \times H^1(\Omega)$, $S(t): H^2 \times H^1 \to H^2 \times H^1$.

1) From **Lemma 1** to **Lemma 2**, we can get that $\forall B \subset H_0^2(\Omega) \times H^1(\Omega)$ is a bounded set that includes in the ball $\left\{\left\|(u,v)\right\|_{H_0^2 \times H^1} \le R\right\}$,

$$\left\|S(t)(u_0,v_0)\right\|_{H^2 \times H_0^1}^2 = \left\|u\right\|_{H^2}^2 + \left\|v\right\|_{H_0^1}^2 \le \left\|u_0\right\|_{H^2}^2 + \left\|v_0\right\|_{H_0^1}^2 + C \le R^2 + C,\ \left(t \ge 0, (u_0,v_0) \in B\right)$$

This shows that $S(t)\,(t \ge 0)$ is uniformly bounded in $H^2(\Omega) \times H_0^1(\Omega)$.

2) Furthermore, for any $(u_0,v_0) \in H^2(\Omega) \times H^1(\Omega)$, when $t \ge \max\{t_1,t_2\}$, we have

$$\left\|S(t)(u_0,v_0)\right\|_{H_0^2 \times H^1}^2 = \left\|u\right\|_{H_0^2}^2 + \left\|v\right\|_{H^1}^2 \le E_0 + E_1$$

So, we get B_0 is the bounded absorbing set.

3) Since $H^2(\Omega) \times H_0^1(\Omega) \to H_0^1(\Omega) \times L^2(\Omega)$ is tightly embedded, which means that the bounded set in $H^2(\Omega) \times H_0^1(\Omega)$ is the tight set in $H_0^1(\Omega) \times L^2(\Omega)$, so the semigroup operator $S(t)$ is completely continuous.

So, the semigroup operators $S(t)$ exist a compact global attractor A. The proof is completed.

Acknowledgements

Funding

References

[1] Messaoudi, S.A. (2003) Blow Up and Global Existence in a Nonlinear Viscoelastic Wave Equation. *Mathematische Nachrichten*, **260**, 58-66. http://dx.doi.org/10.1002/mana.200310104

[2] Cavalcanti, M.M., Domingos Cavalcanti, V.N. and Ferreira, J. (2001) Existence and Uniform Decay for Nonlinear Viscoelastic Equation with Strong Damping. *Mathematical Methods in the Applied Sciences*, **24**, 1043-1053. http://dx.doi.org/10.1002/mma.250

[3] Berrimi, S. and Messaoudi, S.A. (2006) Existence and Decay of Solutions of a Viscoelastic Equation with a Nonlinear Source. *Nonlinear Analysis*: *Theory*, *Methods* & *Applications*, **64**, 2314-2331. http://dx.doi.org/10.1016/j.na.2005.08.015

[4] Lu, L.Q. and Li, S.J. (2011) Cauchy Problem for a Nonlinear Viscoelastic Equation with Nonlinear Damping and Source Term. *Applied Mathematics Letters*, **24**, 1275-1281. http://dx.doi.org/10.1016/j.aml.2011.01.009

[5] Kafini, M. and Mustafa, M.I. (2014) Blow-Up Result in a Cauchy Viscoelastic Problem with Strong Damping and Dispersive. *Nonlinear Analysis*: *Real World Applications*, **20**, 14-20. http://dx.doi.org/10.1016/j.nonrwa.2014.04.005

[6] Araújo, R.O., Ma, T. and Qin, Y.M. (2013) Long-Time Behavior of a Quasilinear Viscoelastic Equation with Past History. *Journal of Differential Equations*, **254**, 4066-4087. http://dx.doi.org/10.1016/j.jde.2013.02.010

[7] Qin, Y.M., Feng, B.W. and Zhang, M. (2014) Uniform Attractors for a Non-Autonomous Viscoelastic Equation with a Past History. *Nonlinear Analysis*: *Theory*, *Methods* & *Applications*, **101**, 1-15. http://dx.doi.org/10.1016/j.na.2014.01.006

[8] Qin, Y.M., Zhang, J.P. and Sun, L.L. (2013) Upper Semicontinuity of Pull Back Attractors for a Non-Autonomous Viscoelastic Equation. *Applied Mathematics and Computation*, **223**, 362-376. http://dx.doi.org/10.1016/j.amc.2013.08.034

[9] Conti, M. and Geredell, P.G. (2015) Existence of Smooth Global Attractors for Nonlinear Viscoelastic Equations with Memory. *Journal of Evolution Equations*. http://dx.doi.org/10.1007/s00028-014-0270-2

[10] Cavalcanti, M.M., Domingos Cavalcanti, V.N., Prates Filho, J.A. and Soriano, J.A. (2001) Existence and Uniform Decay Rates for Viscoelastic Problems with Non-Linear Boundary Damping. *Differential and Integral Equations*, **14**, 85-116.

[11] Muñoz Rivera, J.E., Lapa, E.C. and Barreto, R. (1996) Decay Rates for Viscoelastic Plates with Memory. *Journal of Elasticity*, **44**, 61-87. http://dx.doi.org/10.1007/BF00042192

[12] Wu, S.T. (2011) General Decay of Solutions for a Viscoelastic Equation with Nonlinear Damping and Source Terms. *Acta Mathematica Scientia*, **31**, 1436-1448. http://dx.doi.org/10.1016/S0252-9602(11)60329-9

[13] Ma, T.F. and Narciso, V. (2010) Global Attractor for a Model of Extensible Beam with Nonlinear Damping and Source Terms. *Nonlinear Analysis*: *Theory*, *Methods* & *Applications*, **73**, 3402-3412. http://dx.doi.org/10.1016/j.na.2010.07.023

[14] Qin, Y., Deng, S. and Schulze, W. (2009) Uniform Compact Attractors for a Nonlinear Non-Autonomous Equation of Viscoelasticity. *Journal of Partial Differential Equations*, **22**, 153-198.

Induction Motor Modeling Based on a Fuzzy Clustering Multi-Model—A Real-Time Validation

Abid Aicha, Bnhamed Mouna, Sbita Lassaad

National Engineering School of Gabes, Photovoltaic, Wind and Geothermal Systems Research, Gabes, Tunisia
Email: aicha.abid@gmail.com, benhamed2209@yahoo.fr, Lassaad.sbita@enig.rnu.tn

Abstract

This paper discusses a comparative study of two modeling methods based on multimodel approach. The first is based on C-means clustering algorithm and the second is based on K-means clustering algorithm. The two methods are experimentally applied to an induction motor. The multimodel modeling consists in representing the IM through a finite number of local models. This number of models has to be initially fixed, for which a subtractive clustering is necessary. Then both C-means and K-means clustering are exploited to determine the clusters. These clusters will be then exploited on the basis of structural and parametric identification to determine the local models that are combined, finally, to form the multimodel. The experimental study is based on MATLAB/SIMULINK environment and a DSpace scheme with DS1104 controller board. Experimental results approve that the multimodel based on K-means clustering algorithm is the most efficient.

Keywords

Multi-Model Modeling, C-means Clustering Algorithm, K-Means Clustering Algorithm, Induction Motor (IM), Experimental Validation

1. Introduction

Induction motors are the basis elements in industrial applications thanks to their economic cost, judicious size, and easy maintenance [1] [2]. However, these motors are complex and have a strongly nonlinear system. It is often hard to determine an adequate model that represents all the dynamic behavior of this machine.

Modeling is an essential initial step in the industrial process control. This fundamental step is necessary either for a control law development or for the development of a diagnosis procedure. Modeling a process consists in establishing relationships between its characteristics variables and in representing the dynamic behavior of this process in a particular field of operation.

Based on a priori knowledge of the studied process, many modeling types are used. The increasing complexity of industrial process pushes many researchers to develop modeling techniques that exploit linear systems tools. Hence, in this paper we will consider the modeling based on multimodel approach that recently, has been implemented in various science and engineering domains, concerning application to modeling, control and fault diagnosis [3]-[10].

The multimodel approach consists in replacing the unique nonlinear model by a set of simpler linear models to create a model-base. Generally, each model of this base contributes to the whole description of the considered system through weighed functions or validities functions.

The modeling via this approach needs to follow up a scheme of four steps that are database acquisition, clustering, structural and parametric identification and fusion.

For clustering, many algorithms are adopted in literature [11]-[14], in this paper we will focus on three fuzzy clustering algorithms that are subtractive, C-means and K-means clustering algorithms. The subtractive algorithm is used to determine the cluster number, whereas the C-means and the K-means will be exploited to generate the cluster centers then to construct the clusters. Thus, we will compare two modeling methods, the first is based on the association of subtractive-C-means algorithm and the second is based on the association of subtractive-K-means algorithm.

The two proposed modeling method are experimentally implemented to an induction motor.

The organization of this paper is as follows. The second part consists in describing the modeling with multimodel approach, the third part develops the application of the two modeling methods based on the two clustering algorithm to the induction motor. The part four is a comparative study of the two modeling method and finally the conclusion is in the fifth part.

2. Multi-Model Modeling

To obtain a multimodel, we have to follow a strategy of four stages that are database acquisition, data clustering, structural and parametric identification and local models fusion.

The system is considered as a black box. Thus, it is exited via a rich frequency input. The collected data is consisting of a set of input/output measurements. Then the collected data will be divided into N clusters through clustering algorithms. Later, three clustering algorithms will be developed: the subtractive, C-means and K-means algorithm. Next, structural and parametric identification follow the clustering to obtain the local models. The structural identification is achieved using the general procedure of order estimation and the Instrumental determinant ratio (IDR). For the parametric identification, the generalized recursive least square is implemented. The obtained local models are combined through weighted functions that are calculated based on residue approach [5]-[8].

Two strategies are adopted. The first is based on the C-means clustering algorithm and the second is based on K-means clustering method as shown in **Figure 1** and **Figure 2**.

3. The Clustering Algorithms

Clustering data consists of organizing and collecting similar data points into group or cluster. The similarity is estimated by a function that computes the distance between the data points, usually, the Euclidean distance.

In literature, various clustering algorithm was proposed to deal with clustering problem [11]-[14]. Subtractive, C-means and K-means are among the most commonly-used clustering algorithm

3.1. Subtractive Clustering

The subtractive clustering algorithm was suggested by Chiu as an extension of the mountain function. It is able to determine the number and the value of cluster centers.

The process is provided with the following steps.
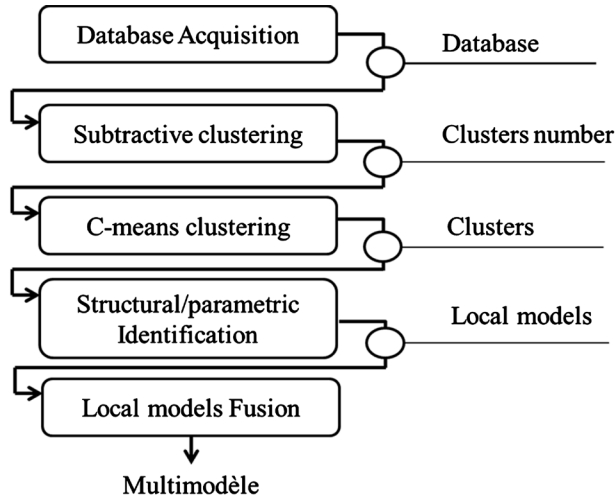
Figure 1. Modeling strategy based on C-means clustering algorithm.
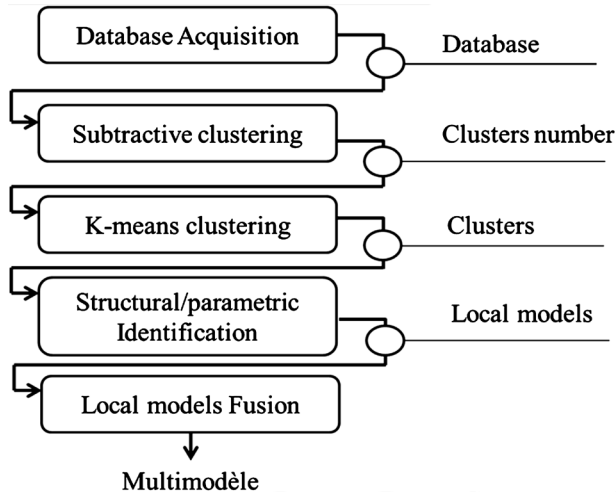
Figure 2. Modeling strategy based on K-means clustering algorithm.

1) Each data point is considered as a cluster center that has the calculated potential p_i given in (1).

$$p_i = \sum_{j=1}^{n} e^{-4\frac{\left\| y_{pi} - y_{pj} \right\|^2}{r_a^2}} \tag{1}$$

where r_a defines the neighborhood radius.

The data with the high potential is the first cluster center.

2) The data potentials are recalculated by (2).

$$p_i \leftarrow p_i - p_1^* e^{-4\frac{\left\| y_{pi} - y_{p1} \right\|^2}{r_b^2}} \tag{2}$$

where $r_b > 0$ is the new neighborhood radius that must be rather greater then r_a to not having cluster centers that are closely spaced. Usually $r_b = 1.5 r_a$.

3) The process is repeated until the obtaining of the k-th center and the potentials are recalculated by (3).

$$p_i \leftarrow p_i - p_k^* e^{-4\frac{\left\| y_{pi} - y_{pk} \right\|^2}{r_b^2}} \tag{3}$$

4) The process is repeated until the following condition (4).

$$P_k^* < \varepsilon P_1^* \qquad (4)$$

3.2. C-Means Clustering

The C-means known as FCM is a data clustering algorithm that considers that each data point belongs to a cluster through a membership function. It consists in producing an optimal partition by minimizing the objective function J on the basis of the following process.

1) Initialize arbitrarily the Fuzzy membership matrix μ_{ik}
2) Calculate the cost function J by (5).

$$J = \sum_{i=1}^{c} J_i = \sum_{i=1}^{c} \sum_{k=1}^{N} \left(\mu_{ik}^g \right) d_{ik}^2 \qquad (5)$$

3) Estimate the clusters centers c_i by the Equation (6).

$$c_i = \frac{\sum_{k=1}^{N} \left(\mu_{ik} \right)^g x_k}{\sum_{k=1}^{N} \left(\mu_{ik} \right)^g} \qquad (6)$$

4) Updates the membership functions as the relation (7).

$$\mu_{ik} = \frac{1}{\sum_{j=1}^{c} \left(\dfrac{d_{ik}}{d_{jk}} \right)^{2/(g-1)}} \qquad (7)$$

5) Recalculate the cost function J. If J is less than a threshold, the process will be ended. If not, return to step 3.

3.3. K-Means Clustering

The K-means clustering algorithm is known as an efficient and rapid one. It is able to construct a fixed finite number of clusters by minimizing the Euclidean distance between the data and the equivalent cluster center.

The K-means clustering algorithm is detailed by the following process.

1) Select arbitrarily cluster centers c_i from the training data set.
2) Calculate the membership matrix u_{ij} using the Equation (8).

$$u_{ij} = \begin{cases} 1 & \text{if } \left\| x_j - c_i \right\|^2 \leq \left\| x_j - c_k \right\|^2, \ k \neq i \\ 0 & \text{else} \end{cases} \qquad (8)$$

3) Calculate the cost function J by the Equation (9). Stop the process if it is less than a certain threshold.

$$J = \sum_{i=1}^{c} J_i = \sum_{i=1}^{c} \left(\sum_{k, x_k \in G_i} \left\| x_k - c_i \right\|^2 \right) \qquad (9)$$

4) Update the cluster center c_i according to the relation (10).

$$c_i = \frac{1}{|G_i|} \sum_{k, x_k \in G_i} x_k \qquad (10)$$

Next, return to step 2.

4. Application of the Two Modeling Strategy on the IM

We propose in this section to modeling the IM by the two multimodel modeling strategies previously described.

Firstly, we have to collect a rich data base from the measurement of input/output of the IM. The electric motor is 1 kw squirrel cage Induction motor.

The training data set is generated through an experimental set-up that is described by **Figure 3**. It is used with the help of Matlab/Simulink and DSpace system with DS1104 controller board to collect the database.

The data collection requires the use of speed and current sensors. For that, Hall type sensors are exploited to measure stator currents and an incremental encoder position sensor delivering 1024 pulses per revolution is mounted on the shaft to measure the IM speed.

To test the robustness of the modeling approach we propose to vary the IM parameter and to apply a wide range of loads.

The load is a resistive bank fed by a DC generator that is connected to the IM.

To vary the stator resistances, three variable resistors are linked in series to the motor phases.

A large data set is selected out after input/output measurements at an operating point of 600 rpm.

4.1. Modeling of IM via the Method Based on C-Means Clustering Algorithm

The subtractive clustering algorithm helps to determine the clusters number that is N = 8. So, the objective of the C-means clustering is to generate these eight clusters.

The obtained clusters will be identified to obtain the local models that are defined by these recurrent equations.

$$M_1\left(q^{-1}\right) = q^{-1}\frac{-0.0583}{1+0.4542q^{-1}} \tag{11}$$

$$M_2\left(q^{-1}\right) = q^{-1}\frac{0.500}{1+0.4974q^{-1}} \tag{12}$$

$$M_3\left(q^{-1}\right) = q^{-1}\frac{0.0212}{1+0.9793q^{-1}} \tag{13}$$

$$M_4\left(q^{-1}\right) = q^{-1}\frac{0.0137}{1+0.9864q^{-1}} \tag{14}$$

$$M_5\left(q^{-1}\right) = q^{-1}\frac{0.0053}{1+0.3514q^{-1}} \tag{15}$$

$$M_6\left(q^{-1}\right) = q^{-1}\frac{0.0459}{1+0.9517q^{-1}+0.1215q^{-2}} \tag{16}$$

Figure 3. Experimental set up.

$$M_7\left(q^{-1}\right)=q^{-1}\frac{0.1853}{1+0.4071q^{-1}} \tag{17}$$

$$M_8\left(q^{-1}\right)=q^{-1}\frac{0.0466}{1+0.4808q^{-1}} \tag{18}$$

The combination of the local models through the validities shown in **Figure 4** helps to construct the final multimodel as shown in **Figure 5**.

4.2. Modeling of IM via the Method Based on K-Means Clustering Algorithm

The same modeling process is respected. In fact, the K-means clustering is applied in order to generate the eight clusters that will be identified and combined to create the multimodel.

The local models are described by the following discrete transfer functions (19)-(26).

$$M_1\left(q^{-1}\right)=q^{-1}\frac{0.0285}{1+0.1313q^{-1}-0.1460q^{-2}} \tag{19}$$

$$M_2\left(q^{-1}\right)=q^{-1}\frac{0.0167}{1+0.0438q^{-1}-0.0460q^{-2}} \tag{20}$$

$$M_3\left(q^{-1}\right)=q^{-1}\frac{0.0818}{1+0.5068q^{-1}-0.4906q^{-2}} \tag{21}$$
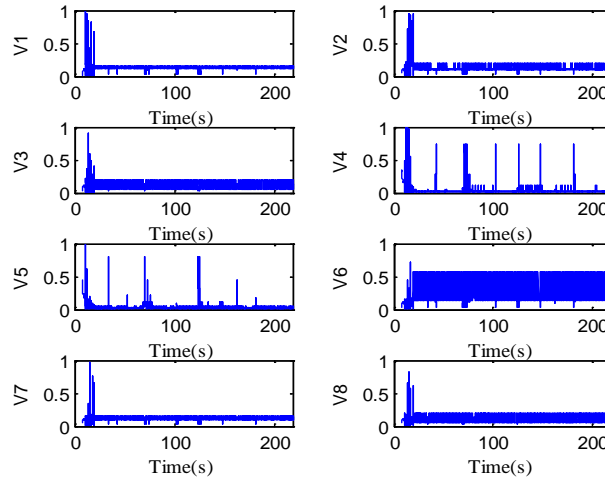
Figure 4. The validities evolutions.
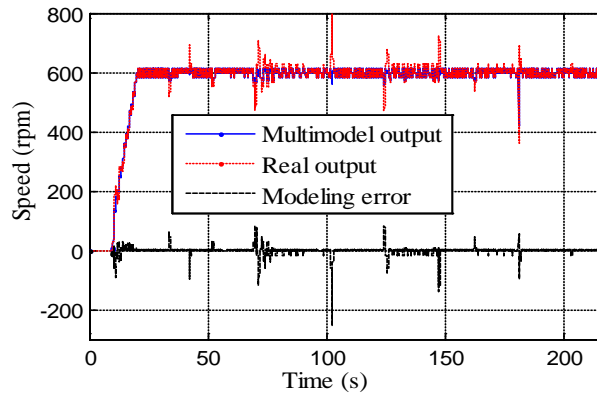
Figure 5. Multimodel modeling of IM based on C-means.

$$M_4\left(q^{-1}\right) = q^{-1}\frac{-0.0003}{1+0.9977q^{-1}-0.0061q^{-2}} \tag{22}$$

$$M_5\left(q^{-1}\right) = q^{-1}\frac{0.0826}{1+0.4881q^{-1}-0.4940q^{-2}} \tag{23}$$

$$M_6\left(q^{-1}\right) = q^{-1}\frac{0.2096}{1+0.3435q^{-1}} \tag{24}$$

$$M_7\left(q^{-1}\right) = q^{-1}\frac{0.985}{1+0.6524q^{-1}+0.2575q^{-2}} \tag{25}$$

$$M_8\left(q^{-1}\right) = q^{-1}\frac{0.4693}{1+0.2808q^{-1}+0.6508q^{-2}} \tag{26}$$

The obtained results are illustrated by **Figure 6** that illustrates the evolution of the real speed and the modeled speed.

The different validities functions are illustrated by **Figure 7**.
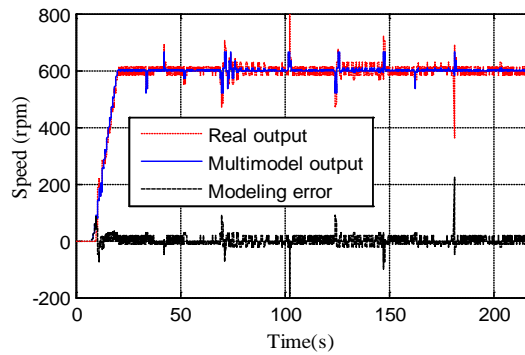
Figure 6. Multimodel modeling of IM based on K-means.
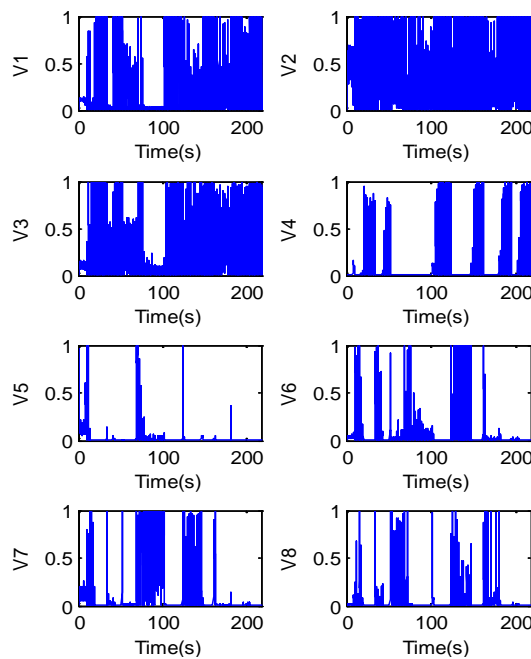
Figure 7. Validities evolutions.

Table 1. Comparative study of the two modeling strategies.

Algorithms	NRMSE
C-means	0.0210
K-means	0.0177

We propose to compare the two modeling strategies. Therefore, we calculate for each strategy the normalized roots mean square modeling error NRMSE. Then, a comparative table (**Table 1**) is dressed.

We can notice that the method based on K-means clustering algorithm is the most convergent as the NRMSE calculated is the lowest.

5. Conclusion

In this paper, the multimodel modeling strategy is described. Two strategies are developed. The first is on the basis of C-means clustering algorithm and the second is based on K-means clustering algorithm. The two methods are applied in real time to an induction motor at an operating point of 600 rpm submissive to load insertion and parameter variation. A comparative study helps to confirm that the method based on K-means is the most convergent. In future work, to improve the modeling performance the modeling should take into account the total behavior of the induction motor.

References

[1] Salahat, M., Barbarawe, O., Abu Zalata, M. and Asad, S. (2011) Modular Approach for Investigation of the Dynamic Behavior of Three-Phase Induction Machine at Load Variation. *Engineering*, **3**, 525-531. http://dx.doi.org/10.4236/eng.2011.35061

[2] Vodovozov, V., Gevorkov, L. and Raud, Z. (2014) Modeling and Analysis of Pumping Motor Drives in Hardware-in-the-Loop Environment. *Journal of Power and Energy Engineering*, **2**, 19-27. http://dx.doi.org/10.4236/jpee.2014.210003

[3] Men, Z.X., Yee, E., Lien, F.-S., Ji, H. and Liu, Y.Q. (2014) Bootstrapped Multi-Model Neural-Network Super-Ensembles for Wind Speed and Power Forecasting. *Energy and Power Engineering*, **6**, 340-348. http://dx.doi.org/10.4236/epe.2014.611029

[4] Shankar, H., Raju P.L.N. and Rao, K.R.M. (2012) Multi Model Criteria for the Estimation of Road Traffic Congestion from Traffic Flow Information Based on Fuzzy Logic. *Journal of Transportation Technologies*, **2**, 50-62. http://dx.doi.org/10.4236/jtts.2012.21006

[5] Abid, A., Ben Hamed, M. and Sbita, L. (2011) Induction Motor Real Time Application of Multimodel Modeling Approach. *International Review of Electrical Engineering* (*IREE*), **6**, 655-660.

[6] Abid, A., Adouni, A., Ben Hamed, M. and Sbita, L. (2012) A New PV Cell Model Based On Multi Model Approach. *The* 4*th International Renewable Energy Congress*, Sousse, 20-22 December 2012, 1447-1452.

[7] Abid A., Ben Mabrouk Z., Ben Hamed M., Sbita L., (2013) Multiple Lunberger Observer for an Induction Motor Represented by Decoupled Multiple Model. 10*th International Multi-Conference on Systems*, *Signals* & *Devices* (*SSD*) Hammamet, March 18-21 2013, 1-6. http://dx.doi.org/10.1109/ssd.2013.6564050

[8] Elfelly, N., Dieulot, J.-Y., Benrejeb, M. and Borne, P. (2012) A Multimodel Approach for Complex Systems Modeling Based on Classification Algorithms. *International Journal of Computers Communications Control*, **7**, 644-659.

[9] Orjuela, R., Marx, B., Ragot, J. and Maquin, D. (2013) Nonlinear System Identification Using Heterogeneous Multiple Models. *International Journal of Applied Mathematics and Computer Science*, **23**, 103-115. http://dx.doi.org/10.2478/amcs-2013-0009

[10] Hamdi, H., Rodrigues, M., Mechmeche, C., Theilliol, D. and BenHadj Braiek, N., (2012) Fault Detection and Isolation in Linear Parameter-Varying Descriptor Systems via Proportional Integral Observer. *International Journal of Adaptive Control and Signal Processing*, **26**, 224-240. http://dx.doi.org/10.1002/acs.1260

[11] Guldemır, H. and Sengur, A. (2006) Comparison of Clustering Algorithms for Analog Modulation Classification. *Expert Systems with Applications*, **30**, 642-649. http://dx.doi.org/10.1016/j.eswa.2005.07.014

[12] Velmurugan, T. (2014) Performance Based Analysis between K-Means and Fuzzy C-Means Clustering Algorithms for Connection Oriented Telecommunication Data. *Applied Soft Computing*, **19**, 134-146. http://dx.doi.org/10.1016/j.asoc.2014.02.011

[13] Chiu, S.L. (1994) Fuzzy Model Identification Based on Cluster Estimation. *Journal of Intelligent and Fuzzy Systems*, **2**, 267-278.

[14] Fan, J.L. and Li, J. (2014) A Fixed Suppressed Rate Selection Method for Suppressed Fuzzy C-Means Clustering Algorithm. *Applied Mathematics*, **5**, 1275-1283. http://dx.doi.org/10.4236/am.2014.58119

A DFIM Sensor Faults Multi-Model Diagnosis Approach Based on an Adaptive PI Multiobserver—Experimental Validation

Abid Aicha, Benhamed Mouna, Sbita Lassaad

National Engineering School of Gabes, Tunisia, Photovoltaic, Wind and Geothermal Systems Research, Gabes, Tunisia
Email: aicha.abid@gmail.com, benhamed2209@yahoo.fr, Lassaad.sbita@enig.rnu.tn

Abstract

This paper studies the problem of diagnosis strategy for a doubly fed induction motor (DFIM) sensor faults. This strategy is based on unknown input proportional integral (PI) multiobserver. Thecontribution of this paper is on one hand the creation of a new DFIM model based on multi-model approach and, on the other hand, the synthesis of an adaptive PI multi-observer. The DFIM Volt per Hertz drive system behaves as a nonlinear complex system. It consists of a DFIM powered through a controlled PWM Voltage Source Inverter (VSI). The need of a sensorless drive requires soft sensors such as estimators or observers. In particular, an adaptive Proportional-Integral multi-observer is synthesized in order to estimate the DFIM's outputs which are affected by different faults and to generate the different residual signals symptoms of sensor fault occurrence. The convergence of the estimation error is guaranteed by using the Lyapunov's based theory. The proposed diagnosis approach is experimentally validated on a 1 kW Induction motor. Obtained simulation results confirm that the adaptive PI multiobserver consent to accomplish the detection, isolation and fault identification tasks with high dynamic performances.

Keywords

Diagnosis, Doubly Fed Induction Motor, Multi-Model Approach, Adaptive PI Multi-Observer

1. Introduction

Doubly-fed induction machine (DFIM) has become the most competitive choice in several applications related with renewable energy especially wind energy as a generator or as a motor for industrial applications such as

rolling, rail traction or even marine propulsion or pumping. Nevertheless, it arrives that this machine presents an electric or mechanical defect.

In recent years, the development of fault diagnosis techniques has become an important issue seen the continuing evolution of modern systems complexity and the increasing demand for improving the reliability and security of controlled systems [1]-[5].

Observer-based diagnosis method is one of the wide variety of different diagnosis approaches that have already been proposed in the literature, these approaches are based on the use of an adequate model [6]-[10]. It is often difficult to synthesize a sufficient model that is able to take into account the system's nonlinearity and complexity. Thus many different approaches have been developed to deal with this problem. As a solution, multi-model approach is one of the most widely used modeling techniques. This approach consists in representing the whole behavior of a nonlinear system by a set of simple local models. Generated sub models are then combined using validity function to contribute to the construction of the whole model [11]-[13]. Indeed, the multi-models facilitate the extension of some analysis tools that are developed in linear context to nonlinear context.

Then, faults diagnosis consists in the use of multiobserver based on decoupled multi-model structure [14]-[19].

Within this diagnosis context, the main objective of this paper is the detection and isolation of different types of sensor faults that may affect the doubly fed induction motor.

As it is the workhorse of industry, the use of the doubly fed induction machine (DFIM) in industrial applications has grown impressively in recent years especially for variable speed applications. Thus, an increasingly growing interest is given to the implementation of a supervision process to ensure a safe application of this machine. As the DFIM is a nonlinear complex system that is subject of load disturbances, it is often difficult to synthesize a single model, therefore, a single observer that is able to detect and isolate the system's faults. Thus the multi-model approach may be a solution to facilitate diagnosis task.

This paper treats the different steps for the study of the diagnosis of DFIM sensor faults based on multimodel approach. Starting with the decoupled multi-model modeling of the DFIM Volt per Hertz drive system which consists of a DFIM powered through a controlled PWM Voltage Source Inverter (VSI) in presence of load disturbances, next the design of an adaptive PI multi-observer that will be exploited finally for the faults detection. The adaptive PI multi-observer is synthesized after modification of the PI multi-observer in the case of variable faults. Finally, the proposed diagnosis approach is validated experimentally on an Induction motor.

Section 2 is dedicated to DFIM modeling in the dq synchronous reference frame. Section 3 deals with the DFIM modeling via decoupled multiple model approach respecting the different steps that lead to the realization of this task. In section 4 an adaptive PI multiobserver is synthesized to be used in section 5 for the detection and isolation of sensor faults that can affect the motor. Section 6 is an experimental validation of the proposed diagnosis method on a squirrel cage induction motor.

Simulation and experimental results for the DFIM multi-model modeling and the implementation of the diagnosis approach are performed by using the environment MATLAB/SIMULINK.

2. Classic DFIM Modeling

The DFIM Volt per Hertz drive system consists of a DFIM powered through the grid in stator side and a PWM inverter in the rotor side [1]-[4].

The mathematical model of the DFIM is presented here via the dq equations in the reference frame.

The equations for the stator and rotor voltage can be written as (1)-(4).

$$
\begin{cases}
V_{sd}(t) = R_s i_{sd}(t) + \dfrac{\mathrm{d}\varphi_{sd}(t)}{\mathrm{d}t} - w_s \varphi_{sq}(t) \\[2mm]
V_{sq}(t) = R_s i_{sq}(t) + \dfrac{\mathrm{d}\varphi_{sq}(t)}{\mathrm{d}t} + w_s \varphi_{sd}(t) \\[2mm]
V_{rd}(t) = R_r i_{rd}(t) + \dfrac{\mathrm{d}\varphi_{rd}(t)}{\mathrm{d}t} - w_r \varphi_{rq}(t) \\[2mm]
V_{rq}(t) = R_r i_{rq}(t) + \dfrac{\mathrm{d}\varphi_{rq}(t)}{\mathrm{d}t} + w_r \varphi_{rd}(t)
\end{cases}
\tag{1}
$$

where

$$w_s = w + w_r \tag{2}$$

The flux equations can be expressed as

$$
\begin{cases}
\varphi_{sd}(t) = L_s i_{sd}(t) + M_{sr} i_{rd}(t) \\
\varphi_{sq}(t) = L_s i_{sq}(t) + M_{sr} i_{rq}(t) \\
\varphi_{rd}(t) = L_r i_{rd}(t) + M_{sr} i_{sd}(t) \\
\varphi_{rq}(t) = L_r i_{rq}(t) + M_{sr} i_{sq}(t)
\end{cases}
\tag{3}
$$

The mechanic equation is described as

$$
\begin{cases}
J_t \dfrac{\mathrm{d}\Omega(t)}{\mathrm{d}t} = T_{em} - f_t \Omega(t) - T_r \\
w = N_p \Omega
\end{cases}
\tag{4}
$$

A Simulink model is built using the Equations (1)-(4) and the DFIM parameters in **Table 1**.

The DFIM model is highly nonlinear since it contains product terms such as speed w with flux φ_d or φ_q, consequently with current i_d or i_q. Thus to cope with this problem the multi-model approach is next suggested.

3. The DFIM Drive System Modeling via Decoupled Multi-Model Approach

The multi-model approach consists in representing the system's behavior with a set of local linear models. Every local model or sub model contributes to this global representation via a validity function which takes its values in {0, 1}.

The DFIM Modeling with multi-model approach is executed through a sequence of four steps which are clusters estimation, structure identification, parametric identification and local models combination.

The performance of the cluster estimation depends on the quality of data base which must be rich in information. The process inputs and outputs are acquired after application of a voltage scalar control strategy as shown in **Figure 1**.

An excitation produced by applying a variable amplitude high frequency signal at the desired speed loop. The acquisition phase consists in the collection of the DFIM's output signals; the speed, the rotor currents i_{rd} and i_{rq}. The rotor frequency fr is considered as the system's input signal. The multi-model modeling is applied in such a way to create the system's model in presence of load disturbances, thus a variable Load torque is produced by a pseudo random binary signal.

Next, the input-output collected data on DFIM are clustered into several groups through a Chui's clustering

Table 1. The DFIM parameters.

Variable	Value
R_s	0.05 Ω
R_r	0.38 Ω
M_{sr}	47.3 H
L_s	50 H
L_r	50 H
J_t	0.05 Kg·m^2
f_t	0.003 N·m/rad/s
N_p	2
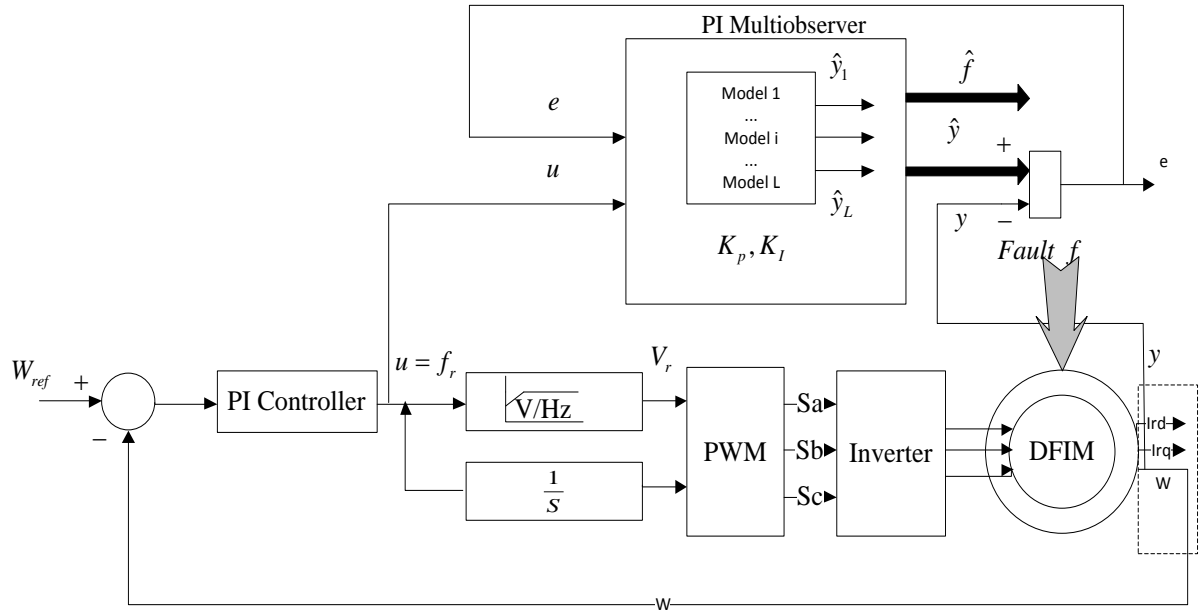
Figure 1. DFIM Volt per Hertz drives system.

algorithm. Then, the structure identification is performed on each cluster using instrumental determinants ration (RDI) method or the general procedure for order estimation while the parameters identification of each sub model are identified using recursive least square (RLS) method. Finally, obtained sub models are combined using the validity concept.

The different steps of multi-model modeling and implementation are performed thanks to MATLAB/ SIMULINK environment

The modeling strategy leads to a decoupled multi-model with six sub models which can be presented as follows.

$$
\begin{cases}
x_i\left(k+1\right) = A_i x_i\left(k\right) + B_i u\left(k\right) + D_i \\
y_i\left(k\right) = C_i x_i\left(k\right) \\
y\left(k\right) = \sum_{i=1}^{L} V_i\left(k\right) y_i\left(k\right)
\end{cases}
\tag{5}
$$

$x_i \in \mathbb{R}^{ni}$, $y_i \in \mathbb{R}^{p}$ and *u* are respectively the system's i^{th} state, output and input. Where $n_i = 3$, $p = 3$.

$$
\begin{cases}
x_i = \begin{bmatrix} w_i & i_{rd_i} & i_{rq_i} \end{bmatrix}', & i = 1, \cdots, 6 \\
u = fr \\
y_i = x_i
\end{cases}
\tag{6}
$$

V_i is the ith validity value which computes the ith sub model's contribution to the creation of the system's global output. These functions have the following properties (7).

$$
\begin{cases}
\sum_{i=1}^{N} V_i\left(k\right) = 1 \\
0 \le V_i\left(k\right) \le 1 & \forall i \in \{1, 2, \cdots, N\}
\end{cases}
\tag{7}
$$

The different obtained DFIM system's matrixes are expressed as (8)-(11).

$$A_1 = \begin{bmatrix} 0.982 & 0 & 0 \\ 0 & -0.970 & 0 \\ 0 & 0 & 0.941 \end{bmatrix}, \quad A_2 = \begin{bmatrix} 0.990 & 0 & 0 \\ 0 & 0.946 & 0 \\ 0 & 0 & 0.960 \end{bmatrix},$$

$$A_3 = \begin{bmatrix} 0.977 & 0 & 0 \\ 0 & 0.945 & 0 \\ 0 & 0 & 0.982 \end{bmatrix}, \quad A_4 = \begin{bmatrix} 0.989 & 0 & 0 \\ 0 & 0.957 & 0 \\ 0 & 0 & 0.968 \end{bmatrix}, \tag{8}$$

$$A_5 = \begin{bmatrix} 0.976 & 0 & 0 \\ 0 & 0.986 & 0 \\ 0 & 0 & 0.959 \end{bmatrix}, \quad A_6 = \begin{bmatrix} 0.999 & 0 & 0 \\ 0 & 0.990 & 0 \\ 0 & 0 & 0.966 \end{bmatrix}$$

$$B_1 = \begin{bmatrix} 0.025 \\ 0.011 \\ 0.070 \end{bmatrix}, \quad B_2 = \begin{bmatrix} 0.081 \\ 0.029 \\ 0.095 \end{bmatrix}, \quad B_3 = \begin{bmatrix} 0.057 \\ -0.019 \\ 0.135 \end{bmatrix},$$

$$B_4 = \begin{bmatrix} 0.012 \\ -0.004 \\ 0.056 \end{bmatrix}, \quad B_5 = \begin{bmatrix} 0.057 \\ 0.016 \\ 0.079 \end{bmatrix}, \quad B_6 = \begin{bmatrix} 0.034 \\ 0.001 \\ 0.067 \end{bmatrix} \tag{9}$$

$$C_1 = \begin{bmatrix} 1 & 0 & 0 \\ 0 & 1 & 0 \\ 0 & 0 & 1 \end{bmatrix}, \quad C_2 = C_3 = C_4 = C_5 = C_6 = C_1 \tag{10}$$

$$D_1 = \begin{bmatrix} -0.048 \\ 0.911 \\ 1.678 \end{bmatrix}, \quad D_2 = \begin{bmatrix} 1.085 \\ 4.690 \\ 2.331 \end{bmatrix}, \quad D_3 = \begin{bmatrix} 0.751 \\ 3.738 \\ -0.856 \end{bmatrix},$$

$$D_4 = \begin{bmatrix} -0.550 \\ 5.323 \\ 3.188 \end{bmatrix}, \quad D_5 = \begin{bmatrix} 4.319 \\ 2.263 \\ -3.662 \end{bmatrix}, \quad D_6 = \begin{bmatrix} 0 \\ 0.025 \\ 0.064 \end{bmatrix} \tag{11}$$

By exciting the system with a variable input, the modeling results of the speed, the current i_{rd} and the current i_{rq} are shown in **Figures 2**-**4**. We can notice that the multi-model outputs follow with acceptable error the real outputs.
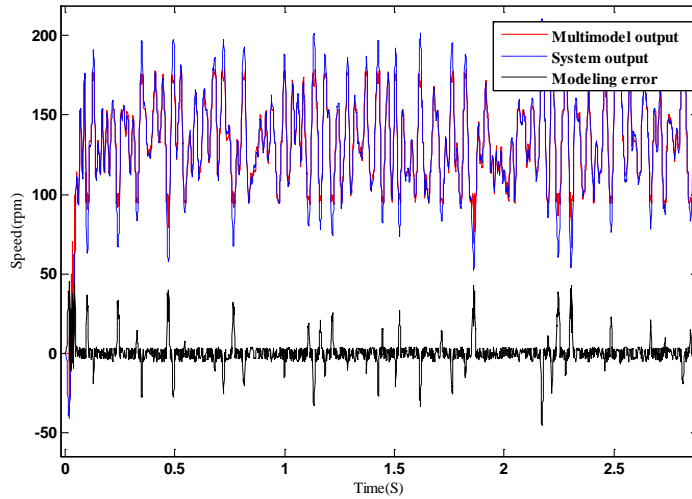
Figure 2. Speed Multi-model modeling.
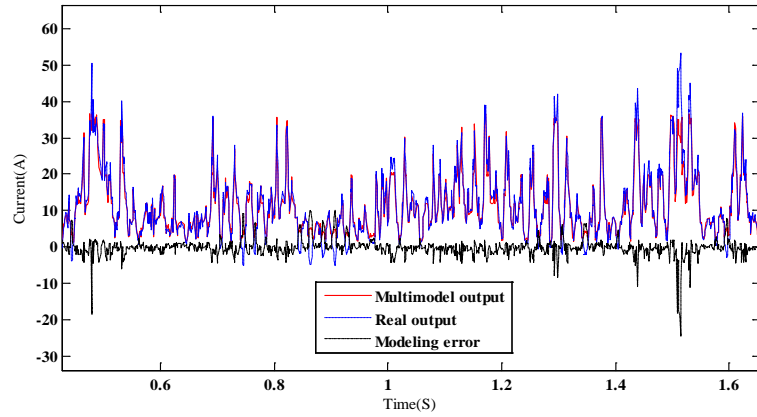
Figure 3. i_{rd} current Multi-model modeling.
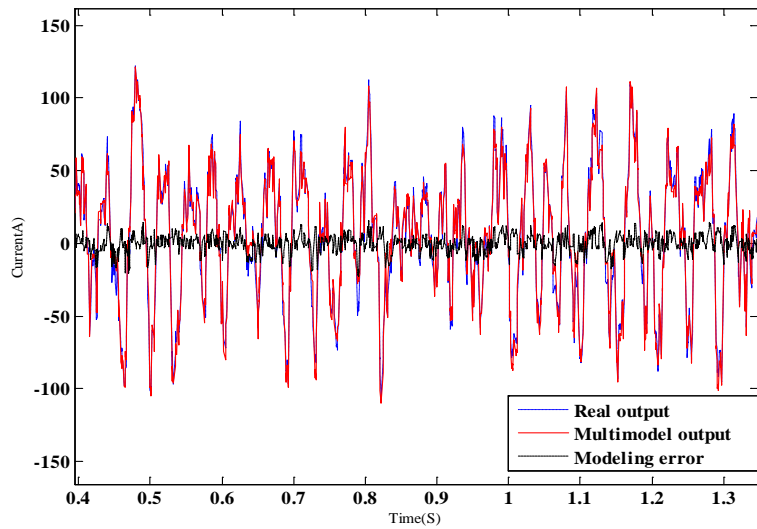
Figure 4. i_{rq} Multi-model modeling.

The normalized roots mean square modeling error NRMSE for each modeling error; the speed, i_{rd} and i_{rq} modeling error are calculated and given in **Table 2**.

The obtained multi-model is compared to a model done by RLS method, **Figure 5** approves the efficiency of the multi-model.

Next this multi-model will be exploited in the multiobserver design.

4. Adaptive Proportional-Integral Multiobserver Designs

In this section we propose to study in the first part the PI multiobserver then the modified or adaptive PI multiobserver in second part of this section.

Firstly, the DFIM decoupled multi-model structure is modified in order to take into account the unknown input vector, and then exploited in the rest of this paper in order to conceive the based observer diagnosis's strategy.

$$\begin{cases} x_i(k+1) = A_i x_i(k) + B_i u(k) + D_i + E_i f(k) \\ y_i(k) = C_i x_i(k) + Mf(k) \\ y(k) = \sum_{i=1}^{N} V_i(k) y_i(k) \end{cases} \tag{12}$$

Table 2. NRMSE for the modeling errors.

	NRMSE
Speed modeling error	0.0243
i_{rd} current modeling error	0.0947
i_{rq} current modeling error	0.0214
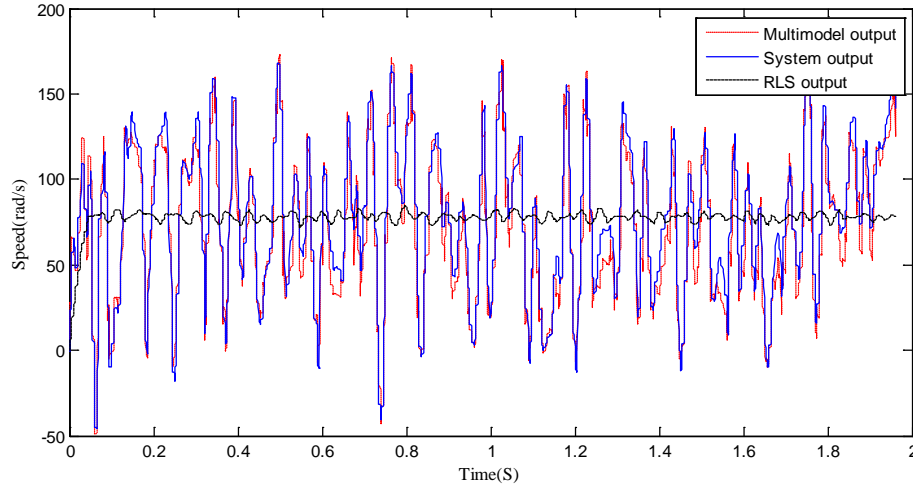
Figure 5. Multi-model, System and RLS outputs.

where E_i and f identify, respectively, the impact of the unknown input on the state's system and the unknown input vector.

4.1. PI Multiobserver

The PI structure is developed below in favor of achieving simultaneously estimation of both state and unknown inputs.

$$\begin{cases} x_i(k+1) = A_i x_i(k) + B_i u(k) + D_i + E_i \hat{f}(k) + K_{pi}(y(k) - \hat{y}(k)) \\ f(k+1) = f(k) + \sum_{i=1}^{N} V_i(k) K_I(y(k) - \hat{y}(k)) \\ y(k) = \sum_{i=1}^{N} V_i(k) C_i x_i(k) + M\hat{f}(k) \end{cases} \tag{13}$$

where x_i and y denote respectively the estimated state vector and output vector. V_i are the validities functions calculated in the modeling phase.

This observer is known as a robust observer regarding the unknown inputs that have feebly variation. The main task of the observer design is to find out the gain matrices K_I and K_{pi}.

The PI observer uses the influence of the rebuilding output's error with a proportional effect to estimate the system's whereas the integral effect is used to estimate the signal of sensor or actuator's defaults.

The sub models' outputs $y_i(k)$, used, as modeling's artificial signals, to represent the real system's behavior are not exploitable to control an observer, indeed only the multi-model's total output $y(k)$ as it is accessible to measurement, can be designed with a system's physical quantity. Thus an augmented system is defined below.

$$\begin{cases} \tilde{x}(k+1) = \tilde{A}\tilde{x}(k) + \tilde{B}u(k) + \tilde{D} + \tilde{E}f(k) \\ \tilde{y}(k) = \tilde{C}(k)\tilde{x}(k) + Mf(k) \end{cases} \tag{14}$$

167

where

$$\tilde{x}(t) = \left[x_1^{\mathrm{T}}(t) \cdots x_i^{\mathrm{T}}(t) \cdots x_N^{\mathrm{T}}(t) \right]^{\mathrm{T}} \in R^n, \ n = \sum_{i=1}^{N} n_i \tag{15}$$

$$\begin{cases} \tilde{A} = diag\left\{ A_1, \cdots, A_N \right\} \in R^{n \times n}, \\ \tilde{B} = \left[B_1^{\mathrm{T}}, \cdots, B_N^{\mathrm{T}} \right]^{\mathrm{T}} \in R^{n \times m}, \\ \tilde{C}(k) = \sum_{i=1}^{N} V_i(k) \tilde{C}_i \in R^{p \times n}, \\ \tilde{C}_i = \left[0 \cdots C_i \cdots 0 \right], \\ \tilde{D} = \left[D_1^{\mathrm{T}}, \cdots, D_N^{\mathrm{T}} \right]^{\mathrm{T}} \in R^{n \times l}, \\ \tilde{E} = \left[E_1^{\mathrm{T}}, \cdots, E_N^{\mathrm{T}} \right]^{\mathrm{T}} \in R^{n \times l} \end{cases} \tag{16}$$

By the use of the Lyapunov's approach defined below and taken advantage of ensuring the employed observer's stability, and in order to guarantee the convergence of the estimation's error, the conditions generated in forms of linear matrix inequalities (LMI) permit to compute the observer's gains. Thus the following theorem proposed in [14] [15] suggests sufficient conditions ensuring the exponential convergence of the estimation's error.

Theorem: The estimation error between the decoupled multi-model (12) and the PI observer (13) converges exponentially towards zero if there exists a symmetric definite positive matrix P and a matrix G verifying the LMI following:

$$\begin{bmatrix} (2\alpha - 1)P & \overline{C}_i^{\mathrm{T}} G^{\mathrm{T}} - A_a P \\ G\overline{C}_i - PA_a & -P \end{bmatrix} < 0, \ i = 1, \cdots, N \tag{17}$$

where

$$A_a = \begin{bmatrix} \tilde{A} & \tilde{E} \\ 0 & I \end{bmatrix}, \ \overline{C}_i(t) = \begin{bmatrix} \tilde{C}_i(t) & M \end{bmatrix} \tag{18}$$

α is the attenuation rate which serves to quantify the convergence speed of the estimation error. Having $0 < \alpha < 0.5$ let to find the KI and Kp gains as:

$$K_a = P^{-1}G \tag{19}$$

The state's estimation e and input's estimation errors ε are given by the following equation:

$$\begin{cases} e(k) = \tilde{x}(k) - \hat{\tilde{x}}(k) \\ \varepsilon(t) = f(k) - \hat{f}(k) \end{cases} \tag{20}$$

Taking into account the fact that the unknown inputs are considered as constant or with very slow dynamics,

$$f(k+1) - f(k) \approx 0 \tag{21}$$

Then

$$\begin{bmatrix} e(k+1) \\ \varepsilon(k+1) \end{bmatrix} = \begin{bmatrix} \tilde{A} - \tilde{K}_P \tilde{C}(k) & \tilde{E} - \tilde{K}_P M \\ -K_I \tilde{C}(k) & I - K_I M \end{bmatrix} \begin{bmatrix} e(k) \\ \varepsilon(k) \end{bmatrix} \tag{22}$$

Considering the definition of augmented system, the augmented error can be defined as

$$e_a(k+1) = \left(A_a - K_a C_a(k) \right) e_a(k), \tag{23}$$

where

$$\begin{cases} e_a(k) = \begin{bmatrix} e(k) \\ \varepsilon(k) \end{bmatrix} \\ K_a = \begin{bmatrix} \tilde{K}_P \\ K_I \end{bmatrix} \\ \tilde{K}_P = \begin{bmatrix} K_{P1}^{\mathrm{T}}, \cdots, K_{PN}^{\mathrm{T}} \end{bmatrix}^{\mathrm{T}} \end{cases} \tag{24}$$

The Lyapunov approach is defined as

$$V(e(k)) = e^{\mathrm{T}}(k) P e(k), \ P > 0 \ P = P^{\mathrm{T}} \tag{25}$$

The exponential convergence is guaranteed if there exists a symmetric definite positive matrix P and a positive scalar α verifying the following condition:

$$\Delta V(e(k)) + 2\alpha V(e(k)) < 0 \tag{26}$$

With

$$\Delta V(e(k)) = V(e(k+1)) - V(e(k)) \tag{27}$$

This PI multiobserver is studied and developed by [17] [18], however, the studied multiobserver is valid only in the case of slowly varying faults.

4.2. Adaptive PI Multiobserver

To consider the case of variable fault, as expressed in (28), we propose to create an adaptive PI multiobserver that is based on the updating of the estimated validity functions $\hat{V}_i$ which are computed as the Equations (29)-(31).

In fact the real system depends on the fault, so the multiobserver design should also consider this fault therefore in each instant a new validities are computed in order to guarantee always the convergence of the residue r_i expressed by (29).

$$f(k+1) - f(k) \neq 0 \tag{28}$$

$$r_i(k) = \| y(k) - \hat{y}_i(k) \| \tag{29}$$

Then simple validities are expressed by (30).

$$v_i(k) = 1 - \frac{r_i(k)}{\sum\limits_{i=1}^{N} r_i(k)} \tag{30}$$

The final adaptive validities after normalization and reinforcement of the simple validities functions are expressed in (31).

$$\hat{V}_i(k) = \frac{v_i(k) \prod\limits_{j=1, j \neq i}^{N} \left(1 - e^{-\left(\frac{r_j(k)}{\sigma} \right)^2} \right)}{\sum\limits_{i=1}^{N} \left(v_i(k) \prod\limits_{j=1, j \neq i}^{N} \left(1 - e^{-\left(\frac{r_j(k)}{\sigma} \right)^2} \right) \right)} \tag{31}$$

The Final adaptive PI multiobserver is developed in (32).

$$\begin{cases} x_i(k+1) = A_i x_i(k) + B_i u(k) + D_i + E_i \hat{f}(k) + K_{pi}(y(k) - \hat{y}(k)) \\ f(k+1) = f(k) + \sum_{i=1}^{N} \hat{V}_i(k) K_I(y(k) - \hat{y}(k)) \\ y(k) = \sum_{i=1}^{N} \hat{V}_i C_i x_i(k) + M\hat{f}(k) \end{cases}$$ (32)

5. Detection and Isolation of DFIM System's Sensors Faults

In this section, the main task to be reached is detection and isolation of the Doubly fed Induction motor's faults by means of a designed adaptive PI multi-observer synthesized to estimate the different system outputs. Within this part the fault effect on the system state is expressed with E_i, $i = 1, \cdots, N$ while M represents the faults effect on the DFIM output.

Three types of sensor faults are considered, they affect respectively the speed Ω, the i_{rd} current and the i_{rq} current. The faults are variable and have sinus form.

The PI multiobserver structure is equivalent to a bank of three multiobservers since

$$\hat{y} = \begin{bmatrix} \hat{\Omega} & i_{rd} & i_{rq} \end{bmatrix}$$ (33)

The different faults are chosen to be occurred in the same date. In this case;

$$M = \begin{bmatrix} 0.2 & 0 & 0 \\ 0 & 0.2 & 0 \\ 0 & 0 & 0.2 \end{bmatrix}$$ (34)

And

$$E_i = 0, \ \forall i = 1, \cdots, N$$ (35)

The resolution of the different LMI helps to find the matrices gains then to construct the PI multiobserver. The K_{Pi} and K_I gains are given by (36).

$$K_{p1} = \begin{bmatrix} 0.121 & 0 & 0 \\ 0 & -0.057 & 0 \\ 0 & 0 & 0.114 \end{bmatrix}, \ K_{p2} = \begin{bmatrix} 0.123 & 0 & 0 \\ 0 & 0.115 & 0 \\ 0 & 0 & 0.118 \end{bmatrix}, \ K_{p3} = \begin{bmatrix} 0.120 & 0 & 0 \\ 0 & 0.115 & 0 \\ 0 & 0 & 0.122 \end{bmatrix},$$

$$K_{p4} = \begin{bmatrix} 0.123 & 0 & 0 \\ 0 & 0.118 & 0 \\ 0 & 0 & 0.120 \end{bmatrix}, \ K_{p5} = \begin{bmatrix} 0.120 & 0 & 0 \\ 0 & 0.124 & 0 \\ 0 & 0 & 0.118 \end{bmatrix}, \ K_{p6} = \begin{bmatrix} 0.273 & 0 & 0 \\ 0 & 0.277 & 0 \\ 0 & 0 & 0.274 \end{bmatrix},$$ (36)

$$K_I = \begin{bmatrix} 0.134 & 0 & 0 \\ 0 & 0.127 & 0 \\ 0 & 0 & 0.131 \end{bmatrix}$$

The residual equations are given as follows:

$$\begin{cases} R_s = \hat{y}_1 - y_1 \\ R_{id} = \hat{y}_2 - y_2 \\ R_{iq} = \hat{y}_3 - y_3 \end{cases}$$ (37)

where R_s, R_{id} and R_{iq} designate respectively the speed residual signal, i_{rd} current residual signal and i_{rq} current residual signal.

$\hat{y}_i$ designate the ith estimated output and y_i designate the ith real system output in no faulty case.

Obtained results approve the performance of the fault estimation method; the different system's outputs y_i, $i = 1, \cdots, 3$ follow rapidly and respectively, the real ones y_i with satisfied error as shown in **Figure 6**, **Figure 7** and **Figure 8**.

The different fault evolutions approve that the estimated fault is occurred at the same time when the real fault is occurred so the detection task is verified.

The three residual signals shown in **Figure 9**, **Figure 10** and **Figure 11** follow with high precision the different sensors fault signals and approve that the faults are well identified.

The isolation task is verified since for each system output a multiobserver is synthesized, *i.e.* each residue is sensitive to only one sensor fault and insensitive to all other faults concerning the residual signals computed in (36).

The isolation of the different sensor faults can be summarized in the **Figure 12**. In fact, if a speed sensor fault f1 is occurred then the residual signal Rs $\neq$ 0, if an i_{rd} current sensor fault f2 is occurred then the residual signal $R_{\text{id}} \neq 0$, and if an i_{rq} current sensor fault f3 is occurred, the residual signal $R_{\text{iq}} \neq 0$.

Considering the previous results, generated relationship can be described in a summarized table as shown in **Table 3**.

6. Experimental Validation

In this section the proposed diagnosis approach is validated experimentally on 1 KW squirrel cage Induction motor.
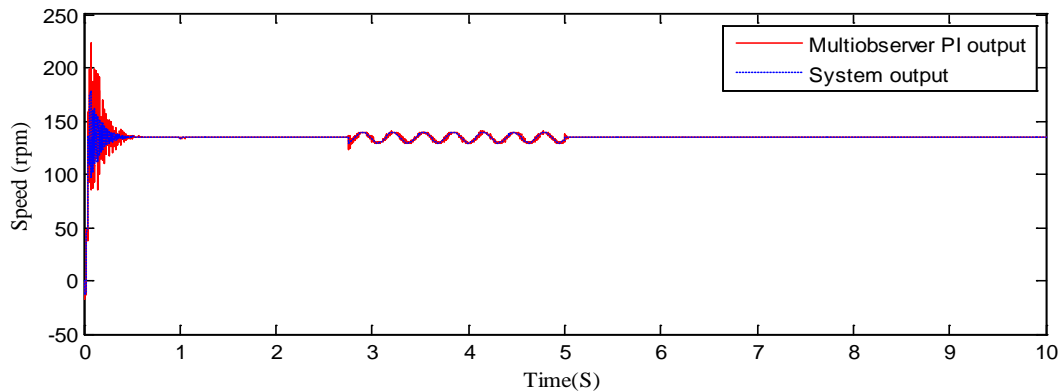
Figure 6. Speed sensor fault identification.
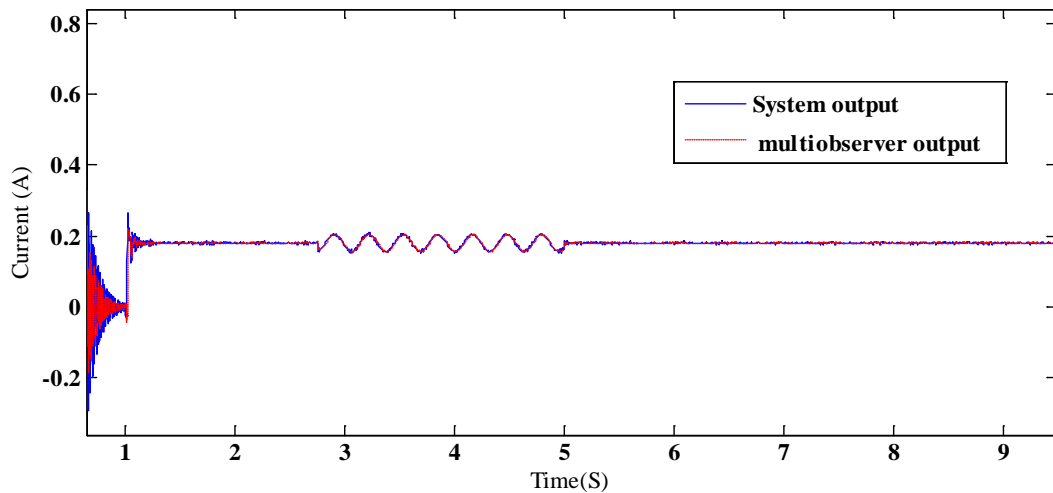
Figure 7. ird current sensor fault identification.
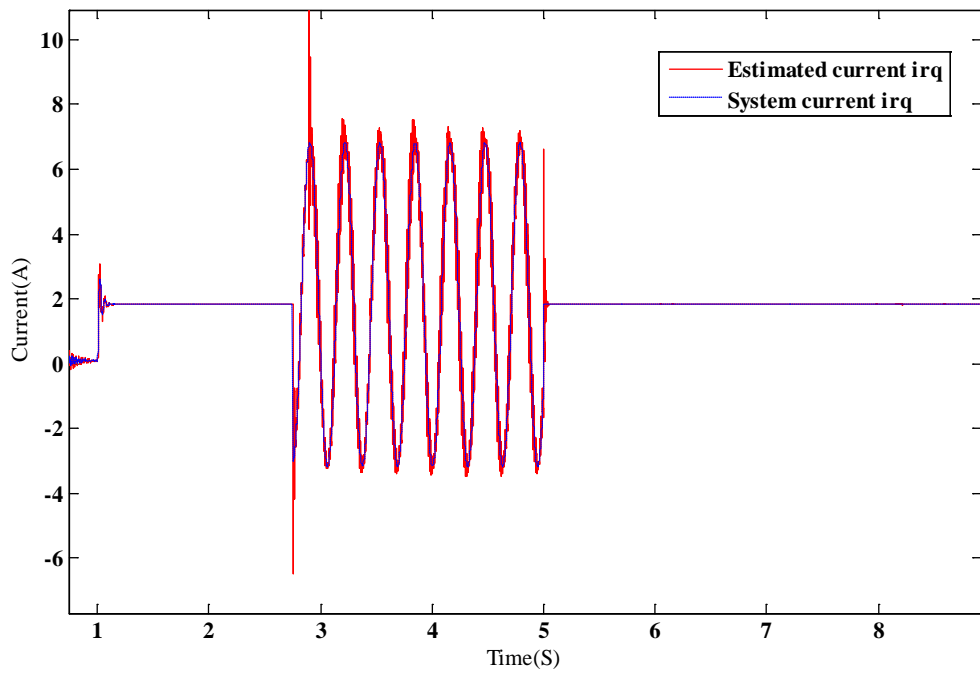
Figure 8. irq current sensor fault identification.
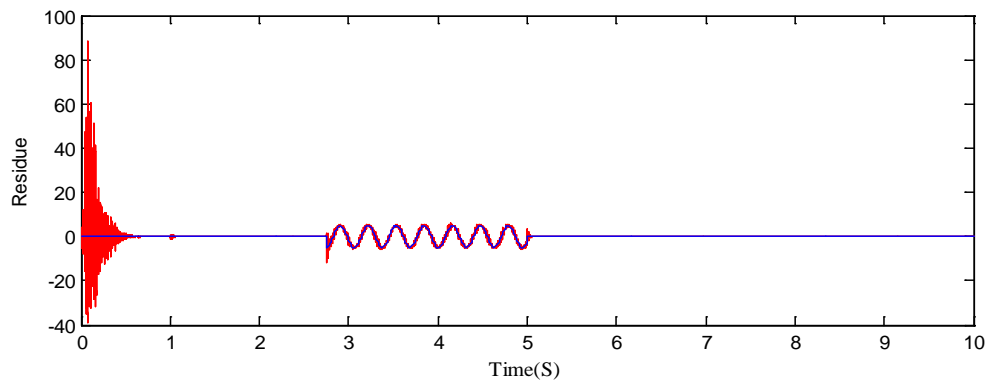
Figure 9. Speed residual signal Rs and speed sensor fault evolution.
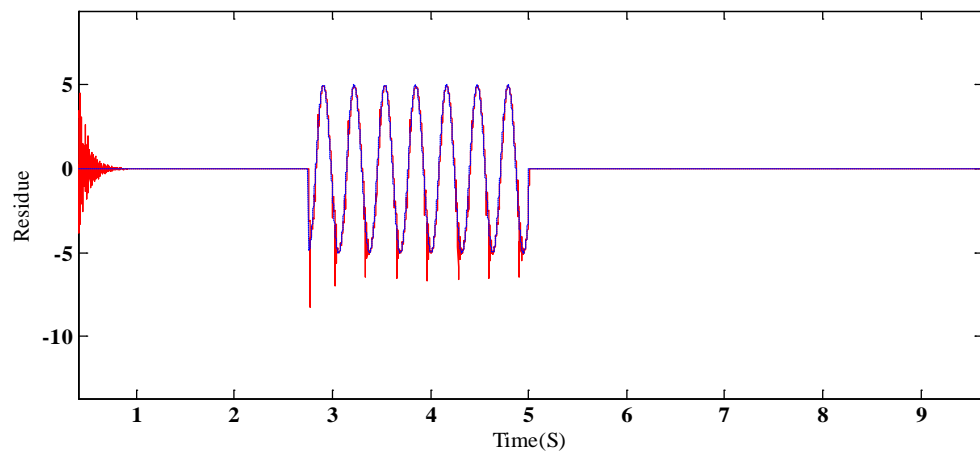
Figure 10. ird current residual signal Rid and current fault evolution.
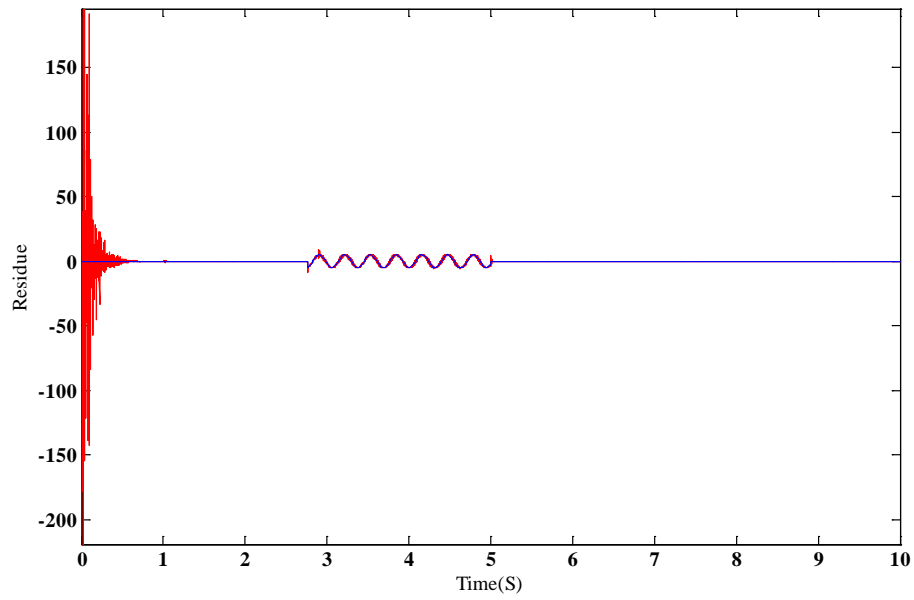
Figure 11. irq current residual signal Riq and current fault evolution.
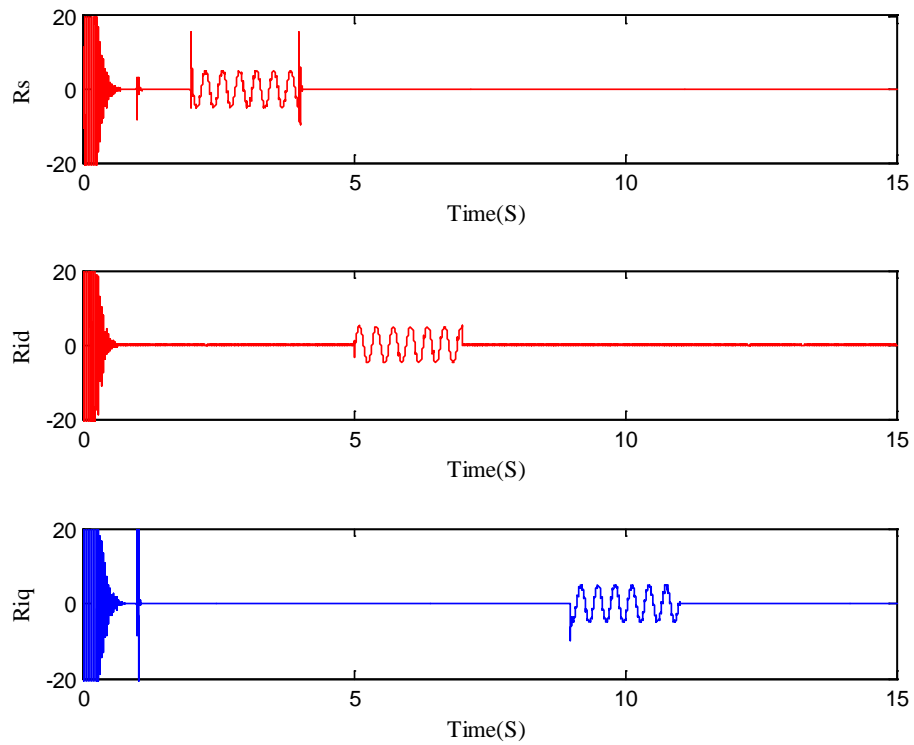
Figure 12. The residual sensor faults evolutions.

Table 3. Fault signature table.

	R_s	R_{id}	R_{iq}
f1	$\neq 0$	0	0
f2	0	$\neq 0$	0
f3	0	0	$\neq 0$

An experimental set up drive system exposed in **Figure 13** is prepared to provide a set of input/output measurement with the help of MATLAB/SIMULINK and DSpace system with DS1104 controller board based on the digital signal processor (DSP) TMS320F240. The measurement of the stator current is achieved via Hall type sensors. An incremental encoder position sensor delivering 1024 pulses per revolution is used to detect The IM speed. Load torque is generated by a resistive bank fed by a DC generator.

To create parameter variation we propose to use a variable resistor that is connected in series to each phase of the motor to vary the stator resistance

The experimental set up is exploited to collect a rich database at 600 rpm with a wide range of loads and stator resistance variations.

The database is then clustered into eight clusters. Next a structural and parametric identification is performed into the obtained cluster to generate the eight local models. Finally a multi-model is created after the combination of the local models pondered by validities functions.

The obtained multi-model is next necessary to synthesize the adaptive PI multiobserver.

The resolution of the different LMI conditions helps to calculate the multiobserver gain matrices that are expressed in Equation (38).

$$K_{I1} = \begin{bmatrix} 0.113 & 0.0348 \\ 0.048 & 0.1184 \end{bmatrix}, \ K_{I2} = \begin{bmatrix} 0.130 & 0.0376 \\ 0.046 & 0.1183 \end{bmatrix}, \ K_{I3} = \begin{bmatrix} 0.121 & 0.0340 \\ 0.025 & 0.0200 \\ 0.026 & 0.0208 \end{bmatrix},$$

$$K_{I4} = \begin{bmatrix} 0.025 & 0.0200 \\ 0.085 & 0.0679 \\ 0.047 & 0.1123 \end{bmatrix}, \ K_{I5} = \begin{bmatrix} 0.148 & 0.0354 \\ 0.057 & 0.0813 \end{bmatrix}, \ K_{I6} = \begin{bmatrix} 0.063 & 0.0503 \\ 0.025 & 0.0200 \\ 0.043 & 0.0349 \end{bmatrix},$$

$$K_{I7} = \begin{bmatrix} 0.025 & 0.0200 \\ 0.072 & 0.0575 \\ 0.047 & 0.1096 \end{bmatrix}, \ K_{I8} = \begin{bmatrix} 0.025 & 0.0200 \\ 0.071 & 0.0572 \\ 0.047 & 0.0376 \end{bmatrix}$$

$$K_p = \begin{bmatrix} 0.025 & 0 \\ 0 & 0.020 \end{bmatrix}$$

(38)

To test the obtained multiobserver, we inject two sensor fault, the first affect the speed sensor between t = 109 s and t = 130 s, while the second affect the current sensor between t = 14 s and 21 s.

Figure 13. Experimental setup system.

Figure 14 and Figure 15 approve that the estimated speed and current signals follow the real ones affected with the faults. Figure 16 and Figure 17 expose the residual signals that approve that the estimated fault follow the real ones.

According to experimental results, we can resume that the detection of the sensor fault is successfully achieved. We can notice that the value of the residual signals (speed and current residue) changes from zeros only when the fault occurs.

The identification of the faults is approved as the two residual signals follow with high precision of the two sensors fault signals.
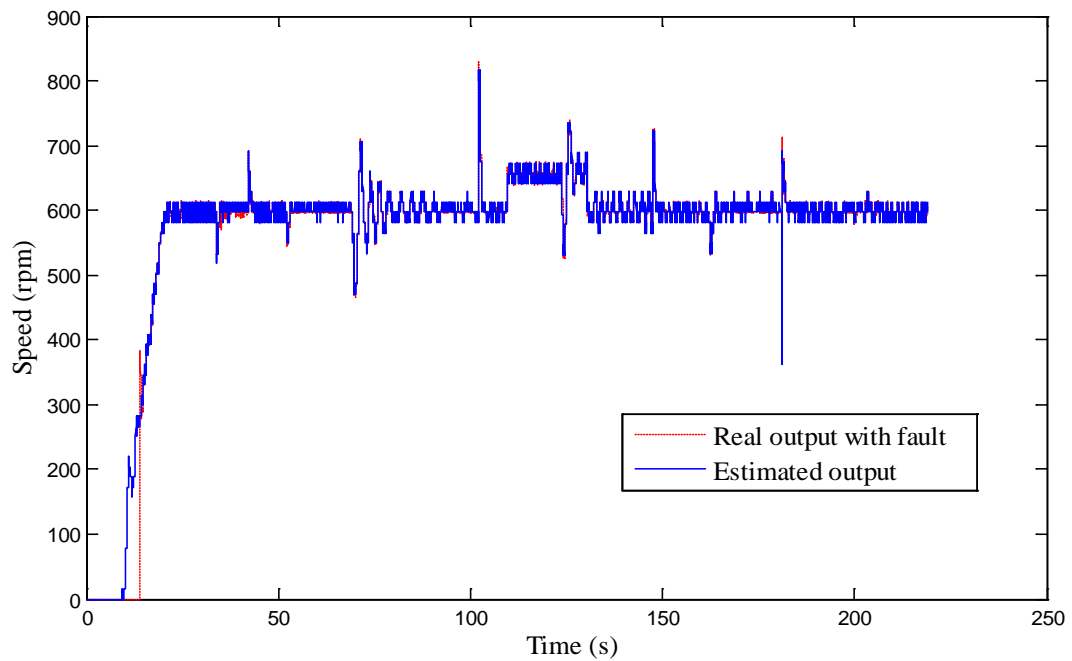
Figure 14. Speed sensor fault identification.
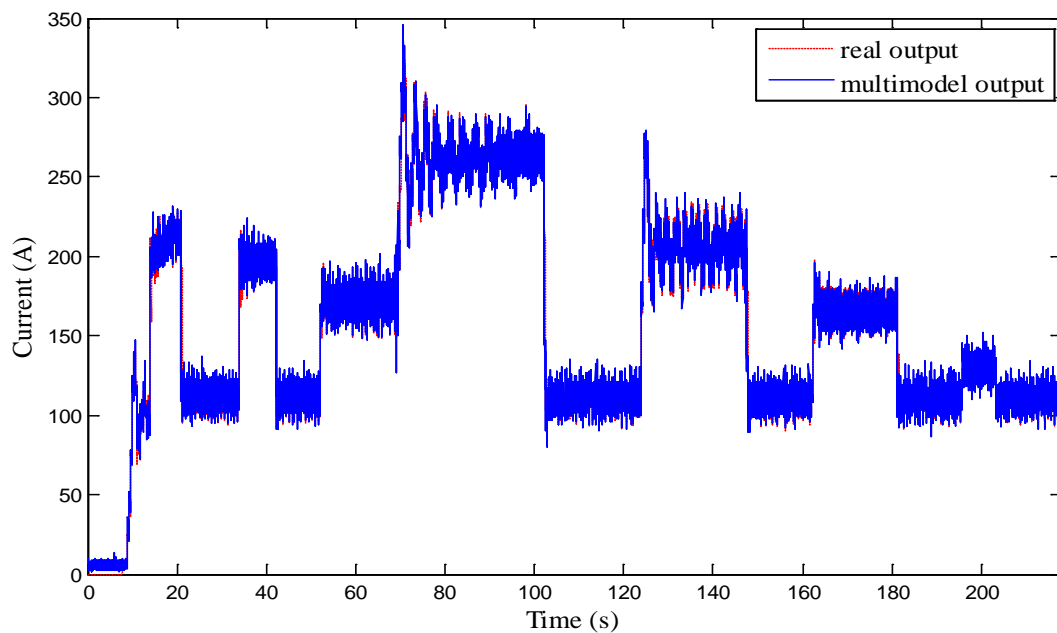
Figure 15. Is current sensor fault identification: Real current with fault and estimated current.
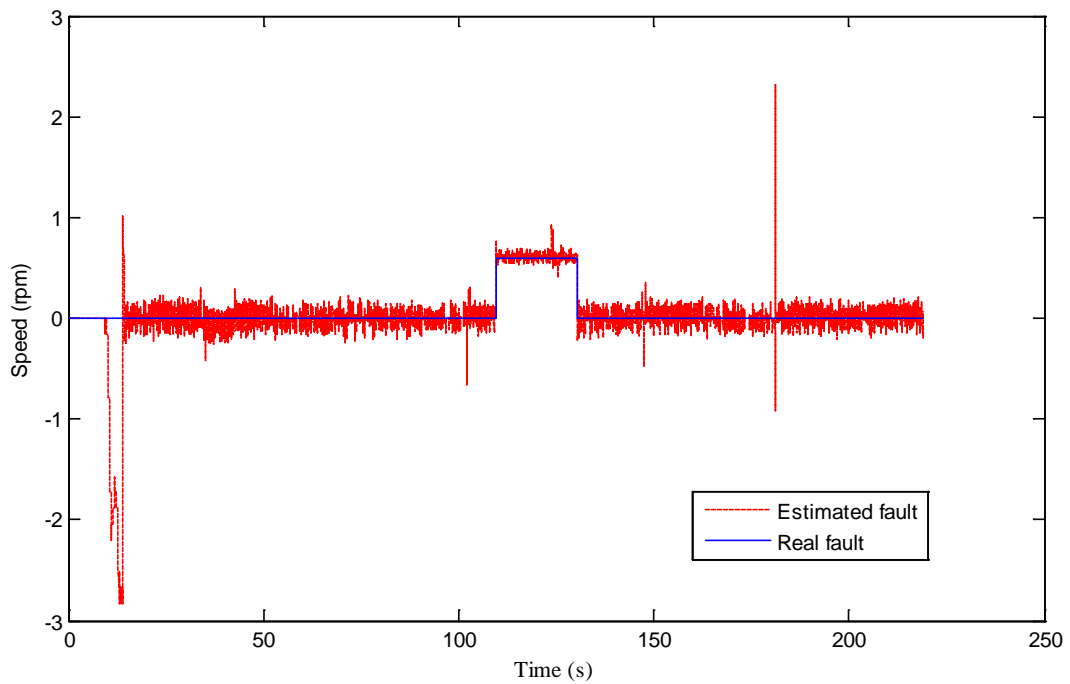
Figure 16. Speed residual signal Rw and speed sensor fault evolution.
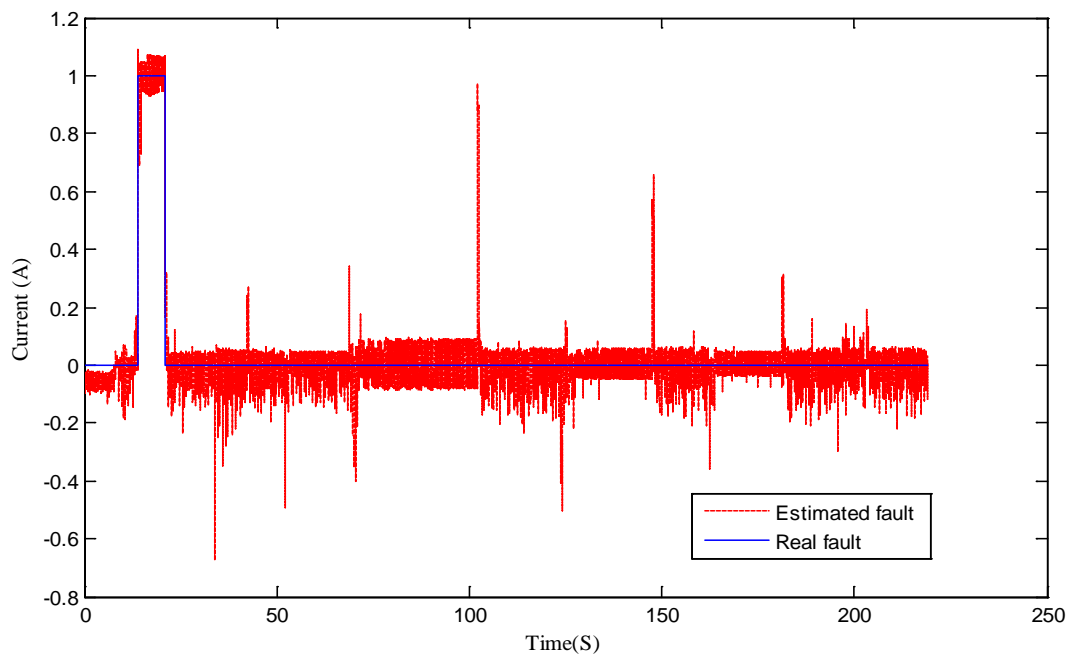
Figure 17. Current residual signal Ris and current sensor fault evolution.

The fault isolation is proved as for each system output an estimated output is generated. Each residue is sensitive to only one sensor fault.

7. Conclusions

In this paper, a multi-model diagnosis strategy is applied to the detection and isolation of the different sensor faults that can affect the induction machine. Firstly the system's modeling is investigated through the multi-

model approach. Then considering the system's decoupled multi-model structure an adaptive PI multi-observer is synthesized. The novel multiobserver is synthesized exploiting the classic PI multiobserver that is modified to obtain the adaptive one. The modification consists in the multiobserver validities calculation. This multiobserver is used in the fault detection and isolation of the different sensor faults that can affect the system's outputs. The obtained experimental and simulation results performed under MATLAB/SIMULINK environment show that the applied method has an excellent capacity to describe the Induction machine under faulty case. The objectives are reached since the different computed residuals signals affirm that the detection, identification and isolation of the sensors faults are well achieved. In this paper the study is limited on simulation and without considering actuators and system faults, thus, in future work experimental study concern the induction motor, in future work we will propose to validate experimentally the diagnosis approach on a DFIM under sensor and actuator faults.

Acknowledgements

References

[1] Gritli, Y., Stefani, A., Rossi, C., Filippetti, F. and Chatti, A. (2011) Experimental Validation of Doubly Fed Induction Machine Electrical Faults Diagnosis under Time-Varying Conditions. *Electric Power Systems Research*, **81**, 751-766. http://dx.doi.org/10.1016/j.epsr.2010.11.004

[2] Djeghali, N., Ghanes, M., Djennoune, S. and Barbot, J.P. (2013) Sensorless Fault Tolerant Control for Induction Motors. *International Journal of Control*, *Automation*, *and Systems*, **11**, 563-576. http://dx.doi.org/10.1007/s12555-012-9224-z

[3] Saha, S., Aldeen, M. and Tan, C.P. (2011) Fault Detection in Transmission Networks of Power Systems. *International Journal of Electrical Power* & *Energy Systems*, **33**, 887-900. http://dx.doi.org/10.1016/j.ijepes.2010.12.026

[4] Chen, J.H., Li, H.K., Sheng, D.R. and Li, W. (2015) A Hybrid Data-Driven Modeling Method on Sensor Condition Monitoring and Fault Diagnosis for Power Plants. *International Journal of Electrical Power* & *Energy Systems*, **71**, 274-284. http://dx.doi.org/10.1016/j.ijepes.2015.03.012

[5] Darouach, M. (2012) On the Functional Observers for Linear Descriptor Systems. *Systems* & *Control Letters*, **61**, 427-434. http://dx.doi.org/10.1016/j.sysconle.2012.01.006

[6] Manuja, S., Narasimhan, S. and Patwardhan, S.C. (2009) Unknown Input Modeling and Robust Fault Diagnosis Using Black Box Observers. *Journal of Process Control*, **19**, 25-37. http://dx.doi.org/10.1016/j.jprocont.2008.02.004

[7] Pertew, A.M., Marquez H.J. and Zhao, Q. (2005) H_∞ Synthesis of Unknown Input Observers for Non-Linear Lipschitz Systems. *International Journal of Control*, **78**, 1155-1165. http://dx.doi.org/10.1080/00207170500155488

[8] Fu, Y.P., Cheng, Y.H. and Jiang, B. (2010) Robust Actuator Fault Estimation for Satellite Control System via Fuzzy Proportional Multiple-integral Observer Method. *Proceedings of the* 29*th Chinese Control Conference*, Beijing, 29-31 July 2010, 3942-3946.

[9] Sören, G. and Horst, S. (2014) Diagnosis of Actuator Parameter Faults in Wind Turbines Using a Takagi-Sugeno Sliding Mode Observer. *Intelligent Systems in Technical and Medical Diagnostics, Advances in Intelligent Systems and Computing*, **230**, 29-40.

[10] Yang, X.-B., Jin, X.-Q., Du, Z.-M., Zhu, Y.-H. and Guo, Y.-B. (2013) A Hybrid Model-Based Fault Detection Strategy for Air Handling Unit Sensors. *Energy and Buildings*, **57**, 132-143. http://dx.doi.org/10.1016/j.enbuild.2012.10.048

[11] Abid, A., BenHamed, M. and Sbita, L. (2011) Induction Motor Real Time Application of Multimodel Modeling Approach. *International Review of Electrical Engineering*, **6**, 655-660.

[12] Capron, B.D.O. and Odloak, D. (2013) LMI-Based Multi-Model Predictive Control of an Industrial C3/C4 Splitter. *Journal of Control*, *Automation and Electrical Systems*, **24**, 420-429. http://dx.doi.org/10.1007/s40313-013-0050-1

[13] Elfelly, N., Dieulot, J.Y. and Borne, P. (2008) A Neural Approach of Multimodel Representation of Complex Processes. *International Journal of Computers*, *Communications* & *Control*, **3**, 149-160.

[14] He, S.P. (2014) Fault Estimation for T-S Fuzzy Markovian Jumping Systems Based on the Adaptive Observer. *International Journal of Control*, *Automation and Systems*, **12**, 977-985. http://dx.doi.org/10.1007/s12555-013-0350-z

[15] Yu, C.H. and Choi, J.W. (2014) Interacting Multiple Model Filter-Based Distributed Target Tracking Algorithm in Underwater Wireless Sensor Networks. *International Journal of Control*, *Automation and Systems*, **12**, 618-627. http://dx.doi.org/10.1007/s12555-013-0238-y

[16] Ichalal, D. (2009) Estimation et diagnostic de systèmes non linéaires décrits par un modèle de Takagi-Sugeno. PhD Thesis, Institut National Polytechnique de Lorraine, Nancy.

[17] Orjuela, R., Marx, B., Ragot, J. and Maquin, D. (2010) Fault Diagnosis for Nonlinear Systems Represented by Heterogeneous Multiple Models. 2010 *Conference on Control and Fault Tolerant Systems*, Nice, 6-8 October 2010, 600-605. http://dx.doi.org/10.1109/SYSTOL.2010.5675969

[18] Hamdi, H., Rodrigues, M., Mechmeche, C., Theilliol, D. and Benhadj Braiek, N. (2012) Fault Detection and Isolation in Linear Parameter-Varying Descriptor Systems via Proportional Integral Observer. *International Journal of Adaptive Control and Signal Processing*, **26**, 224-240. http://dx.doi.org/10.1002/acs.1260

[19] Zhou, D., Spée, R. and Wallace, A.K. (1993) Laboratory Control Implementations for Doubly-Fed Machines. *Proceedings of the International Conference on Industrial Electronics*, *Control*, *and Instrumentation*, *IECON*'93, Maui, 15-19 November 1993, 1181-1186. http://dx.doi.org/10.1109/iecon.1993.339234

Call for Papers

International Journal of Modern Nonlinear Theory and Application

ISSN: 2167-9479 (Print)   ISSN: 2167-9487 (Online)
http://www.scirp.org/journal/ijmnta

International Journal of Modern Nonlinear Theory and Application (*IJMNTA*) is an international peer-reviewed journal dedicated to publishing original papers on all topics related to nonlinear dynamics and its applications such as, electrical, mechanical, civil, and chemical systems and so on. The contributions concerned will be discussion of a practical problem, the formulating nonlinear model, and determination of closed form exact or numerical solutions.

Editor-in-Chief

Subject Coverage

This journal invites original papers and review papers that address the following issues in modern nonlinear Theory and its applications. The interested topics that may be covered, but not limited to:

- Application of Modern Nonlinear Theory in:
  - Biology
  - Business
  - Chemical Systems
  - Electrical and Power Systems
  - Fluid Mechanics
  - Mechanical Systems
  - Medicine
  - Physics
- Applied Mechanics
- Bifurcation and Chaos
- Chaos Control
- Classic Control Systems
- Electrical Drives and Power Electronics
- Fractal Order Systems
- High Dimensional Chaos and Applications
- Intelligent Control Systems (Fuzzy, Neural, Genetic...)
- Nonlinear Control
- Nonlinear Differential Equations and Applications
- Nonlinear Dynamic Stability
- Nonlinear Dynamics
- Nonlinear Mathematical Physics
- Nonlinear Optical Physics & Materials
- Nonlinear Oscillations
- Nonlinear Phenomena
- Nonlinear Science and Numerical Simulation
- Power Systems and Energy
- Security in Communication Systems

We are also interested in: 1) Short Reports—2-5 page papers where an author can either present an idea with theoretical background but has not yet completed the research needed for a complete paper or preliminary data; 2) Book Reviews—Comments and critiques.

Notes for Intending Authors

Submitted papers should not have been previously published nor be currently under consideration for publication elsewhere. Paper submission will be handled electronically through the website. All papers are refereed through a peer review process. For more details about the submission, please access the website.

Website and E-Mail

http://www.scirp.org/journal/ijmnta   E-mail: ijmnta@scirp.org

What is SCIRP?

Scientific Research Publishing (SCIRP) is one of the largest Open Access journal publishers. It is currently publishing more than 200 open access, online, peer-reviewed journals covering a wide range of academic disciplines. SCIRP serves the worldwide academic communities and contributes to the progress and application of science with its publication.

What is Open Access?

All original research papers published by SCIRP are made freely and permanently accessible online immediately upon publication. To be able to provide open access journals, SCIRP defrays operation costs from authors and subscription charges only for its printed version. Open access publishing allows an immediate, worldwide, barrier-free, open access to the full text of research papers, which is in the best interests of the scientific community.

- High visibility for maximum global exposure with open access publishing model
- Rigorous peer review of research papers
- Prompt faster publication with less cost
- Guaranteed targeted, multidisciplinary audience

Scientific Research Publishing